# Localization in Wireless Sensor Networks

by

Xue Zhang

A Dissertation Presented in Partial Fulfillment
of the Requirements for the Degree
Doctor of Philosophy

Approved March 2016 by the
Graduate Supervisory Committee:

Cihan Tepedelenlioğlu, Co-Chair
Andreas Spanias, Co-Chair
Konstantinos Tsakalis
Visar Berisha

ARIZONA STATE UNIVERSITY

May 2016

ABSTRACT

In many applications, measured sensor data is meaningful only when the location of sensors is accurately known. Therefore, the localization accuracy is crucial. In this dissertation, both location estimation and location detection problems are considered.

In location estimation problems, sensor nodes at known locations, called anchors, transmit signals to sensor nodes at unknown locations, called nodes, and use these transmissions to estimate the location of the nodes. Specifically, the location estimation in the presence of fading channels using time of arrival (TOA) measurements with narrowband communication signals is considered. Meanwhile, the Cramer-Rao lower bound (CRLB) for localization error under different assumptions is derived. Also, maximum likelihood estimators (MLEs) under these assumptions are derived.

In large WSNs, distributed location estimation algorithms are more efficient than centralized algorithms. A sequential localization scheme, which is one of distributed location estimation algorithms, is considered. Also, different localization methods, such as TOA, received signal strength (RSS), time difference of arrival (TDOA), direction of arrival (DOA), and large aperture array (LAA) are compared under different signal-to-noise ratio (SNR) conditions. Simulation results show that DOA is the preferred scheme at the low SNR regime and the LAA localization algorithm provides better performance for network discovery at high SNRs. Meanwhile, the CRLB for the localization error using the TOA method is also derived.

A distributed location detection scheme, which allows each anchor to make a decision as to whether a node is active or not is proposed. Once an anchor makes a decision, a bit is transmitted to a fusion center (FC). The fusion center combines all the decisions and uses a design parameter $K$ to make the final decision. Three scenarios are considered in this dissertation. Firstly, location detection at a known location is considered. Secondly, detecting a node in a known region is considered. Thirdly, location detection in the presence of fading is considered. The optimal thresholds are derived and the total probability of false alarm and detection under different scenarios are derived.

To my parents.

ACKNOWLEDGMENTS

I would like to express utmost gratitude to my advisors, Professor Cihan Tepedelenlioğlu and Professor Andreas Spanias, for their constant support and encouragement. Their sincere enthusiasm, strong dedication, and serious attitude towards research have motivated me to do my best. I am very fortunate to have them as my advisors.

I would like to express my sincere gratitude to Professor Konstantinos Tsakalis and Professor Visar Berisha for agreeing to serve on my dissertation committee. Their useful feedback and advice are very important to my research. I also want to thank Professor Tolga Duman, who asked many valuable questions on my research. I would like to thank Professor Mahesh Banavar for his insightful discussions. His willingness to share ideas, solve hard problems, and focus on details have taught me how to become a better researcher.

I would like to thank my friends Shuai Jiang and Jinjin Li for their side-by-side support through these difficult years. Many thanks to my current and former colleagues, Sai Zhang, Jongmin Lee, Huan Song, Jayaraman Jayaraman Thiagarajan, Karthikeyan Natesan Ramamurthy, Ahmed Ewaisha, Xiaofeng Li, Ruochen Zeng, Adithya Rajan and Sivaraman Dasarathan for their kindness, and support.

Most importantly, I would like to thank my parents for their unconditional love and support in all my pursuits, without whom I could have come this far.

TABLE OF CONTENTS

Page

LIST OF TABLES . . . viii

LIST OF FIGURES . . . ix

CHAPTER

1 INTRODUCTION . . . 1

1.1 Wireless Sensor Networks . . . 1

1.2 Applications of WSNs . . . 2

1.3 Localization in WSNs . . . 3

1.4 Classifications of Localization Algorithms . . . 6

1.5 Sequential Localization in WSNs . . . 11

1.6 Estimators for Localization . . . 12

1.7 Location Detection in WSNs . . . 12

1.7.1 Location Detection versus Location Estimation in WSNs . . . 13

1.8 Motivation of the Dissertation . . . 14

1.9 Contributions and Organization of the Dissertation . . . 15

2 LOCALIZATION IN WSNs . . . 17

2.1 Range-based Localization Algorithms . . . 17

2.2 Range-free Localization Algorithms . . . 22

2.3 Calculating the Coordinate of Node Locations . . . 24

2.4 Review of Some Existing Approaches . . . 27

2.4.1 Nonlinear Least Squares . . . 27

2.4.2 Linear Least Squares . . . 28

2.4.3 Projection onto Convex Sets . . . 29

2.4.4 Projection onto Rings . . . 31

2.5 Performance Analysis on Location Estimation and Detection . . . 31

2.6 Conclusions . . . 34

3 LOCATION ESTIMATION IN THE PRESENCE OF FADING . . . 35

3.1 System Model . . . 35

CHAPTER Page


3.2 Fading Coefficients Are Known at Each Anchor . . . . . 38

3.3 Effect of Unknown Fading Amplitude . . . . . 39

3.4 Unknown Fading Amplitude: Nakagami Fading . . . . . 39

3.5 No CSI Available at Anchors . . . . . 43

3.6 Extension to Cooperative Location Estimation in the Presence of Fading . . . . . 46

3.7 Simulation Results . . . . . 47

3.8 Conclusions . . . . . 49

4 SEQUENTIAL LOCATION ESTIMATION . . . . . 50

4.1 Performance Comparison of Localization Techniques for Sequential Location Estimation . . . . . 50

4.1.1 Simulation Results . . . . . 52

4.2 CRLB for Sequential Localization in the Absence of Fading . . . . . 55

4.3 CRLB for Sequential Localization in the Presence of Nakagami Fading . . . . . 60

4.3.1 Simulation Results . . . . . 61

4.4 Conclusions . . . . . 61

5 DISTRIBUTED LOCATION DETECTION . . . . . 63

5.1 Distributed Location Detection at A Point . . . . . 64

5.1.1 Simulation Results . . . . . 65

5.2 Distributed Location Detection in A Region . . . . . 66

5.2.1 Detecting A Node in A Region Using the TOA Method . . . . . 68

5.2.1.1 Simulation Results . . . . . 70

5.2.2 Detecting A Node in A Region Using the RSS Method . . . . . 70

5.2.2.1 Simulation Results . . . . . 74

5.3 Conclusions . . . . . 77

6 DISTRIBUTED LOCATION DETECTION IN THE PRESENCE OF FADING . . . . . 78

6.1 Fading Coefficients Known at Anchors . . . . . 79

6.2 Fading Coefficients with Known Phase but Unknown Amplitude . . . . . 82

CHAPTER Page

6.3 No CSI is Available at Any Anchor . . . . . 83

6.3.1 The Choice of the Design Parameter $K$ . . . . . 85

6.4 Simulation Results . . . . . 85

6.5 Conclusions . . . . . 87

7 CONCLUSIONS . . . . . 90

REFERENCES . . . . . 93

LIST OF TABLES

Table Page

2.1 The Sequential Localization Algorithms. . . . . 26

4.1 Linear Equations for Node Localization Using TOA, TDOA, RSS, DOA and LAA techniques in $\mathbb{R}^2$ Space. . . . . 53

LIST OF FIGURES


Figure Page

1.1 An Example of Sensor Nodes. . . . . 2

1.2 Some Applications of WSNs. . . . . 3

1.3 Mobile WSNs Apply in Localization. . . . . 4

1.4 An Example of Cooperative WSNs. . . . . 5

1.5 An Example of non-Cooperative WSNs. . . . . 6

1.6 Classifications of Localization Algorithms. . . . . 7

1.7 Flow Chart for Centralized Algorithms. . . . . 8

1.8 Flow Chart for Distributed Algorithms. . . . . 8

1.9 Flow Chart of Range-based Localization. . . . . 9

1.10 An Example of Locating Nodes Using the Sequential Algorithm. . . . . 11

2.1 Two-step Localization Method. . . . . 17

2.2 The TOA Measurement. . . . . 19

2.3 The Node is Located on the Hyperbola. . . . . 20

2.4 The TDOA Measurements. . . . . 21

2.5 The DOA Measurement. . . . . 22

2.6 The LAA Measurement. . . . . 23

2.7 The Flowchart of DV-hop Algorithm. . . . . 24

2.8 Projection onto Convex Sets . . . . . 29

2.9 Projection onto Rings . . . . . 31

2.10 The CRLB on the TOA Measurement When the Node is Locating Inside A 1m by 1m Square. . . . . 33

2.11 The CRLB on the RSS Measurement When the Node is Locating Inside A 1m by 1m Square. . . . . 33

3.1 The System Model of Location Estimation in WSNs. . . . . 36

3.2 Coherent TOA Estimation Scheme. . . . . 36

3.3 non-Coherent TOA Estimation Scheme. . . . . 37

3.4 Alternate non-Coherent TOA Estimation Scheme. . . . . 37

Figure Page


3.5 CRLBs Comparison Between the non-Fading and the Rayleigh Fading Case. . . . . 47

3.6 The Ratio $k$ in (3.23) versus the Nakagami $m$ Parameter. . . . . 48

3.7 ML Estimators Comparison. . . . . 48

3.8 CRLB Comparison When SNR is Large. . . . . 49

4.1 TOA/TDOA Based Localization of A Node Located at $\mathbf{z}$ Using $M$ Anchors at Locations $\mathbf{p}_1, \mathbf{p}_2, \ldots, \mathbf{p}_M$. . . . . 54

4.2 RSS Based Localization of A Node Located at $\mathbf{z}$ Using $M$ Anchors at Locations $\mathbf{p}_1, \mathbf{p}_2, \ldots, \mathbf{p}_M$. 55

4.3 DOA Based Localization of A Node Located at $\mathbf{z}$ Using $M$ Arrays with Local Geometries $\mathbf{p}_1, \mathbf{p}_2, \ldots, \mathbf{p}_M$ and DOAs $\theta_1, \theta_2, \ldots, \theta_M$. . . . . 56

4.4 LAA Based Localization of A Node Located at $\mathbf{z}$ Using $M$ Anchors at Known Locations $\mathbf{p}_1, \mathbf{p}_2, \ldots, \mathbf{p}_M$ and AOAs $\theta_1, \theta_2, \ldots, \theta_M$. . . . . 57

4.5 Sequential Discovery Using LAA Technique. . . . . 58

4.6 Performance Comparison of Different Localization Techniques for Network Discovery. 59

4.7 System Model of the 1-D Sequential Localization Scheme. . . . . 59

4.8 Comparisons Between the Sequential CRLB with the Non-sequential CRLB when $N =$ 10 Nodes Located Inside a $10 \times 10$ Square. . . . . 62

4.9 Comparisons Between the Sequential CRLB with the Sequential CRLB When $N = 10$ Nodes and $N = 100$ Nodes Located Inside a $10 \times 10$ Square. . . . . 62

5.1 The Complete ROC Curve. . . . . 66

5.2 ROC Curve When $\bar{P}_{FA}$ is Low. . . . . 67

5.3 System Model for Location Detection in A Circle. . . . . 67

5.4 ROC Curves at the $i^{th}$ Anchor Under Different Circle Radius. . . . . 71

5.5 ROC Curves at the $i^{th}$ Anchor Under Different $d_{\min}$. . . . . 71

5.6 ROC Curves Comparison Between the Gaussian Approximation and the Original Detector. . . . . 72

5.7 ROC Curves Under Different Choices of $K$ When Using (5.11). . . . . 72

5.8 ROC Curves Under Different Choices of $K$ When Using (5.17). . . . . 73

Figure Page

5.9 ROC Curves at the $i^{th}$ Anchor Under Different $d_{\min}$. . . . . 75

5.10 ROC Curves at the $i^{th}$ Anchor Under Different $r$. . . . . 75

5.11 ROC Curves at the $i^{th}$ Anchor Under Different SNR. . . . . 76

5.12 ROC Curves at the $i^{th}$ Anchor Under Different Choice of $K$ Using the RSS Method. . . 76

6.1 ROC Curves for Different Scenarios. . . . . 85

6.2 ROC Curves When the Fading Coefficients are Known to All Anchors When SNR = 15dB. . . . . 86

6.3 ROC Curves When the Amplitude of the Fading Coefficients are Unknown to the Anchors but with A Prior Distribution When SNR = 15dB. . . . . 87

6.4 ROC Curves When No CSI is Available at Any Anchor When SNR = 15dB. . . . . 88

6.5 $\bar{P}_{\mathrm{D}}^{\mathrm{T}}$ vs. SNR Under Different Fading Scenarios. . . . . 88

6.6 Comparisons Between the Threshold is A Function of Fading Coefficients and the Threshold is not A Function of Fading Coefficients When SNR = 15dB. . . . . 89

# Chapter 1

# INTRODUCTION

## 1.1 Wireless Sensor Networks

A sensor node is usually a low size, weight and power (SWAP) device with an antenna, a CPU, an expansion connector, a power switch, a radio, and is powered by battery. Figure 1.1 shows an example of a sensor node. A sensor network, which consists of multiple sensor nodes, is a group of specialized transducers with a communications infrastructure intended to monitor and record conditions at diverse locations. It can be used to monitor quantities such as location, temperature, humidity, pressure, among others [1–3], and can be either wired or wireless depending on the connection between sensor nodes. In a wired sensor network, two sensor nodes are connected through a wire. In a wireless sensor network (WSN), sensor nodes communicate with each other through agreed protocols. Therefore, comparing wired sensor networks with WSNs, wired sensor networks are more secure and faster than wireless sensor networks in data transfer speed [4]. However, they lack flexibility. Meanwhile, the implementation of a wired sensor network is more expensive than a WSN due to the cost of wires, connectors and labor. Also, a large wired sensor network is more difficult to manage than a WSN. On the other hand, WSNs are more flexible and power efficient than wired sensor networks [2].

A WSN can be either fully connected, in which case all sensor nodes communicate with each other, or partly connected, in which case one sensor node only communicates with its neighbors. In a fully connected WSN, sensor nodes exchange information by transmitting and receiving signals from all other nodes. On the other hand, in a partly connected WSN, each sensor node collects limited information. Therefore, a fully connected WSN benefits from a global network knowledge and provides more accurate results than a partly connected WSN, but costs more in terms of energy and bandwidth. A WSN can be either homogeneous or heterogeneous [5]. In a homogeneous network, all sensor nodes are identical in terms of battery life, communication range, and hardware complexity. On the other hand, in heterogeneous networks, sensor nodes have different communication ranges and functions. Generally speaking, the algorithms which are designed for homogeneous networks are not suitable for heterogeneous networks.

Figure 1.1: An Example of Sensor Nodes.

The sensor node is developed by Genetlab and has been used for intrusion detection in border and facility surveillance systems [6].

Comparing to traditional devices, the greatest advantages of WSNs are improved robustness and scalability [3]. In general, WSNs have energy advantage compared to other devices since sensors are small, have low power cost and detection advantage since a more dense sensor field improves the odds of detecting a signal source within the range. Although the main driving forces for WSNs are fault tolerance, energy gain and spatial capacity gain, WSNs have bandwidth limits [10]. Meanwhile, due to mobile applications, one of the most important constraints on sensor nodes is the low power consumption requirements [2]. Therefore, sensor network protocols must focus primarily on power conservation. Also, to make sure the nodes work efficiently, these nodes must operate in high volumetric densities, have low production cost and be dispensable, be autonomous and operate unattended and be adaptive to the environment [2, 11, 12].

## 1.2 Applications of WSNs

WSNs are deployed in both civilian and military applications. Figure 1.2 shows some applications of WSNs, such as security surveillance [13], health and wellness [14], smart home [15], fire pro-

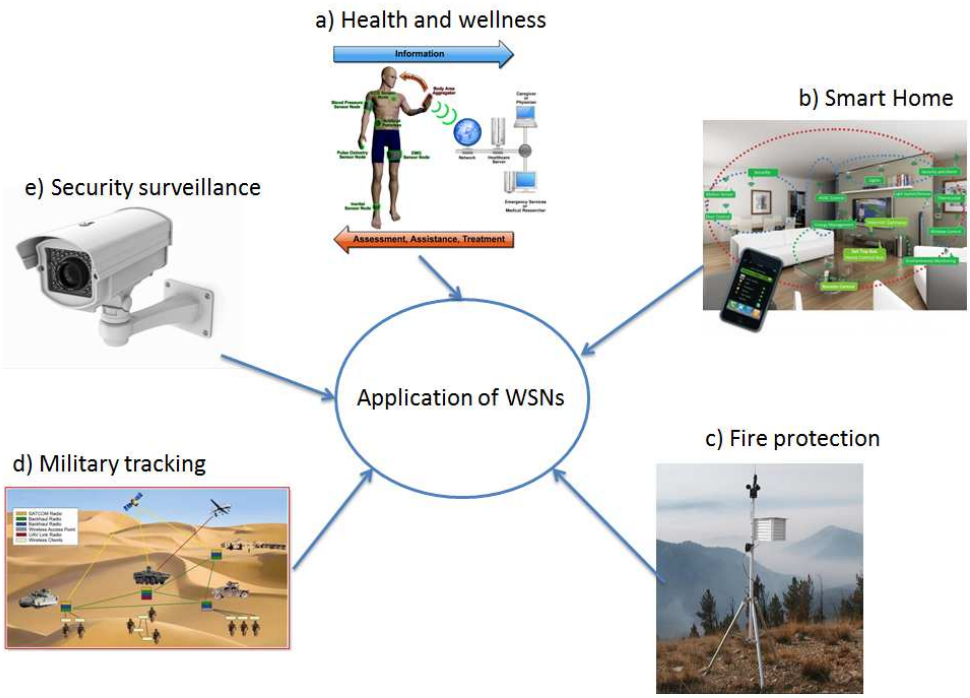


Figure 1.2: Some Applications of WSNs.

WSNs are deployed in a) health and wellness [7], b) smart home [8], c) fire protection, d) military tracking [9], and e) security surveillance applications.

tection in forest [16], and tracking [17]. Reference [18] gives a general literature review on the applications of WSNs, which includes military applications, indoor monitoring, outdoor monitoring and robotics. Meanwhile, reference [19] discusses the applications in automobiles. Applications in the area of human health, medical care, and emergency rescue are found in reference [20]. In [21], the authors discuss WSNs applications in weather and disaster alarm systems. In [22], WSNs are applied in air pollution monitoring systems. Mobile wireless sensor networks (MWSNs) has raised attention in recent years. For example, in [23], cell phones are used for mobile localization as shown in Figure 1.3.

## 1.3 Localization in WSNs

In many applications, measured sensor data are meaningful only when the location of sensors is accurately known. Nowadays, the most widely used technique for localization purpose is the Global Positioning System (GPS), which was developed in 1973 to overcome the limitations of previous


Figure 1.3: Mobile WSNs Apply in Localization.

By sending acoustic signals among anchors and the device at unknown location, the location can be estimated.

navigation systems [24, 25] and it has been used for both military and industry purposes. GPS offers 3D localization based on direct line-of-sight(LOS) with at least four satellites, providing an accuracy up to three meters. However, GPS has some limitations [26–28]. First of all, GPS cannot be implemented under harsh environments. For example, in the presence of dense forests, mountains or other obstacles that block the LOS from GPS satellite, GPS cannot work. Second, GPS cannot be implemented under the indoor environment. Third, while the cost for GPS equipment has been dropping over the years, it is still not suited for mass-produced cheap sensor boards, phones and even PDAs. On the other hand,the Federal Communications Commission (FCC) in the US has required wireless providers to locate mobile users within 10 meters for 911 calls [29]. There-

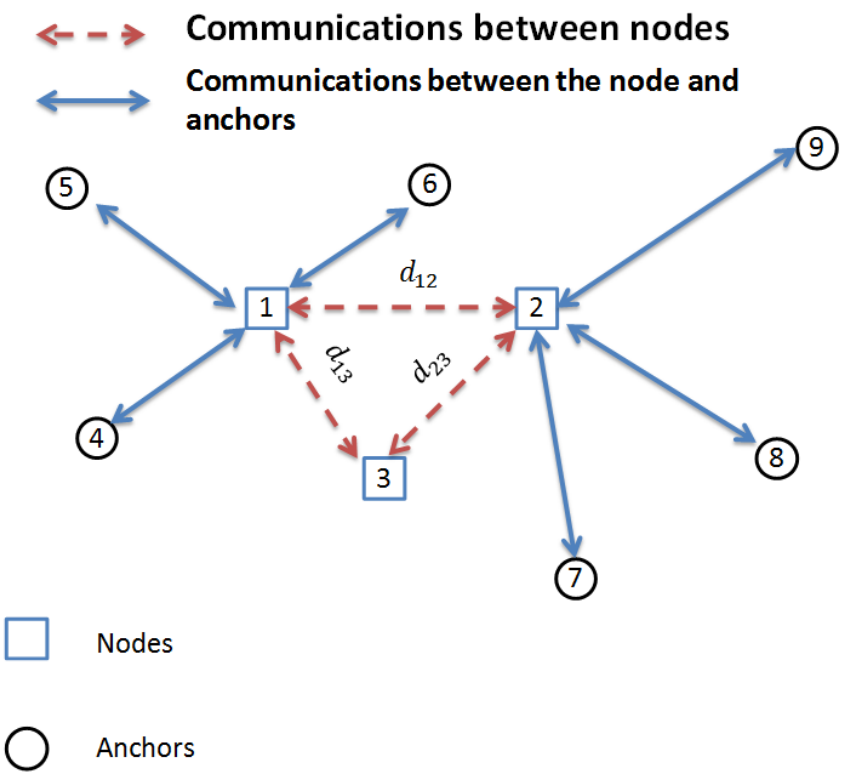


Figure 1.4: An Example of Cooperative WSNs.

Here $d_{12}$ $d_{13}$ and $d_{23}$ are the distances between nodes.

fore, the accurate estimation of position should be performed even in challenging environments. To overcome GPS limitations, researchers have developed fully GPS-free techniques for locating nodes as well as techniques where few nodes, commonly called anchors, use GPS to determine their location and, by broadcasting it, help other nodes in calculating their own position without using GPS. Therefore, the problem of location estimation using WSNs is formulated. To localize a node, several reference nodes, termed anchors with known locations are used to localize nodes with unknown locations. Localization in WSNs has been used in many applications, such as inventory tracking, forest fire tracking, home automation and patient monitoring [30]. When both anchors and other nodes communicate with the node that needs to be localized, a sensor network is called a cooperative WSN. In general, WSNs can be classified as cooperative and non-cooperative WSNs. The concept of cooperative WSNs relies on direct communication between nodes, which means nodes can communicate with each other and in localization problems, a node can estimate its loca-

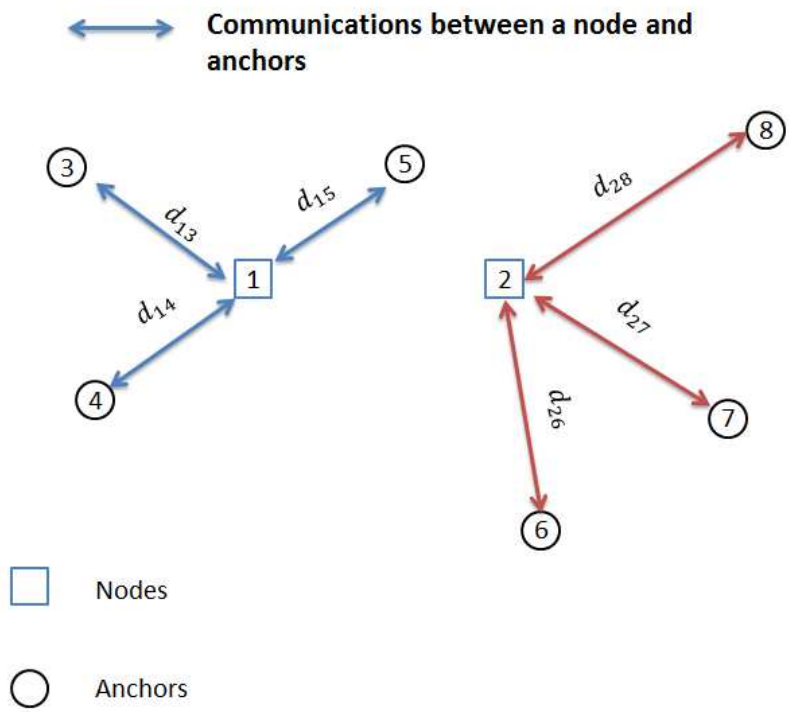


Figure 1.5: An Example of non-Cooperative WSNs.

Here node 1 communicates with anchor 3, 4 and 5. Node 2 communicates with anchor 6, 7, and 8. Nodes do not communicate with each other.

tion by sending or receiving signals from other nodes [31]. On the other hand, in non-cooperative WSNs, no communications take place between nodes. Nodes can only communicate with anchors and estimate their locations through anchors. Figure 1.4 shows an example of cooperative WSNs. In the figure, node 1, 2 and 3 communicate with each other, which indicates that distance measurements $d_{12}$, $d_{13}$, and $d_{23}$ are available, and the network is a cooperative WSN because nodes communicates with each other. Figure 1.5 shows an example of non-cooperative WSNs. In the figure, the link between node 1 and node 2 is not present. Therefore, the network is a non-cooperative WSN.

## 1.4 Classifications of Localization Algorithms

Localization algorithms can be classified in three categories. Figure 1.6 shows the classifications of localization algorithms. According to the computational capability at each anchor, localization

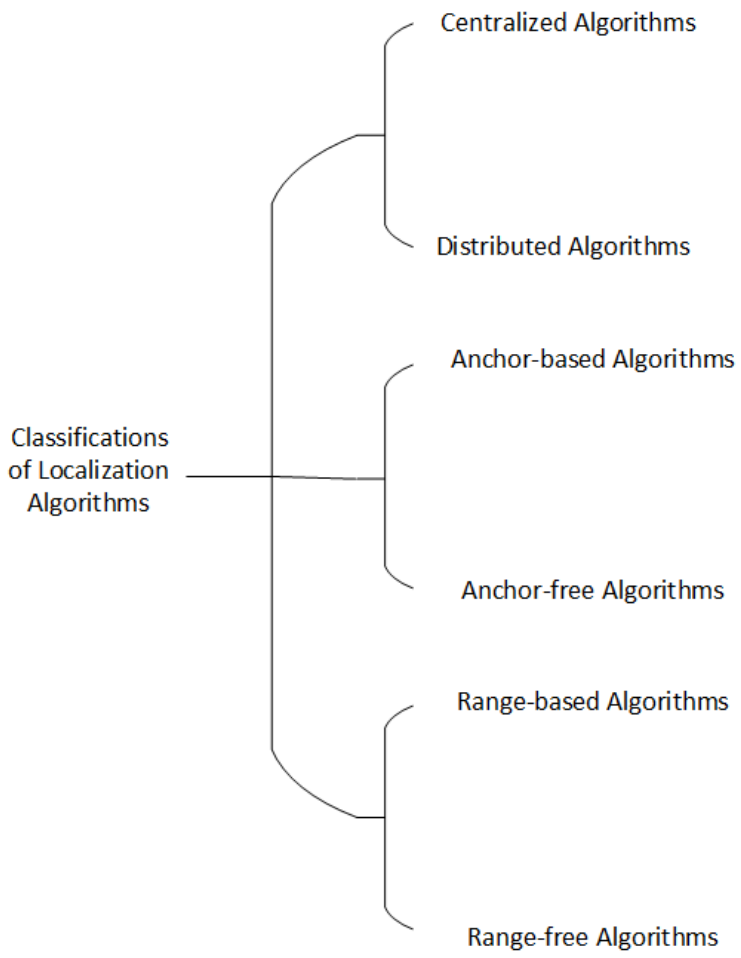


Figure 1.6: Classifications of Localization Algorithms.

algorithms can be classified as centralized and distributed algorithms. For centralized algorithms, as shown in Figure 1.7, a fusion center (FC) is used to collect all information from sensor nodes and is responsible for a majority of the computations. For distributed algorithms, as shown in Figure 1.8, each sensor node exchanges information with its neighbor or a group of sensor nodes, and computes or estimates parameters locally. A FC is optional, and if it exists, is used to collect computed or estimated parameters from each sensor node. Centralized algorithms require more energy than distributed algorithms due to transmissions between sensor nodes and a FC. On the other hand, centralized algorithms provide more accurate results compared to distributed algorithms. However, in large WSNs, efficient utilization of energy is crucial for large area and long distance communications. In order to implement centralized algorithms more efficiently in large WSNs,

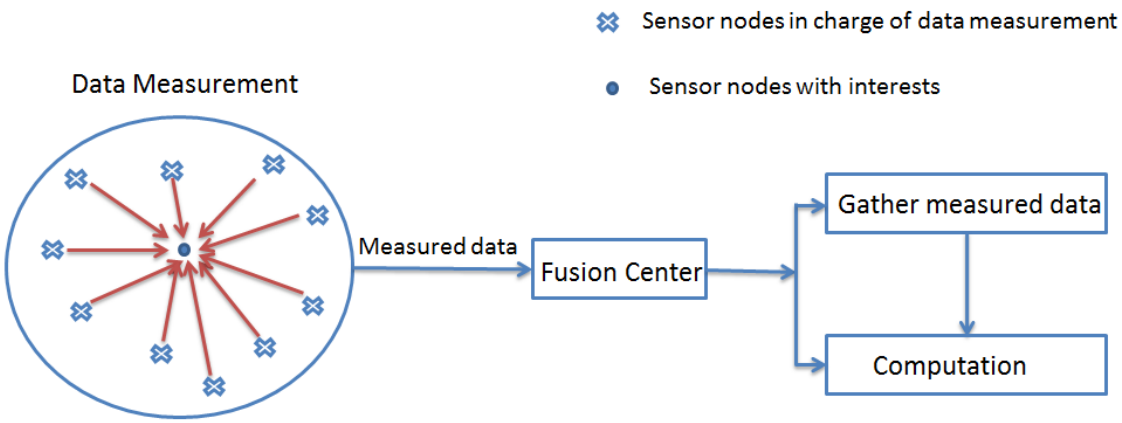


Figure 1.7: Flow Chart for Centralized Algorithms.

Sensor nodes collect measurements, then the measured data are passed to a FC. The fusicon center is in charge of computing parameters of interest.

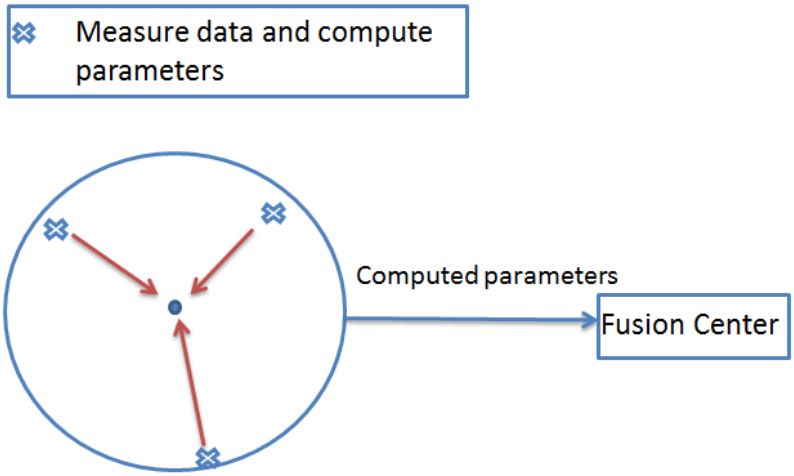


Figure 1.8: Flow Chart for Distributed Algorithms.

The measured data are used for computation at each sensor node. A FC is optional.

many researchers focus on developing energy efficient protocol for WSNs [32, 33]. Comparing a distributed system with a centralized system, a distributed system is inherently more robust than a centralized system, such as less possible of link failures. Distributed algorithms are also far more scalable in practical deployment and may be the only way to achieve the large scales needed for some applications.

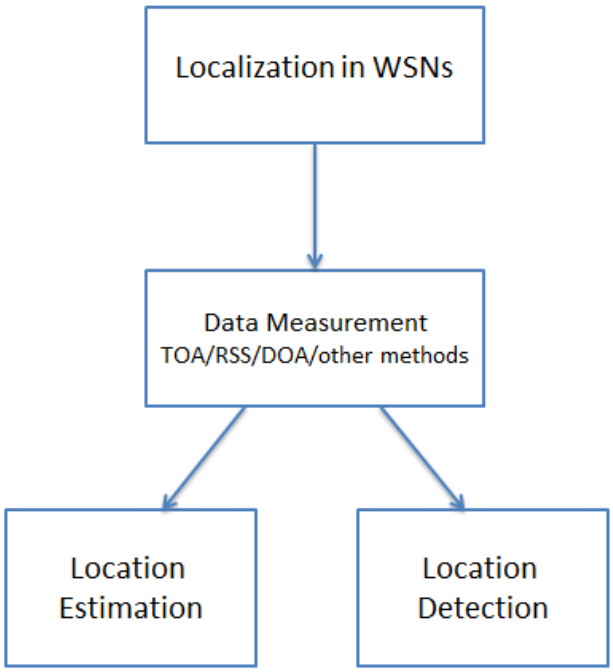


Figure 1.9: Flow Chart of Range-based Localization.

According to the dependency of range measurements, the localization schemes can be classified as range-based approaches and range-free approaches. In range-based localization scheme, location related parameters are firstly measured. Figure 1.9 shows the flow chart of the range-based localization approach. Commonly used range-based techniques include time of arrival (TOA) [34], received signal strength (RSS) [35], time difference of arrival (TDOA) [36], direction of arrival (DOA) [37], large aperture array (LAA) [38] or other hybrid techniques [39]. The TOA technique is one of the most popular techniques used for localization. Here, the time delay from the transmitting node to the receiving node is measured, which can be either one-way transmission or two-way transmission. For the one-way transmission, the time synchronization between the transmitter and the receiver is required [31, 36]. For the two-way transmission, there is no need for time synchronization between the transmitter and the receiver, and the actual transmitting time is half of the measured time. However, the two-way transmission scheme requires more energy and bandwidth compares to the one-way transmission, and has limitations in large WSNs. In contrast to TOA,

TDOA measures the difference between arrival times at the receiving nodes which removes the need for synchronization between the transmitter and receiver [40, 41]. However, this technique is known to suffer if there is insufficient bandwidth. In RSS, a path loss model is used to estimate location on power loss measurements [42]. This is a simple and cheap technique to implement but suffers from problems in the presence of channel impairments such as multipath and frequency flat fading. The DOA approach employs small aperture arrays at each sensor node to estimate the direction of the transmitted source. This method uses spatial diversity more optimally to achieve a better localization performance and does not require nodes to be synchronized but has increased hardware and processing requirements. Finally, in the LAA approach, nodes used for localization are aggregated to form an array system [38]. This approach is robust to frequency flat fading and may be extended to overcome co-channel interference. On the other hand, range-free algorithms include neighborhood and hop counting techniques. The commonly used anchor-free localization algorithms includes DV-hop [43], in which each node counts the minimum hop number to the neighbors, and estimate the distance by multiplying the number of hops with the averaged distance between two hops. Range-based algorithms have higher accuracy compared to range-free, but require additional hardware.

According to the number of anchors that is used to localize a node, the localization algorithms can be classified as anchor-based algorithms and anchor-free algorithms. In anchor-based algorithms, several reference nodes, termed anchors with known locations are used to localize nodes with unknown locations. In this scheme, the accuracy of the estimation highly depends on the number of anchors and the performance is improved when more anchors are added to the network. In the anchor-free scheme, there is no anchor node with perfectly known location. Nodes communicates with each other to estimate relative locations instead of computing absolute locations [44]. Comparing the anchor-based scheme with the anchor-free scheme, the anchor-based scheme provides more accurate results than the anchor-free scheme. However, since GPS receivers are expensive, to obtain the accurate anchor locations, the hardware cost for the anchor-based scheme is much higher than the anchor-free scheme.

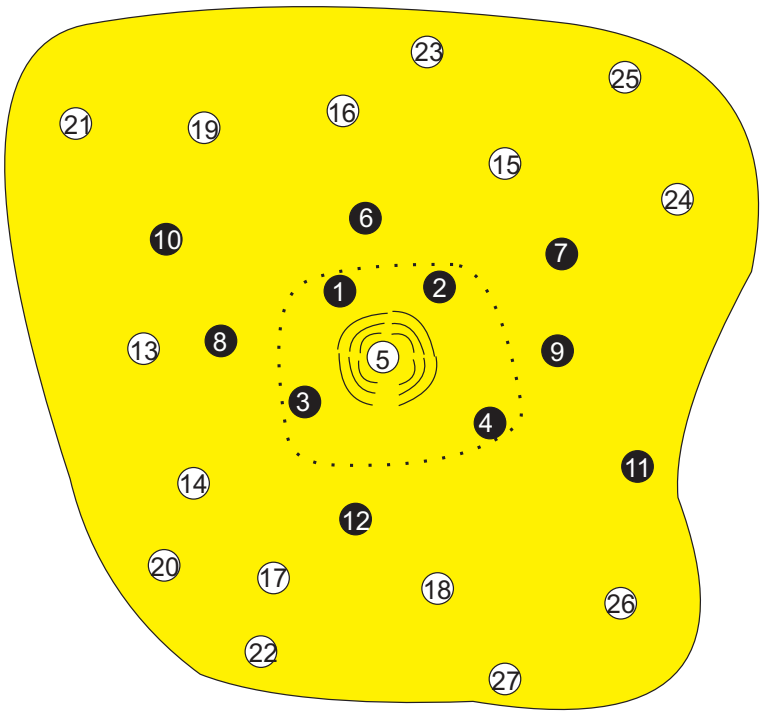


Figure 1.10: An Example of Locating Nodes Using the Sequential Algorithm.

Black nodes are at known or previously estimated locations. Transmitting node 5 is localizaed using nodes 1, 2, 3 and 4. Once a white node is localized, it becomes an anchor to localize other neighbour white nodes [38].

## 1.5 Sequential Localization in WSNs

WSN discovery may be performed in a centralized or distributed manner [34]. In the centralized approach, all the measurements are transmitted to a FC to estimate unknown locations. The main drawback of this approach is that anchors must be within the coverage area of all nodes which will lead to an undesirably large cost in power. On the other hand, distributed sensor networks allow nodes only communicates with small portion of neighbors. Therefore, distributed algorithms are more power efficient. One of the distributed localization algorithms, which is called sequential localization algorithm [38], attempts to overcome the limited power in WSNs by allowing nodes which have previously been localized to be used to localize other nodes [45]. Figure 1.10 shows an example of locating nodes using sequential algorithm. In the figure, black nodes are at known or previously estimated locations. The node 5 is localized using node 1, 2, 3 and 4 only. Once more nodes are localized, they become anchors to localize neighbor white nodes. The main drawback

of this approach is that localization errors will propagate through the network during the iterative localization process. This is because it is assumed that the estimated locations of the nodes are the actual locations. However, due to the errors associated in localizing the nodes, this may not be the case. This makes the order in which nodes are localized markedly important as well as the localization algorithm used. In [45], the performance of TOA, TDOA, RSS, DOA and LAA localization algorithms using the sequential localization approach are compared.

## 1.6 Estimators for Localization

After location related parameters are estimated, the location can be computed using the measured parameters. To compute the node location, many algorithms have been proposed in the literature. If the data is known to be described well by a particular statistical model, then the maximum likelihood estimator (MLE) can be derived and implemented [34]. Since MLE can asymptotically achieve the Cramer-Rao lower bound (CRLB), it is the optimal estimator. However, there are some difficulties with this approach. Firstly, it is possible that the maximization search may find a local maxima not a global maxima. Secondly, if the measurements are obtained from the assumed model, the results are no longer guaranteed to be optimal. Thirdly, in a large WSN, finding a global maxima is computationally intense, which makes the computation much slower than other approaches. Therefore, to overcome the difficulties, other approaches have been applied. One way to prevent local maxima is to formulate the location estimation as a convex optimization problem [46]. Convex constraints are presented that can be used to require a sensor's location estimate to be within a radius $r$ from a second sensor. In [47], the linear programming using a "taxi metric" is suggested to provide a quick means to obtain rough localization estimates. More general constrains can be considered if semidefinite programming (SDP) techniques are used [48]. In [49] a distributed SDP-based localization algorithm was presented to simplify the complexity of computation.

## 1.7 Location Detection in WSNs

In some applications, such as in a surveillance network, the accuracy of the nodes's reading is crucial. Once any node behaves abnormal, the location of the node with abnormal activity needs to be localized. To detect the malicious node, many researchers work on designing algorithms and

protocols. In the literature, researches have been working on designing algorithms and protocols to detect abnormal nodes. Reference [50] proposed detecting malicious nodes through detection of malicious message transmission in a network. In [51] studies a distributed node detection protocol. In other applications, the node location is known to all anchors, but whether the node is active or not is unknown. In many applications such as detecting fire in buildings, each node is placed inside a room, and the location is known to all anchors. Anchors detect an event based on whether the node is transmitting. In the absence of transmission, each anchor receives only noise. In the presence of the node, each anchor receives signal with noise. Therefore, location detection in WSNs is formulated as a binary hypothesis testing problem, and Neyman-Pearson lemma [52] is applied to solve the problem.

### 1.7.1 Location Detection versus Location Estimation in WSNs

Comparing with the estimation formulation, the detection formulation is different from the estimation formulation in the following aspects. First of all, in detection problems, the goal is to detect the activity or silence of a node or multiple nodes at known locations; however, in estimation problems, the goal is to estimate the location of a node or multiple nodes, which are at unknown locations. Secondly, to estimate the location of a node, multiple anchors are needed in order to avoid ambiguity. For example, when using range-based methods, a minimum of two anchors are needed for one dimension (1-D), and three anchors are needed for two dimensions (2-D). On the other hand, to detect a node, each anchor can make a local decision on whether the node is active or not by correlating the received signal with the transmitted signal and then comparing with a threshold. The final decision can be made by exchanging this data with other anchors and a FC. Therefore, the detection problem can be solved by using a distributed implementation based on exchange of bits between anchors and a FC. Thirdly, the performance analysis is different. In the estimation formulation, the variance of the location estimation error is used as a performance metric, whereas for detection, metrics such as the probability of false alarm and the probability of detection are used [52] [53].

## 1.8 Motivation of the Dissertation

Both location estimation and detection problems have been studied in the literature. Many researchers have discussed the method of location estimation using WSNs [31, 34, 40], and different performance analysis bounds have been proposed, for example, reference [31] derived the CRLB on the estimation error by using TOA and RSS measurements, and reference [54] studied the position error bound in which the nuisance parameters were considered. However, none of the existing work considered fading scenario. Although some work has considered fading environments for TOA measurements [55, 56], the CRLB of location estimation by considering fading coefficients as random unknown parameters has not been derived. The accuracy of measurements is highly affected by the bandwidth, therefore, wide band or ultra wide band (UWB) signals are often used for localization [27]. However, in some applications, localization needs to be done with the narrowband signals that are also used for communications. When the bandwidth of the transmitted signal is limited, the performance is affected by multipath fading and noise. Therefore, localization in the presence of fading needs to be studied.

In other applications, such as fire protection in a building, one node is placed inside each room, whose location is known to all anchors. If a fire actives a node in any room, the active node at this known location needs to be detected. In the absence of transmission from a node, each anchor only receives noise, and in the presence of transmission from a node, each anchor receives signal plus noise. Therefore, location detection is needed to decide whether a node is active or not. In this case, the problem of location detection using WSNs is formulated. In the literature, location detection in WSNs has been studied in [57], which discretizes the problem to obtain an $N$-ary hypothesis testing problem. However, the performance depends on the grid size. In [58], a centralized sensor network with unknown fading coefficients has been studied. Although centralized methods may give a better performance, it is costly in large WSNs. None of these works have studied location detection using distributed methods, also none of these works consider fading environments with explicit incorporation of the fading distribution in deriving the threshold for location detection. Therefore, distributed location detection problems in the absence of fading

and in the presence of fading need to be studied.

## 1.9 Contributions and Organization of the Dissertation

In this section, contributions and organization of the dissertation are provided.

In Chapter 2, localization methods and algorithms are revisited, and performance analysis metrics for both location estimation and detection are discussed.

In Chapter 3 and Chapter 4, location estimation is studied. Specifically, in Chapter 3, the problem of location estimation in the presence of fading is proposed. The followings are the main contributions in this chapter.

- In the location estimation problem, we assume narrow band communication signals are transmitted between a node and anchors, and we derive the CRLBs in the presence of fading scenarios for both 1-D and 2-D with TOA measurements. Specifically, the Nakagami fading with different knowledge at each anchor is considered.
  - Firstly, the fading coefficients are assumed to be known at each anchor. In this case, the CRLB depends on the fading coefficients.
  - Secondly, the phase of the fading coefficients are assumed to be known but unknown amplitude. Specifically, we assume the amplitude of the fading coefficients are Nakagami distributed. In this case, the CRLB can be derived by integrating the fading effect.
  - Thirdly, no CSI is available at any anchor. In this case, a non-coherent detector is applied to extract both in-phase and channel components. The CRLB depends on both the phase and the amplitude of the fading coefficients.
- Finally, the MLEs under difference fading scenarios are derived and compared with the MLE in the absence of fading.

In Chapter 4, a sequential localization algorithm is applied and different localization methods are compared under different SNR conditions. Also, to characteristic the error propagation in

the sequential localization algorithm, CRLBs for the TOA measurement in the absence and in the presence of fading are derived.

In Chapter 5 and Chapter 6, a distributed location detection scheme is proposed. In Chapter 5, detecting a node at a point and in a region are studied. The followings are the main contributions in Chapter 6.

- The location detection in the presence of fading is considered. Specifically, The Rayleigh fading with different knowledge at each anchor is considered.
- Firstly, The fading coefficients are assumed to be known at each anchor. Secondly, the phase of the fading coefficients are assumed to be unknown but known amplitude. Thirdly, no CSI is available at any anchor. The knowledge of the fading coefficients affects finding the optimal threshold.

Chapter 7 summarizes the dissertation and conclusions are made.

Chapter 2

# LOCALIZATION IN WSNs

Localization in WSNs is needed in both civilization and military. To localize a node, several reference nodes, termed anchors with known locations are used to localize nodes with unknown locations. In this chapter, existing localization algorithms are revisited. Following that, the Fisher information and the CRLB, which provide a benchmark on the performance of location estimation are reviewed. For location detection, the Neyman-Pearson detector is applied to find the threshold and the corresponding detection probability and false alarm probability.

## 2.1 Range-based Localization Algorithms

According to the dependency of range measurements, the localization schemes can be classified as range-based approaches and range-free approaches. In this section, some classical range-based localization algorithms are revisited. To determine the node location, two different location estimation schemes can be performed, which are direct positioning determination method [59], in which case the location estimation is performed directly from the transmitted signals, and the two-step localization scheme [30] as shown in Figure 2.1, in which case the location related parameters that are firstly extracted and the location estimation is performed based on the extracted parameters. Although the two-step localization scheme is suboptimal, it can significant lower complexity than the direct approach. Therefore, the two-step localization method is the common technique in most localization systems.

In the two-step localization system, location related parameters need to be measured. In

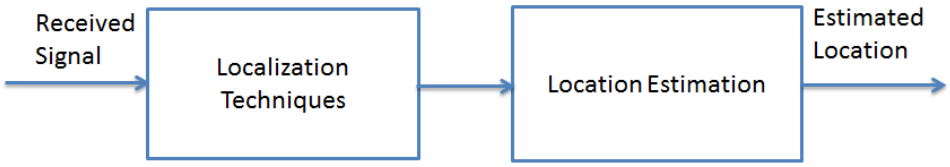


Figure 2.1: Two-step Localization Method.

range-based approaches, distant related measurements, such as TOA, RSS and TDOA, and angle related measurements, such as DOA are collected. Also, some hybrid measurements, such as LAA, which measures distance and angle simultaneously are investigated [34, 35, 60–62].

TOA measures the transmitting time between a node and an anchor. The measurement can be either one way or two way mode [63]. In the one way transmission scheme, a signal is transmitted from an anchor to a node, and the node estimates its location based on the transmission time. It is more efficient than two way transmission in large WSNs, but the synchronization between anchors and nodes is crucial. In the two way transmission scheme, a signal is transmitted from an anchor to a node, and the node transmits the signal back immediately after it receives the signal. The one way transmission time is half of the measured time. The two way transmission scheme consumes more time and energy but does not need the time synchronization. In Figure 2.2, the node location is estimated using the TOA measurement. In the absence of noise, the node is located in the intersection of three circles with radius $d_1$, $d_2$ and $d_3$ respectively. However, in the presence of noise, the estimation error occurs. For a given bandwidth and SNR, the time delay estimate can only achieve a certain accuracy. The CRLB provides a lower bound on the variance of the TOA estimate in a multipath free channel. Define $\hat{\tau}$ as the time delay estimate, $B$ is the signal bandwidth, and $f_0$ is the center frequency which is much higher than the bandwidth $B$, and $T_s$ is the signal duration in seconds, the CRLB is given as

$$\mathrm{var}(\hat{\tau}) \geq \frac{1}{8\pi^2 B T_s f_0^2 \mathrm{SNR}}. \tag{2.1}$$

From (2.1) one can see that in the absence of multiple signals, the accuracy of the arrival time is limited by additive noise [34]. But in multipath channels, TOA based range errors can be much greater than those caused by additive noise alone. Therefore, TOA measurements suffer from two problems, early arriving multipath and attenuated LOS.

To overcome the time synchronization error in the TOA measurement, the TDOA based localization techniques can be applied. The key concept of the TDOA measurement is to determine the location of the source by evaluating the difference in arrival time of the signal at spatially separated sensor nodes. For each pair of anchors, as shown in Figure (2.3), the node is located in the hyperbola of anchor 1 and anchor 2. The hyperbola is the set of points at a constant distance

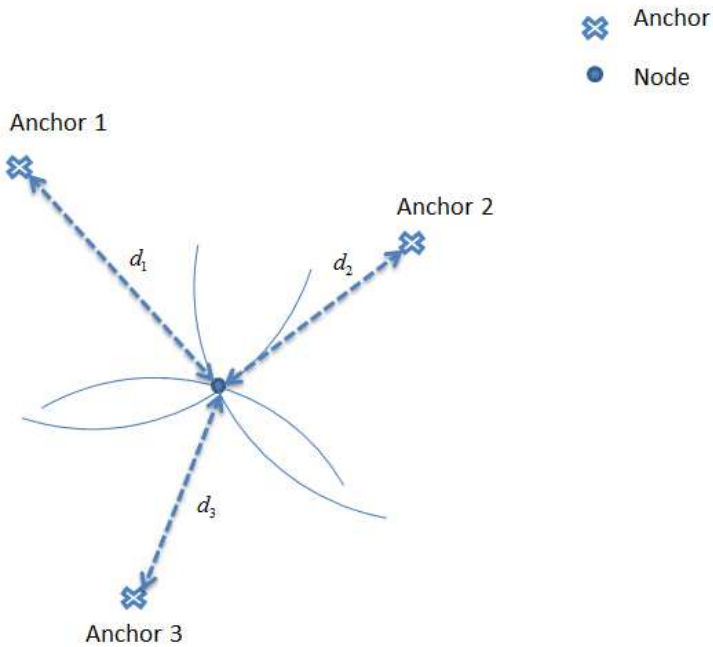


Figure 2.2: The TOA Measurement.

In the absence of the noise, the estimate of the node location is at the intersection point of three circles which have the radius $d_1$, $d_2$ and $d_3$ respectively.

difference from two foci. Here the distance difference is defined as $c\Delta t$, where $c$ is the speed of propagation, and $\Delta t = |d_1 - d_2|$. The intersection point of multiple hyperbola is the estimated location of the node as shown in Figure 2.4. Since TDOA is taking the time difference between arriving signals, it does not depend on the clock bias. Therefore, the synchronization between nodes and anchors is not needed. However, same as the TOA measurement, TDOA also suffers from multipath and noise, especially in the low SNR regime.

Another commonly used localization measurement is called received signal strength. In RSS, the measured received power at the node transmitted by an anchor, which is defined as $P$ is used to estimate the distance $d$. The path loss formula is given as [34]

$$P(dBm) = P_0(dBm) - 10\alpha \log 10\,(d/d_0)\,, \tag{2.2}$$

here $P_0$ is the reference power at reference distance $d_0$, $\alpha$ is the pathloss component. RSS can be measured using simple circuits, but has limited accuracy due to the difficulty measuring the

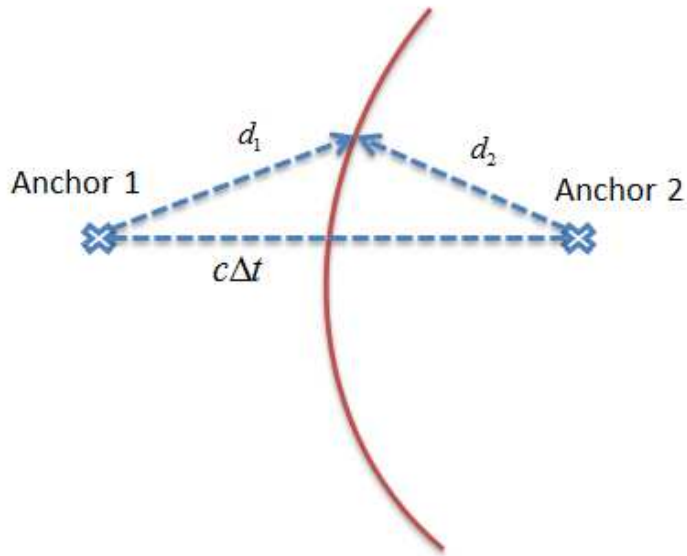


Figure 2.3: The Node is Located on the Hyperbola.

appropriate path loss model. Multipath signals and shadowing are two major sources of environment dependence in the measured RSS [34]. Multiple signals with different amplitudes and phases arrive at the receiver, and these signals add constructively or destructively as a function of the frequency, causing frequency-selective fading. To deal with the frequency-selective fading, one can use a spread-spectrum method that average the received power over a wide range of frequencies. In the absence of fading, shadowing becomes the major source of error, such as the attenuation of a signal due to obstructions that a signal must pass through or diffract around on the path between the transmitter and receiver.

Besides measure distance related parameters, nodes can also be localized using angle related measurements. The DOA measurement determines the direction of a node by measuring the propagation direction of the signal between a node and an anchor [64]. In Figure 2.5, $\theta_1$ is the angle between the node and anchor 1, and $\theta_2$ is the angle between the node and anchor 2. Also, the orientation, which is defined as a fixed direction against which AOAs are measured, is the North. Therefore, the DOA measurement corresponding to anchor 1 and the node restricts the location of

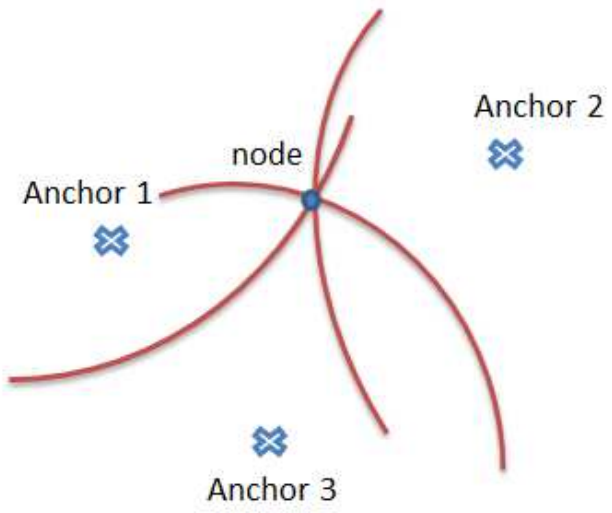


Figure 2.4: The TDOA Measurements.

In the absence of noise, the node is located at the intersection of three hyperbolas.

the node along a ray starting at anchor 1. Similarly, the node is also located along the ray which starts at anchor 2. The estimate of the node location is at the joint point of two rays. In general, the node is located at the intersection of all rays when two or more non-collinear anchors are available. Since it is not likely that all anchors are placed with known orientation, when the orientation at any anchor is unknown, the problem is more complicated than the case when the orientation at all anchors is the same.

Since different localization techniques have different disadvantages, in order to overcome different downfalls, one common way is to mix different localization approaches simultaneously. Reference [62] studies a hybrid localization technique, which is called large aperture array. The LAA technique is an array processing technique that measures direction and distance related information. The measurements are jointly used to localize transmitting nodes by forming a large aperture array of nodes. Figure 2.6 shows an example of locating a node location using the LAA measurement. In this example, the location of the node is estimated by using 3 anchors as an array

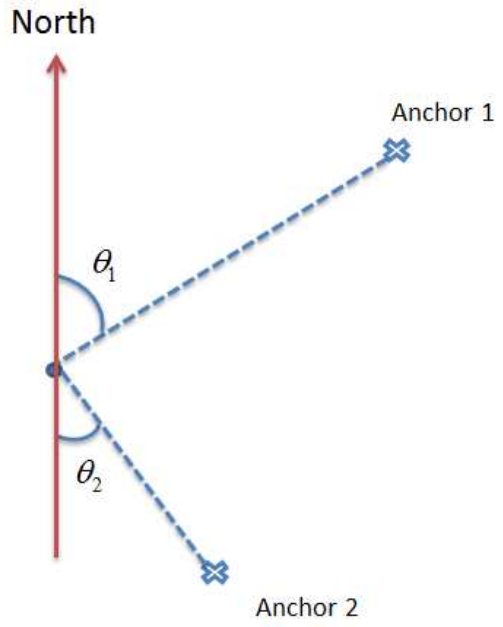


Figure 2.5: The DOA Measurement.
Here, the orientation is the North.

of large aperture of known geometry. The eigenvalue of the covariance matrix corresponding to a specified reference point is proportional to the distance between the node and that reference point. By repeatedly selecting reference point for the covariance matrix, the position of the node can be estimated as the intersection point of three circular loci. In [38], the LAA technique is proved that it leads to improve localization accuracy. In addition, in [45], the LAA technique is compared with conventional techniques using the sequential localization algorithm, and the simulation results show that the LAA technique outperforms all other conventional techniques in high SNR regimes.

## 2.2 Range-free Localization Algorithms

Although range-based localization algorithms provide high accuracy on location estimation, they are costly in terms of hardware. In order to overcome this issue, researchers have developed range-free methods. Comparing the range-based localization algorithms with the range-free localization algorithms, instead of measuring location related parameters, range-free methods counts the num-

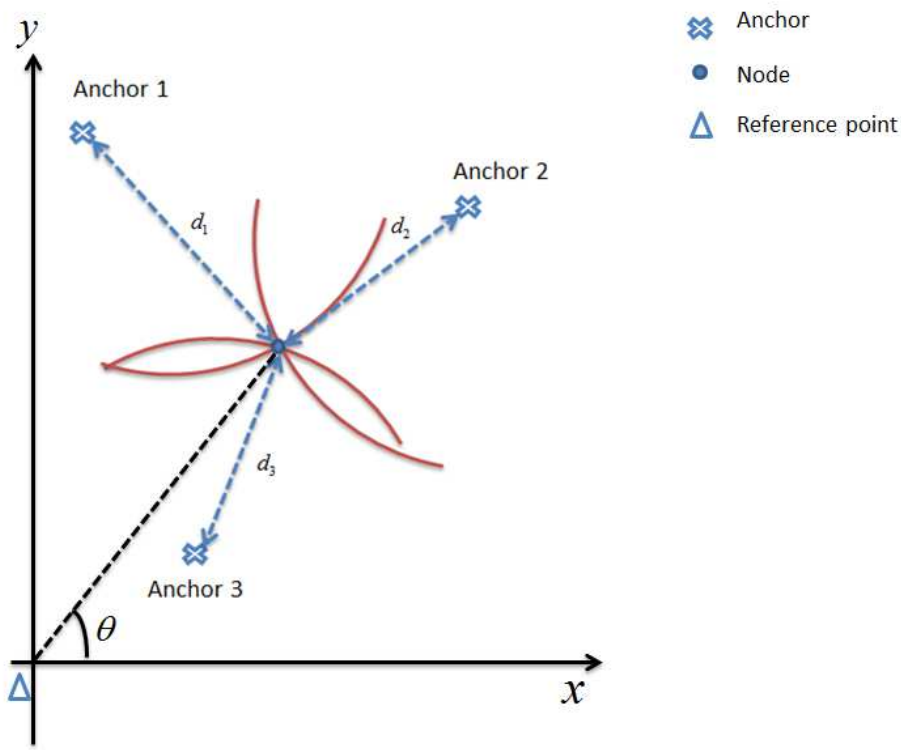


Figure 2.6: The LAA Measurement.

Each anchor measures both distance and angles between the node and the anchor.

ber of hops or using the area information to estimate distance to neighbors in order to estimate locations. One of the most commonly used anchor-free techniques, DV-hop, allows each node counts the minimum number of hops between itself and an anchor. The number of hops is multiplied by the averaged distance between two hops to estimate the distance. Figure 2.7 shows the flow chart of the DV-hop algorithm. Firstly, Each anchor broadcasts its location and the initial hop-count value initialized to one. Each node counts the number of hops from itself to an anchor, and only save the one with minimum number of hops to each anchor. Secondly, each anchor estimates an average size for one hop by exchanging information with another anchor, and broadcasts the average size to other nodes. Thirdly, the distance between the node an anchor can be estimated by multiplying the hop size with the minimum number of hops.

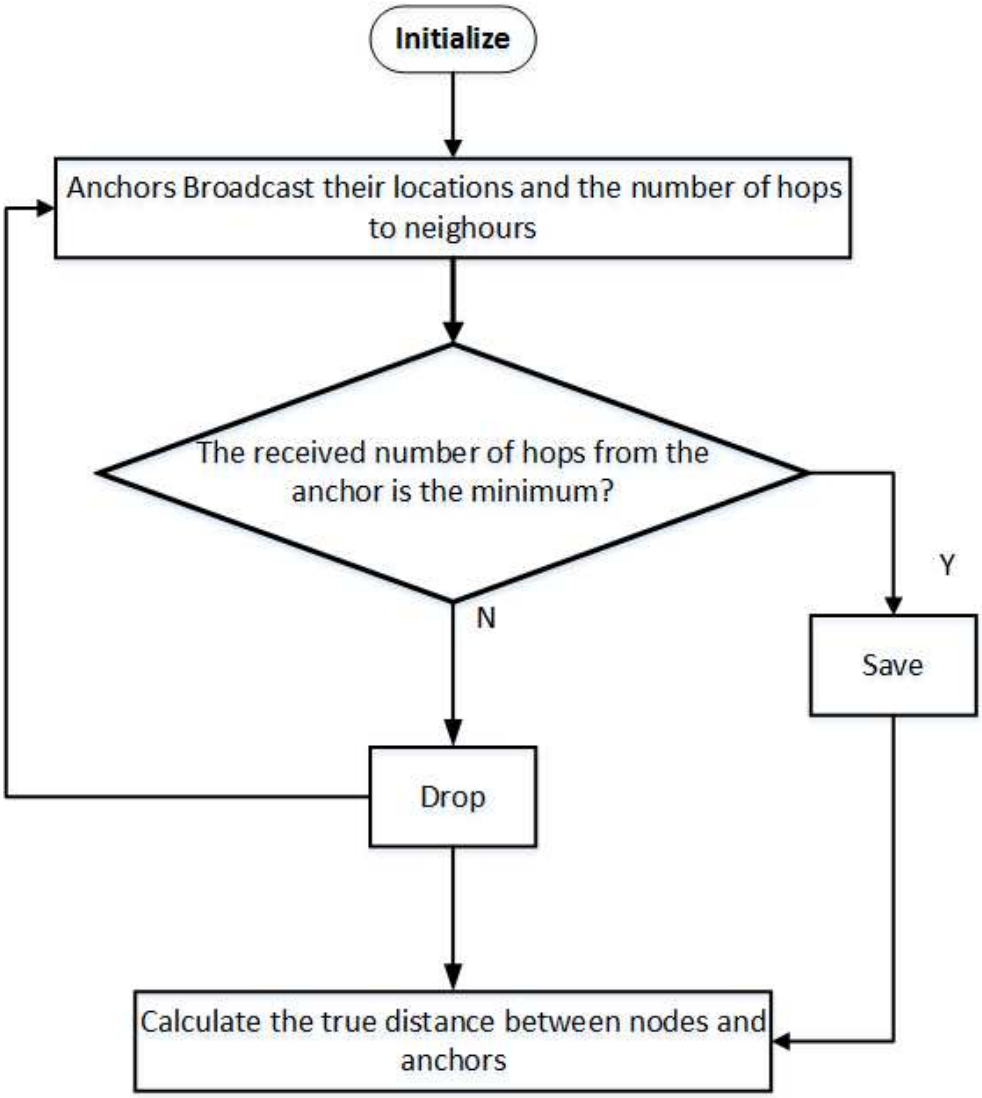


Figure 2.7: The Flowchart of DV-hop Algorithm.

## 2.3 Calculating the Coordinate of Node Locations

After distance or angle related measurements are collected at each anchor, unknown locations are estimated using either centralized or distributed algorithms. In a centralized algorithm, the collected measurements at each anchor are transmitted to a fusion center prior to calculate. On the other hand, in a distributed algorithm, each anchor estimate unknown locations and share the estimates with their neighbors. In general, centralized algorithms are more likely to provide more accurate location estimates than distributed algorithms. However, centralized algorithms suffer

from computing complexity and are not feasible to be implemented in large WSNs. In centralized algorithms, if the measured data is known to be described well by a particular statistical model, then the maximum likelihood estimator (MLE) can be derived and implemented [31] [65]. One reason that these estimators are used is that their variance asymptotically approaches the lower bound given by the CRLB. However, there are two difficulties with this approach. Firstly, MLE suffers from local maxima. It is possible that the maximization search may not find the global maxima unless the initialed value is close to the true location. Secondly, MLE depends on the actual model. If measurements deviate from the assumed model, the results are no longer guaranteed to be optimal. One way to prevent local maxima is to formulate the localization as a convex optimization problem [46–49].

There are two big motivations for developing distributed localization algorithms. First, for some applications, there is no FC (or none with enough computational power) is available to handle the calculations. Second, when a large network of sensors must forward all measurement data to a single central processor, there is a communication bottleneck and higher energy drain at and near the central processor. To overcome this issue, distributed localization algorithms, such as sequential localization scheme, can be applied. In the sequential estimation approach, only a small number of anchors is needed at the initial stage, and the anchors are used to localize nodes within a certain range. Once the nodes are localized, they become anchors and are used to localize other nodes. Therefore, the number of anchors increases after each node is localized. Table 2.1 gives the detail for the sequential algorithms. Since anchors only are used to localize nodes within its range, this approach is more power efficient comparing to centralized methods. However, the sequential location estimation has some drawbacks. Firstly, the localization errors will propagate through the network during the iterative localization process. This is because it is assumed that the estimated locations of the nodes are the actual locations. Secondly, the order in which nodes are localized is markedly important and affects the localization accuracy. Therefore, the estimates for the nodes that are localized later may not satisfy the error tolerance. Thirdly, since anchors only communicate with nodes within the range, it is possible that one node or multiple nodes is not localized within any of the anchor's range. In that case, the node will not be successfully localized.

| |
|---|
| **Initialization**<br>*Step 1*: Initially there are $M$ anchors and $N$ nodes.<br>Each anchor can communicate with a node within a range $D$.<br>*Step 2*: Set $k = 1$.<br>**Algorithm**<br>For the $i$th undiscovered node that transmits within<br>a coverage range $D$, repeat the following steps until<br>all the node locations have been estimated:<br>*Step 1*: Find the number of nodes at known or<br>estimated locations $M_{\text{set}}$ within the coverage range.<br>*Step 2*: **If** $M_{\text{set}} \geq M_{\min}$<br>**Then** Using TOA/RSS/TDOA/LAA to measure the data.<br>**Else** Move to Step 4.<br>*Step 3*: Estimate the location of the node<br>using localization algorithms.<br>*Step 4*: $M = M + 1$, $i = i + 1$, and $k = k + 1$.<br>**Refinement**<br>*Step 1*: For the $k$th localization iteration,<br>set $i = 1$ and<br>repeat the **Algorithm** using all localized node location estimates<br>from previous iterations until $k = K$. |

Table 2.1: The Sequential Localization Algorithms.

Here, $i$ is the node index, and $i = 1, 2, \ldots, N$; $k$ is the iteration index, and $k = 1, 2, \ldots, K$; $M_{\text{set}}$ is the number of anchors or previously localized nodes that is used to localize the $i^{th}$ node, and $M_{\min}$ is the minimum number of anchors that is required for each measurement to avoid ambiguity. For the TOA measurement, $M_{\min} = 3$, for the RSS, $M_{\min} = 3$, and for LAA, $M_{\min} = 2$.

Distributed algorithms for cooperative localization generally fall into one of the two categories. Firstly, network multilateration. In this case, each node estimates its multihop range to the nearest reference nodes. These ranges can be estimated via the shortest path between the sensor and anchors. Note that finding the shortest path is readily distributed across the network. When each sensor has multiple range estimates to known positions, its coordinates are calculated locally via multilateration [66]. Secondly, successive refinement. In this case, the algorithms try to find the optimum of a global cost function, e.g., least squares (LS) , weighted least squares (WLS) [67], or maximum likelihood (ML). Each sensor estimates its location and then transmits that assertion to its neighbors [68]. Neighbors must then recalculate their location and transmit again until converge. Typically, better statistical performance is achieved by successive refinement compared to network multilateration, but convergence issues must be addressed. Bayesian networks provide

another distributed successive refinement method to estimate the probability density of sensor network parameters. These methods are particularly promising for sensor localization-each sensor sores a conditional density on its own coordinates, based on its measurements.

## 2.4 Review of Some Existing Approaches

Once the distance measurements are available, node location can be estimated using different approaches. In this section, some existing approaches, for example, non linear least squares (NLS), linear least squares (LLS), projection onto convex sets (POCS), and projection onto rings (POR) are revisited. Consider a 2-D network with $N+M$ sensor nodes. Suppose that $N$ nodes are placed at positions $\mathbf{z}_i \in \mathbb{R}^2$, $i = 1,\ldots N$, and the remaining $M$ nodes are anchors. Suppose that anchors are able to estimate distances to the nodes with the following observation:

$$\hat{d}_{ij} = d_{ij} + n_{ij},\ j = 1,\ldots,M, i = 1,\ldots,N, \tag{2.3}$$

where $d_{ij} = \|\mathbf{z}_i - \mathbf{z}_j\|$ is the Euclidean distance between $\mathbf{z}_i$ and $\mathbf{z}_j$ and $n_{ij}$ is the measurement error. We assume the measurement errors are independent and identically distributed (i.i.d).

### 2.4.1 Nonlinear Least Squares

The nonlinear least squares location estimate based on the range measurement can be found as the solution to the non-convex optimization problem

$$\hat{\mathbf{z}}_i = \arg\min_{\mathbf{z}_i \in \mathbb{R}^2} \sum_{i=1}^{N} \sum_{j=1,\ldots,M} (\hat{d}_{ij} - d_{ij})^2, \tag{2.4}$$

and the algorithm is given in Algorithm 1.

**Algorithm 1** NLS

1. Initialization: choose arbitrary initial target position $\mathbf{z}_i^0 \in \mathbb{R}^2$ for node $i$
2. for k=0 until convergence or predefined number of K do
3. Update:
$$\hat{\mathbf{z}}_i = \arg\min_{\mathbf{z}_i \in \mathbb{R}^2} \sum_{j \in M} (\hat{d}_{i,j} - \|\mathbf{z}_i - \mathbf{z}_j\|)^2$$
4. End for

We note if $n_{ij}$ are identically distributed, zero-mean Gaussian random variables for all $j = 1,\ldots,M$, the NLS estimate is also the maximum likelihood estimate [69]. Solving the NLS

problems require minimizing a nonlinear and non-convex function, which can not be solved analytically. Therefore, numerical algorithms are applied to approximate NLS estimations. However, numerical algorithms require intensive computation and require a good initialization, in order to avoid minimization problem and obtain a closed form solution, location estimation problems can be solved by using the linear least squares approach.

### 2.4.2 Linear Least Squares

Based on [30, 70], an alternative approach to the NLS estimation is the LLS approach. In a LLS technique, a new measurement set is obtained from the measurements by certain operation that result in linear relations.

Let $\hat{d}_{ij}$ represents the distance estimate obtained from the $i$th TOA measurement, and $M$ represents the total number of anchors, we have:

$$\hat{d}_{ij}^2 = (x_j - x_i)^2 + (y_j - y_i)^2, \text{ for } j = 1, \ldots, M \tag{2.5}$$

where each distance measurement is assumed to define a circle of uncertain region. Then one of the equations in (2.5), say the $r$th one, is fixed and subtracted from all of the other equation. After some manipulation, the following linear relation can be obtained:

$$\mathbf{A}\mathbf{l} = \mathbf{P} \tag{2.6}$$

where $\mathbf{l} = [\mathbf{x}\ \mathbf{y}]^T$,

$$\mathbf{A} = 2 \begin{bmatrix} x_1 - x_r & y_1 - y_r \\ \vdots & \vdots \\ x_{r-1} - x_r & y_{r-1} - y_r \\ x_{r+1} - x_r & y_{r+1} - y_r \\ \vdots & \vdots \\ x_M - x_r & y_M - y_r \end{bmatrix} \tag{2.7}$$

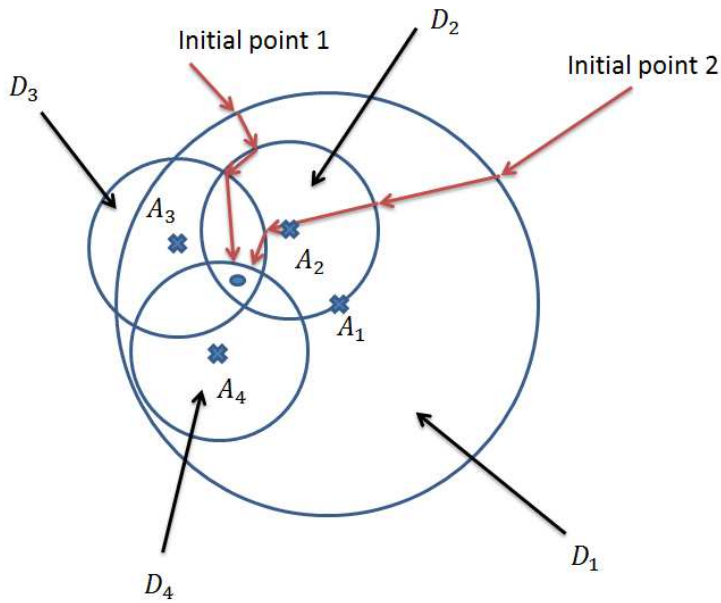


Figure 2.8: Projection onto Convex Sets

and

$$\mathbf{P} = 2 \begin{bmatrix} d_r^2 - d_1^2 - k_r + k_1 \\ \vdots \\ d_r^2 - d_{r-1}^2 - k_r + k_{r-1} \\ d_r^2 - d_{r+1}^2 - k_r + k_{r+1} \\ \vdots \\ d_r^2 - d_M^2 - k_r + k_M \end{bmatrix} \tag{2.8}$$

with $k_j = x_j^2 + y_j^2$ and $r$ being the selected reference node index that is used to obtain linear relations. Therefore, the LLS solution can be obtained as

$$\hat{\mathbf{l}} = (\mathbf{A}^T\mathbf{A})^{-1}\mathbf{A}^T\mathbf{P} \tag{2.9}$$

Compared to the NLS estimator, it has low computational complexity. However, it is suboptimal in general and the amount of its sub-optimality can be quantified in terms of the CRLB.

### 2.4.3 Projection onto Convex Sets

To solve NLS based problems using numerical approximations, a good initialization is required. Projection onto convex sets algorithm can provide a good initialization and a estimate on a node

location. POCS was originally introduced to solve convex feasibility problems [71]. POCS then been applied to different problems in various fields, such as image restoration problem and radiation therapy treatment planning. Reference [72] discusses the POCS in localization problems. In the absence of measurement error, it is clear that node $i$, at location $\mathbf{z}_i$ , can be found in the intersection of a number of circles with radii $d_{ij}$ and centers $\mathbf{z}_j$. For non-negative measurement errors, we can relax circles to discs because a target definitely can be found inside the circles. We define the disc $\mathscr{D}_{ij}$ centered at $\mathbf{z}_j$ as

$$\mathscr{D}_{ij} = \{\mathbf{z}_i \in \mathbb{R}^2 \ \|\mathbf{z}_i - \mathbf{z}_j\| \leq \hat{d}_{ij}\},\ j = 1, \ldots, M \tag{2.10}$$

Define an estimate of $\mathbf{z}_i$ as a point in the intersection $\mathscr{D}_i$ of the disc $\mathscr{D}_{ij}$

$$\hat{\mathbf{z}}_i \in \mathscr{D}_i = \bigcap_{j=1,\ldots,M} \mathscr{D}_{ij} \tag{2.11}$$

Therefore, the positioning problem can be transformed to the following convex feasibility problem:

$$\text{find } \mathbf{z} = [\mathbf{z}_1, \ldots, \mathbf{z}_N] \text{ such that } \mathbf{z}_i \in \mathscr{D}_i,\ i = 1, \ldots, N. \tag{2.12}$$

**Algorithm 2** POCS

1. Initialization: choose arbitrary initial target position $\mathbf{z}_i^0 \in \mathbb{R}^2$ for node $i$
2. for k>0 until convergence or predefined number of K do
3. Update:
$$\mathbf{z}_i^{k+1} = \mathbf{z}_i^k + \lambda_k^i(\mathscr{P}_{\mathscr{D}_{ij}(k)}(\mathbf{z}_i^k) - \mathbf{z}_i^k)$$
4. End for

In Algorithm 2, we have introduced $\mathscr{P}_{\mathscr{D}_{ij}(k)}$, which is the orthogonal projection of $\mathbf{z}$ onto set $\mathscr{D}_{ij}$. To find the projection of a point $\mathbf{z} \in \mathbb{R}^n$ onto a closed convex set $\Omega \subseteq \mathbb{R}^n$, we need to solve an optimization problem:

$$\mathscr{P}_\Omega(\mathbf{z}) = \arg\min \|\mathbf{z} - \mathbf{x}\| \tag{2.13}$$

When $\Omega$ is a disc, there is a closed-form solution for the projection:

$$\mathscr{P}_{\mathscr{D}_{ij}}(\mathbf{z}) = \begin{cases} \mathbf{z}_j + \frac{\mathbf{z}-\mathbf{z_j}}{||\mathbf{z}-\mathbf{z}_j||}\hat{d}_{ij} & ||\mathbf{z}-\mathbf{z_j}|| \geq \hat{d}_{ij} \\ \mathbf{z} & \|\mathbf{z}-\mathbf{z}_j\| \leq \hat{d}_{ij} \end{cases} \tag{2.14}$$

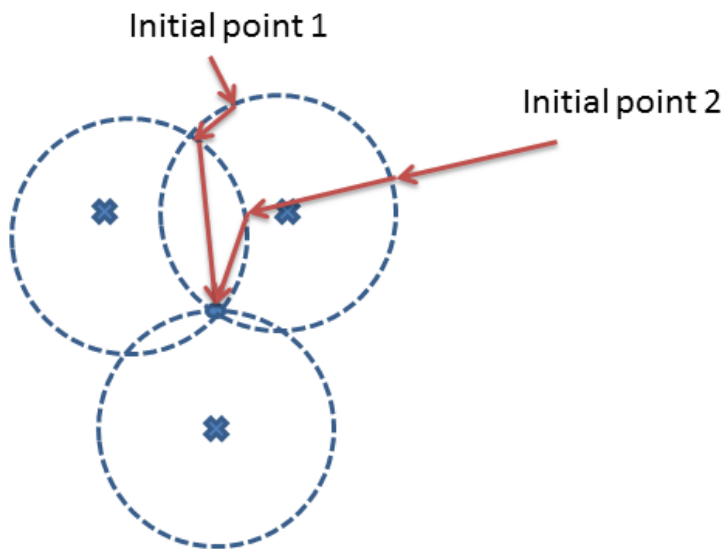


Figure 2.9: Projection onto Rings

### 2.4.4 Projection onto Rings

In the case when the measurement noise is small, we can often improve POCS by replacing the disc $\mathscr{D}_{ij}$ with a ring defined as

$$\mathscr{R}_{ij} = \{\mathbf{x} \in \mathbb{R}^2 : \hat{d}_{ij} - \varepsilon_l \leq d_j(\mathbf{z}) \leq \hat{d}_{ij} + \varepsilon_u\},\ j = 1, \ldots, M \tag{2.15}$$

where $\varepsilon_l + \varepsilon_u$ determines the width of the ring. The width is tuning parameter of the resulting algorithm. The projection onto rings (POR) is computed as in Algorithm 3.

**Algorithm 3** POR

1. Initialization: choose arbitrary initial target position $\mathbf{z}_i^0 \in \mathbb{R}^2$ for node $i$
2. for k >0 until convergence or predefined number of K do
3. Update:
$$\mathbf{z}_i^{k+1} = \mathbf{z}_i^k + \lambda_k^i(\mathscr{P}_{\mathscr{R}_{ij}(k)}(\mathbf{z}_i^k) - \mathbf{z}_i^k)$$
4. End for

## 2.5 Performance Analysis on Location Estimation and Detection

In the previous section, the measurements that are used to estimate node locations are reviewed. To evaluate the performance of different measurements, the Cramer-Rao lower bound (CRLB), which provides a lower bound on the variance achievable by any unbiased location estimator, can

be applied to evaluate the performance. An unbiased estimator is defined as that on the average the estimator will yield to the true value of the unknown parameter. Since the parameter may in general be anywhere in the interval $a \leq \theta \leq b$, unbiasedness asserts that no matter what the true value of $\theta$, our estimator will yield it on the average. Mathematically, an estimator is unbiased if

$$E(\hat{\theta}) = \theta. \tag{2.16}$$

The CRLB provides a lower bound on the variance achievable by any unbiased location estimator. Any unbiased estimator $\hat{\theta}$ must satisfy

$$\text{cov}(\hat{\theta}) \geq \left\{\mathbb{E}[-\nabla_\theta(\nabla_\theta \log f(\mathbf{X}|\theta))^T]\right\}^{-1}, \tag{2.17}$$

where $f(\mathbf{X}|\theta)$ is the pdf of the observation $\mathbf{X}$, $\text{var}(\hat{\theta})$ is the covariance of the estimator, and $\nabla_\theta$ is the gradient operator w.r.t the vector $\theta$. The Fisher Information of the unknown parameter $\theta$ is defined as

$$\mathbf{F}_\theta = \mathbb{E}[-\nabla_\theta(\nabla_\theta \log f(\mathbf{X}|\theta))^T]. \tag{2.18}$$

The CRLBs on the TOA and RSS measurement in the absence of fading have been derived in [31]. To locate a node in a 1m by 1m square, the CRLBs on the TOA measurement and the RSS measurement are shown in Figure 2.10 and Figure 2.11 respectively. From the figure one can see that the CRLB depends on the node location. When the node is located in the center of the square, the CRLB is the smallest in both cases.

In detection theory, Neyman-Pearson hypothesis testing techniques are frequently used. Specially, in a binary hypothesis problem, suppose one hypothesis is called null hypothesis, states that the observed data only contains noise, and is denoted as $H_0$, another hypothesis, states that the observed data contains both signal plus noise, and is denoted as $H_1$, the Neyman-Pearson detector, which is denoted as $L(\mathbf{x})$ is defined as the ratio of the log likelihood function under two hypothesis, which is given as

$$L(\mathbf{x}) = \frac{f(\mathbf{x}; H_1)}{f(\mathbf{x}; H_0)} \lessgtr \gamma. \tag{2.19}$$

It is proved that the Neyman-Pearson detector is the optimal detector that maximizing the probability of detection ($\bar{P}_{\text{D}}$) while satisfying the constraint on the probability of false alarm ($\bar{P}_{\text{FA}}$). They

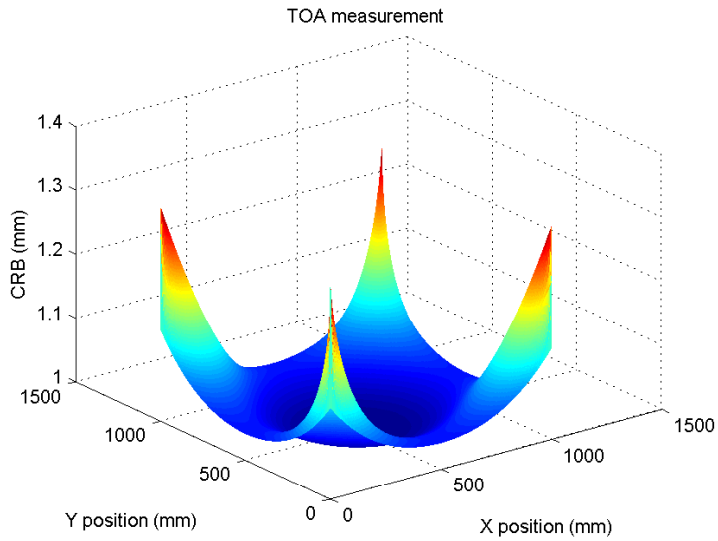


Figure 2.10: The CRLB on the TOA Measurement When the Node is Locating Inside A 1m by 1m Square.

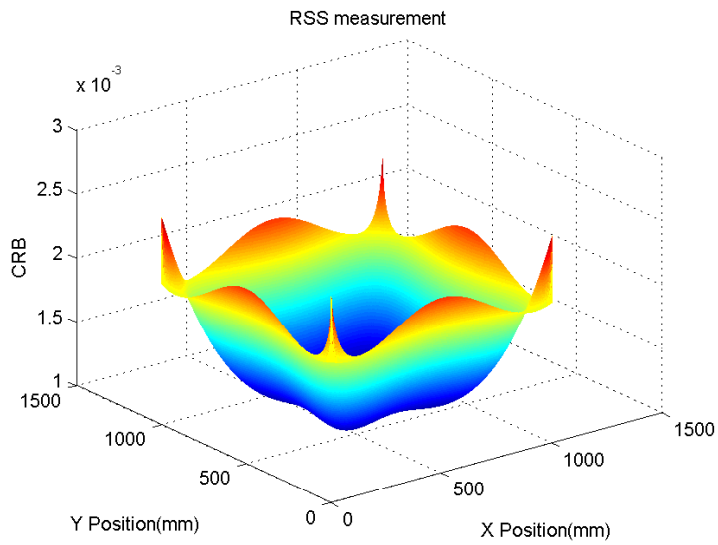


Figure 2.11: The CRLB on the RSS Measurement When the Node is Locating Inside A 1m by 1m Square.

Neyman-Pearson detector has been widely used in detection problems. When the prior distribution is known, one can simply find the optimal threshold that satisfies constrains on $\bar{P}_{\mathrm{FA}}$. When the prior distribution is unknown, machine learning algorithms can be applied to train the measured data and find the NP classifier [73, 74].

## 2.6 Conclusions

In this chapter, both range-based and range-free algorithms are revisited. Also, distance related measurements, such as TOA, TDOA and RSS, angle related measurements, such as DOA, and hybrid measurements, such as LAA, are discussed in details. To overcome the limits in centralized algorithms, a sequential location estimation scheme, which is one of distributed algorithms, is reviewed. To compute the coordinate of node locations, many approaches can be applied. In this chapter, the NLS, LLS, POCS, and POR approaches are reviewed.

Chapter 3

# LOCATION ESTIMATION IN THE PRESENCE OF FADING

In this chapter, we consider localization in the presence of fading. Several fading scenarios are considered, and CRLBs are derived for both 1-D and two 2-D localization problems with TOA measurements. Our results are compared with the CRLBs in the absence of fading that were derived in [31]. The ML estimators under different fading scenarios are also derived.

## 3.1 System Model

Assume a non-cooperative WSN, in which nodes do not communicate with each other, with $M$ anchors and 1 node in $\mathbb{R}^n$, where $n = 1,2$. In 1-D, the location of the $i^{th}$ anchor, $\mathbf{p}_i = x_i$, and the node, $\mathbf{z} = x$ are scalars. In 2-D, $\mathbf{p}_i = [x_i, y_i]^T$ and $\mathbf{z} = [x, y]^T$ are vectors. Figure 3.1 shows a sensor network with $M = 3$ anchors and 1 node. We assume the node communicates with all anchors. The measured TOA between the node and the anchor located at $\mathbf{p}_i$, is defined as $\hat{\tau}_i$. In location estimation, each anchor transmits a modulated signal to a node, and the node transmits back immediately after it receives the signal. The two way transmit time is measured by each anchor, which can be halved to estimate the transmit time and distance. Define $d_i = ||\mathbf{p}_i - \mathbf{z}||_2$ as the true distance between the node located at $\mathbf{z}$ and the anchor located at $\mathbf{p}_i$. In the absence of fading, $\hat{\tau}_i$ is Gaussian distributed [75], and is given by

$$\hat{\tau}_i \sim \mathcal{N}\left(\frac{d_i}{c}, \sigma^2\right), \tag{3.1}$$

where $c$ is the speed of propagation of signals in the free space, and $\sigma^2$ is the variance of the TOA measurements [31]. We will assume throughout that $\{\hat{\tau}_i\}_{i=1}^M$ are independent.

Define $h_i = |h_i|e^{j\theta_i}$ as the fading coefficient for the channel between the node and the $i^{th}$ anchor, where $|h_i|$ and $\theta_i$ are the amplitude and phase of the fading coefficient respectively, and $i \in \{1, 2, \ldots, M\}$. In the presence of fading, the statistics of $\hat{\tau}_i$ is a function of $h_i$. In this paper, we consider the following scenarios: (a) $h_i$ is assumed to be known at each anchor; (b) $\theta_i$ is assumed to be known at each anchor, but $|h_i|$ is an unknown random variable with a known prior distribution; (c) No CSI (amplitude or phase) is available at any anchor. Although only 1-D and 2-D cases are

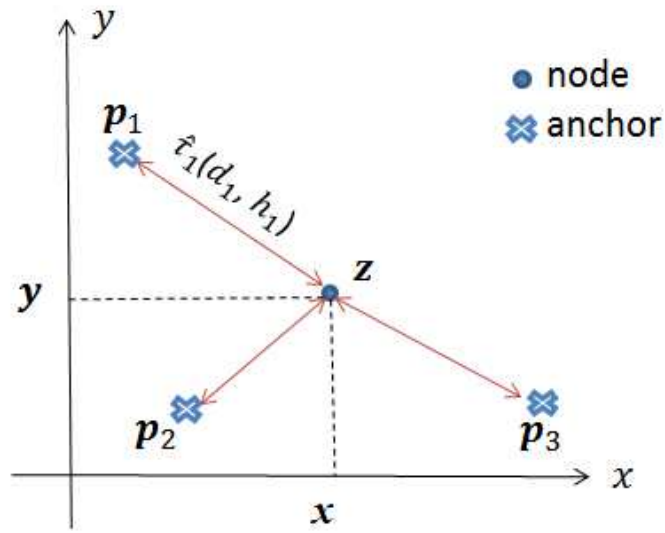


Figure 3.1: The System Model of Location Estimation in WSNs.

Three anchors are present at positions $\mathbf{p} = [\mathbf{p}_1, \mathbf{p}_2, \mathbf{p}_3]$, and 1 node at the position $\mathbf{z} = [x, y]^T$. Variables $\hat{\tau}_i$, $d_i$ and $h_i$ are the TOA measurement, distance and the channel fading coefficient between the node and the $i^{th}$ anchor respectively, where $\hat{\tau}_i$ is the function of $d_i$ and $h_i$ in the presence of fading.

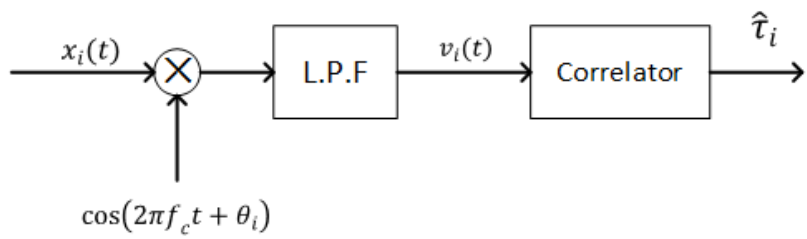


Figure 3.2: Coherent TOA Estimation Scheme.

considered, the results can be generalized to three dimension (3-D).

Consider a carrier modulated signal with carrier frequency $f_c$ transmitted on a fading channel for TOA estimation. When the received phase is known at each anchor, a coherent estimation strategy, as shown in Figure 3.2 is applied to estimate the TOA. The received signal is given by

$$x_i(t) = |h_i| \sum_n s[n] g(t - nT - \tau_i) \cos(2\pi f_c t + \theta_i), \tag{3.2}$$

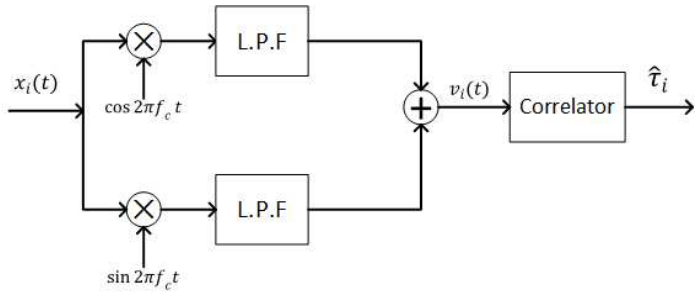


Figure 3.3: non-Coherent TOA Estimation Scheme.

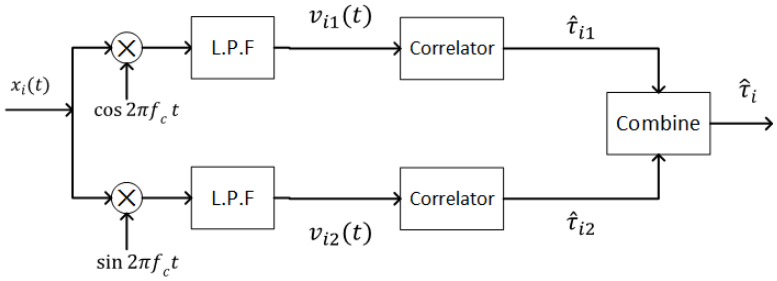


Figure 3.4: Alternate non-Coherent TOA Estimation Scheme.

is multiplied by $\cos(2\pi f_c t + \theta_i)$ and then low pass filtered. The output of the low pass filter

$$v_i(t) = \frac{|h_i|}{2} \sum_n s[n] g(t - nT - \tau_i) \tag{3.3}$$

is correlated with a regenerated template signal

$$s_i(t) = \sum_n s[n] g(t - nT - \tau^*) \tag{3.4}$$

with delay $\tau^*$. The TOA is estimated by finding the maximum value of the output of the correlator.

When the phases are unknown, a non-coherent estimation strategy is needed. We will consider non-coherent architectures that correlate with a base-band signal. Figure 3.3 and Figure 3.4 shows two such non-coherent estimation schemes. Figure 3.3 correlates the received signal with a regenerated modulated signal and its 90 degree shifted regenerated signal. In this scheme, the input of the correlator is the summation of the output of two low pass filters, which is

$$v_i(t) = \frac{1}{2}(|h_i|\cos(\theta_i) - |h_i|\sin(\theta_i)) \sum_n s[n] g(t - nT - \tau_i). \tag{3.5}$$

Similar to the coherent estimation scheme, $v_i(t)$ in (3.5) is correlated with the signal given in (3.4) to estimate TOA. Another alternate non-coherent estimation scheme is shown in Figure 3.4. In this

scheme, in-phase and quadrature components estimate TOA independently. Firstly, the received signal $x_i(t)$, which is given in (3.2), is multiplied by $\cos(2\pi f_c t)$ and $\sin(2\pi f_c t)$ separately, and then passed to two low pass filters. The output of the two low pass filters are given by

$$v_{i1}(t) = \frac{|h_i|}{2}\cos(\theta_i)\sum_n s[n]g(t - nT - \tau_i), \tag{3.6}$$

and

$$v_{i2}(t) = \frac{|h_i|}{2}\sin(\theta_i)\sum_n s[n]g(t - nT - \tau_i). \tag{3.7}$$

Then $v_{i1}(t)$, which contains the in-phase component, and $v_{i2}(t)$, which contains the quadrature component, estimate TOA separately by correlating the signal with the regenerated signal that is given in (3.4), and two TOA estimates on each branch are given as $\hat{\tau}_{i1}$ and $\hat{\tau}_{i2}$ respectively. The final TOA estimate $\hat{\tau}_i$ can be computed by combing $\hat{\tau}_{i1}$ and $\hat{\tau}_{i2}$ using different combing methods. The CRLB comparisons between these non-coherent estimation schemes will be compared in Section 3.5.

## 3.2 Fading Coefficients Are Known at Each Anchor

Assume $h_i$ is known at each anchor. Since both amplitude and phase are known, a coherent estimation strategy is used for location estimation as in Figure 3.2. Conditioned on the fading coefficients, the TOA measurement $\hat{\tau}_i$ in (3.1) is Gaussian distributed, and is given by

$$\hat{\tau}_i \sim \mathcal{N}\left(\frac{d_i}{c}, \frac{\sigma^2}{|h_i|^2}\right), \tag{3.8}$$

where $\mathrm{E}\left[|h_i|^2\right] = 1$. In this case, the CRLB can be expressed as a function of the fading coefficients, with analysis very similar to the case with only additive white Gaussian noise (AWGN) [31]:

$$\mathrm{CRLB}_{\text{1-D}} = \frac{c^2\sigma^2}{\sum_{i=1}^{M}|h_i|^2}. \tag{3.9}$$

Recall that the CRLB in 1-D in the absence of fading [31] is a special case of (3.9) with $|h_i| = 1$, and is given as

$$\mathrm{CRLB}_{\text{1-D}}^{\text{AWGN}} = \frac{c^2\sigma^2}{M}. \tag{3.10}$$

Similarly, we can also calculate the CRLB where the fading coefficients are known at each anchor in 2-D. Note that in 2-D, the CRLB depends on the geometry of the network, and it is more

complicated than the 1-D case. However, a similar conclusion as the 1-D case that when $|h_i| = 1$, $\text{CRLB}_{\text{2-D}} = \text{CRLB}_{\text{2-D}}^{\text{AWGN}}$, can be reached when compared with the AWGN case in [31].

### 3.3 Effect of Unknown Fading Amplitude

When the amplitude of fading coefficients is unknown at any anchor, we will show that the presence of fading always degrades the CRLB. To show this, we use the modified CRLB (MCRLB) [76], which is defined as

$$\text{MCRLB} = \text{tr}\left(\left(-\text{E}_{\mathbf{T},\mathbf{h}}\left[\nabla_{\mathbf{z}}^2 \ln f(\mathbf{T}|\mathbf{h},\mathbf{z})\right]\right)^{-1}\right), \tag{3.11}$$

where $\nabla_{\mathbf{z}}^2$ is the Hessian operator, $\text{tr}(\mathbf{A})$ is the trace of the matrix $\mathbf{A}$, $\mathbf{h} = [|h_1|, |h_2|, \ldots, |h_M|]$ contains the amplitude of the fading coefficients, $\mathbf{T} = [\hat{\tau}_1, \hat{\tau}_2, \ldots, \hat{\tau}_M]$ contains all TOA measurements, and $\mathbf{z}$ is the location of the node. In one dimension, using (3.8), (3.11) can be calculated as

$$\text{MCRLB}_{\text{1-D}} = \frac{c^2\sigma^2}{\sum_{i=1}^{M} \text{E}\left[|h_i|^2\right]}. \tag{3.12}$$

Since $\text{E}\left[|h_i|^2\right] = 1$, (3.12) can be simplified as $\text{MCRLB}_{\text{1-D}} = c^2\sigma^2/M = \text{CRLB}_{\text{1-D}}^{\text{AWGN}}$, and the MCRLB for the localization error equals to the AWGN case in (3.10), which is also seen in (3.9) with $|h_i| = 1$. Since the MCRLB is known to be a lower bound on the CRLB in the presence of fading [76], we can conclude that the presence of fading will always degrade the performance for *any* fading amplitude distribution. For the MCRLB in 2-D, the derivation is very similar as 1-D, and it turns out the MCRLB in 2-D is the same as the CRLB of the 2-D AWGN case as well. The details are omitted for brevity.

### 3.4 Unknown Fading Amplitude: Nakagami Fading

Having seen that fading degrades the performance, we quantify this degradation in the Nakagami envelope case. We assume that fading does not change during the TOA measurements, the phases of the fading coefficients are known at each anchor, and the amplitudes $|h_i|$ are Nakagami distributed, corresponding to a Gamma distributed $|h_i|^2$. Since the phase is known, the coherent estimation strategy which is used in Section 3.2 can be applied. The TOA measurements $\hat{\tau}_i$ are assumed to be i.i.d., and conditioned on the fading coefficients satisfy (3.8), where the fading power is Gamma

distributed and given by [77]:

$$f_{|h_i|^2}(x) = m^m x^{m-1}\Gamma(m)^{-1}\exp(-mx), \tag{3.13}$$

where $\frac{1}{2} \leq m < \infty$ is the Nakagami fading parameter, and as before, $\mathrm{E}\left[|h_i|^2\right] = 1$. When $m = \frac{1}{2}$, the envelope $|h_i|$ is one-sided Gaussian distributed; when $m = 1$, $|h_i|$ is Rayleigh distributed; and as $m \to \infty$, the channel exhibits no fading corresponding to an AWGN channel.

The unconditional distribution of $\hat{\tau}_i$ can be calculated by using the total probability theorem:

$$f_{\hat{\tau}_i}(\hat{\tau}_i|\mathbf{z}) = \int_0^\infty f\left(\hat{\tau}_i \middle| |h_i|^2, \mathbf{z}\right) f_{|h_i|^2}(x)dx. \tag{3.14}$$

By substituting (3.8) and (3.13) into (3.14), and using [78, p.310] we obtain

$$f_{\hat{\tau}_i}(\hat{\tau}_i|\mathbf{z}) = \frac{m^m(m-\frac{1}{2})!}{\sqrt{2\pi\sigma^2}\Gamma(m)\left(\frac{1}{2\sigma^2}(\hat{\tau}_i - \frac{d_i}{c})^2 + m\right)^{(m+\frac{1}{2})}}. \tag{3.15}$$

For convenience, let $l(\hat{\tau}_i|\mathbf{z}) = \ln f_{\hat{\tau}_i}(\hat{\tau}_i|\mathbf{z})$ be the log likelihood function of each TOA measurement. Due to the independence of the TOA measurements, we define $l(\mathbf{T}|\mathbf{z}) = \sum_{i=1}^M \ln f_{\hat{\tau}_i}(\hat{\tau}_i|\mathbf{z})$. The CRLB can be expressed as [52]

$$\mathrm{CRLB}(\mathbf{z}) = \mathrm{tr}\left(\mathbf{F}_\mathbf{z}^{-1}\right), \tag{3.16}$$

where $\mathbf{F}_\mathbf{z} = -\mathrm{E}_\mathbf{T}\left[\nabla_\mathbf{z}^2 l(\mathbf{T}|\mathbf{z})\right]$ is the Fisher information matrix (FIM). We can calculate the $(j,k)$ element of $\mathbf{F}_\mathbf{z}$, denoted by $[\mathbf{F}_\mathbf{z}]_{jk}$

$$[\mathbf{F}_\mathbf{z}]_{jk} = \begin{cases} \sum_{i=1}^M \mathrm{E}_{\hat{\tau}_i}\left[\left(\frac{\partial l(\hat{\tau}_i|\mathbf{z})}{\partial \mathbf{z}_j}\right)^2\right] & j = k \\ -\mathrm{E}_{\hat{\tau}_i}\left[\frac{\partial^2 l(\hat{\tau}_i|\mathbf{z})}{\partial \mathbf{z}_j \partial \mathbf{z}_k}\right] & j \neq k \end{cases}. \tag{3.17}$$

In 1-D, the location of the node is a scalar $\mathbf{z} = x$, the distance between the node and the $i^{th}$ anchor is $d_i = ||x_i - x||_2 = |x_i - x|$, and $F_z$ is a scalar. Using $F_z = \sum_{i=1}^M \mathrm{E}_{\hat{\tau}_i}\left[\left(\frac{\partial l(\hat{\tau}_i|x)}{\partial x}\right)^2\right]$, $\mathrm{E}_{\hat{\tau}_i}\left[\left(\frac{\partial l(\hat{\tau}_i|x)}{\partial x}\right)^2\right]$ can be calculated using (3.15) as

$$\mathrm{E}_{\hat{\tau}_i}\left[\left(\frac{\partial l(\hat{\tau}_i|x)}{\partial x}\right)^2\right] = \frac{m^m(m-\frac{1}{2})!(m+\frac{1}{2})^2}{\Gamma(m)\sqrt{2\pi}c^2\sigma^5}X(d_i), \tag{3.18}$$

where

$$X(d_i) = \int_0^\infty \frac{(\hat{\tau}_i - \frac{d_i}{c})^2}{\left(\frac{1}{2\sigma^2}(\hat{\tau}_i - \frac{d_i}{c})^2 + m\right)^{\frac{5}{2}+m}} d\hat{\tau}_i. \tag{3.19}$$

Unlike the AWGN case, the Fisher information depends on $d_i$ through $X(d_i)$ in (3.19). However, using [78, p.292], it is possible to express it as

$$X(d_i) \leq \frac{\sqrt{2}\sigma^3\Gamma(\frac{3}{2})\Gamma(m+1)}{m^{1+m}\Gamma(m+\frac{5}{2})} + \frac{\left(\frac{d_i}{c}\right)^2}{\left(\frac{1}{2\sigma^2}(\frac{d_i}{c})^2 + m\right)^{\frac{5}{2}+m}}. \tag{3.20}$$

Since the second term in (3.20) is small, it is clear that $X(d_i)$ can be approximated by the first term, and therefore approximately independent of $d_i$. The exact CRLB in the presence of Nakagami fading in 1-D can be expressed as

$$\text{CRLB}_{\text{1-D}}(\mathbf{z}) = \frac{\Gamma(m)\sqrt{2\pi}c^2\sigma^5}{m^m(m-\frac{1}{2})!(m+\frac{1}{2})^2\sum_{i=1}^M X(d_i)}, \tag{3.21}$$

with an approximation as

$$\text{CRLB}_{\text{1-D}}(\mathbf{z}) \approx \frac{2c^2\sigma^2\Gamma\left(m+\frac{5}{2}\right)}{\left(m-\frac{1}{2}\right)!\left(m+\frac{1}{2}\right)^2}\frac{1}{M}. \tag{3.22}$$

The approximation of the loss due to fading can be expressed as

$$\frac{\text{CRLB}_{\text{1-D}}(\mathbf{z})}{\text{CRLB}_{\text{1-D}}^{\text{AWGN}}} \approx k = \frac{\sqrt{\pi}\Gamma(m+\frac{5}{2})}{\Gamma(\frac{3}{2})(m+\frac{1}{2})^2\left(m-\frac{1}{2}\right)!}, \tag{3.23}$$

where we recall from (3.10) that $\text{CRLB}_{\text{1-D}}^{\text{AWGN}} = c^2\sigma^2/M$. As $m \to \infty$, the second term in (3.20) goes to 0 and $k$ in (3.23) goes to 1 so that the CRLB in the presence of fading converges to the AWGN case.

When $m = 1$, the fading is Rayleigh distributed, and the exact CRLB in (3.21) is simplified as

$$\text{CRLB}_{\text{1-D}}(\mathbf{z}) = \frac{8\sqrt{2}c^2\sigma^5}{9\sum_{i=1}^M X(d_i)}. \tag{3.24}$$

To simplify even further, we use the first term of (3.20) because $\frac{d_i}{c} \approx 0$ and set $m = 1$ to obtain

$$\text{CRLB}_{\text{1-D}} = \frac{\sigma^2c^2}{M}\frac{10}{3}. \tag{3.25}$$

This shows that the loss in SNR due to Rayleigh fading is a factor of $k = \frac{10}{3}$ which is about 5dB, compared to the AWGN case.

In 2-D, the distance between the node and the $i^{th}$ anchor is $d_i = \sqrt{(x_i - x)^2 + (y_i - y)^2}$. Letting $Y(m) = m^m (m - \frac{1}{2})!(m + \frac{1}{2})^2 \left[\Gamma(m)\sqrt{2\pi}\sigma^3\right]^{-1}$. The FIM is

$$\mathbf{F_z} = \frac{Y(m)}{c^2\sigma^2} \sum_{i=1}^{M} X(d_i) \begin{bmatrix} \frac{(x_i - x)^2}{d_i^2} & \frac{(y_i - y)(x_i - x)}{d_i^2} \\ \frac{(y_i - y)(x_i - x)}{d_i^2} & \frac{(y_i - y)^2}{d_i^2} \end{bmatrix}. \tag{3.26}$$

The CRLB on the variance of the localization error in 2-D is

$$\text{CRLB}_{\text{2-D}}(\mathbf{z}) = \text{tr}\left(\mathbf{F}_{\mathbf{z}}^{-1}\right). \tag{3.27}$$

The FIM in the absence of fading for the 2-D case is given in [31], and can be written the same as (3.26) except without the $Y(m)$ and $X(d_i)$ terms. Comparing (3.27) with the CRLB in the absence of fading in [31], both CRLBs in 2-D depend on the true location of the node. When $\frac{d_i}{c} \approx 0$, similar to the 1-D case, $X(d_i)$ in (3.20) can be simplified. After simplifications and substituting into (3.27), we see that the CRLB in the presence of fading is also a factor of $k$ higher than the AWGN counterpart, i.e. when $m = 1$, $k = \frac{10}{3}$ in both 1-D and 2-D. Further, as $m \to \infty$, the CRLB in 2-D converges to the AWGN case.

Extension To Multiple Nodes Case

When $N$ nodes exist in a WSN, $\mathbf{F_z}$ becomes a $N \times N$ matrix, and the diagonal elements in (3.17) is summed from $i = 1$ to $i = M + N - 1$. Using the approximation of $X(d_i)$ in (3.20), after simplifications, in 1-D, the CRLB for the $i^{th}$ node is the $(i,i)$ element of $\mathbf{F}_{\mathbf{z}}^{-1}$, which is given by

$$\text{CRLB}_{\text{1-D}}(\mathbf{z}_i) \approx \frac{2c^2\sigma^2\Gamma\left(m + \frac{5}{2}\right)}{\left(m - \frac{1}{2}\right)!\left(m + \frac{1}{2}\right)^2} \frac{M+1}{M(N+M)}. \tag{3.28}$$

We can prove that in cooperative WSNs, the ratio of location estimation in the presence of fading and in the absence of fading keeps the same.

ML Estimator in the Presence of Nakagami Fading

The ML estimator for location estimation in the presence of fading is denoted as

$$\hat{\mathbf{z}} = \underset{\mathbf{z}}{\text{argmax}} \prod_{i=1}^{M} f_{\hat{\tau}_i}(\hat{\tau}_i | \mathbf{z}). \tag{3.29}$$

Substituting (3.15) into (3.29), we have

$$\hat{\mathbf{z}} = \underset{\mathbf{z}}{\text{argmin}} \sum_{i=1}^{M} \ln\left(\frac{1}{2\sigma^2 m}\left(\hat{\tau}_i - \frac{d_i}{c}\right)^2 + 1\right), \tag{3.30}$$

where $d_i = ||\mathbf{p}_i - \mathbf{z}||_2$.

In the absence of fading, the ML estimator which is derived in [31] is

$$\hat{\mathbf{z}} = \arg\min_{\mathbf{z}} \sum_{i=1}^{M} \left( \hat{\tau}_i - \frac{d_i}{c} \right)^2, \tag{3.31}$$

which is different from (3.30). Since $\ln(1+x) \approx x$ for small $x$, it is straightforward to see that if $m$ is large, (3.30) and (3.31) are approximately the same.

## 3.5 No CSI Available at Anchors

In the previous sections, we assumed that the phases of the fading coefficients are known at each anchor. When there is no CSI (phase or amplitude) available at any anchor, a non-coherent estimator is applied. Since the optimal non-coherent estimator is hard to implement, one of the suboptimal non-coherent estimators as shown in Figure 3.3 and Figure 3.4 can be applied. When the non-coherent estimator in Figure 3.3 is applied, using (3.5) and [75, p.233], conditioned on amplitudes and phases of the fading coefficients, the pdf of the TOA measurements is Gaussian with mean and variance given by

$$\hat{\tau}_i \sim \mathcal{N}\left( \frac{d_i}{c}, \frac{\sigma^2}{|h_i|^2 \left(1 - \sin\left(2\theta_i\right)\right)} \right). \tag{3.32}$$

As in Section 3.4, we assume that $|h_i|^2$ is Gamma distributed. In addition, we assume $\theta_i$ is uniformly distributed over $[0, 2\pi)$, and is independent of $|h_i|^2$. We can calculate the unconditional distribution of $\hat{\tau}_i$ by integrating the effect of $|h_i|^2$ and $\theta_i$, which is given by

$$f_{\hat{\tau}_i}(\hat{\tau}_i|\mathbf{z}) = \int_0^{2\pi} \int_0^{\infty} f\left( \hat{\tau}_i \middle| \left(|h_i|^2, \theta_i\right), \mathbf{z} \right) f_{|h_i|^2}(x) f\left(\theta_i\right) dx d\theta_i. \tag{3.33}$$

where $f\left(\theta_i\right) = \frac{1}{2\pi}$, $\theta_i \in [0, 2\pi)$, and $f_{|h_i|^2}(x)$ is given in (3.13). After simplifications,

$$f_{\hat{\tau}_i}(\hat{\tau}_i|\mathbf{z}) = \frac{2\sigma m^m \left(m - \frac{1}{2}\right)! m^{\frac{1}{2}-m}}{\Gamma(m)\pi^{\frac{3}{2}} \left( \left( \hat{\tau}_i - \frac{d_i}{c} \right)^2 + m\sigma^2 \right)} \times {}_2F_1\left( 1, 1-m, \frac{3}{2}; \frac{\left( \hat{\tau}_i - \frac{d_i}{c} \right)^2}{\left( \hat{\tau}_i - \frac{d_i}{c} \right)^2 + m\sigma^2} \right), \tag{3.34}$$

where ${}_2F_1(a,b,c;z)$ is the hypergeometric function [78], defined as

$${}_2F_1(a,b,c;z) = \sum_{n=0}^{\infty} \frac{(a)_n (b)_n}{(c)_n} \frac{z^n}{n!}, \tag{3.35}$$

and $(a)_n$ is a Pochhammer symbol, which is defined as $(a)_n = a(a+1)\ldots(a+n-1)$ for $n > 1$, and $(a)_0 = 1$.

When the amplitude of the fading coefficients is Rayleigh distributed, which means $m = 1$, (3.34) can be simplified as

$$f_{\hat{\tau}_i}(\hat{\tau}_i|\mathbf{z}) = \frac{\sigma}{\pi\left(\sigma^2 + \left(\hat{\tau}_i - \frac{d_i}{c}\right)^2\right)}, \tag{3.36}$$

which interestingly is the Cauchy distribution with a scale factor $\sigma$, and median $\frac{d_i}{c}$.

Using (3.17), in 1-D, the Fisher information can be expressed as

$$F_z = \frac{4}{c^2\sigma^5\pi}\sum_{i=1}^{M} Y(d_i), \tag{3.37}$$

where

$$Y(d_i) = \int_0^\infty \left(\hat{\tau}_i - \frac{d_i}{c}\right)^2 \left(1 + \frac{\left(\hat{\tau}_i - \frac{d_i}{c}\right)^2}{\sigma^2}\right)^{-3} d\hat{\tau}_i. \tag{3.38}$$

Similar to $X(d_i)$ in (3.19) and (3.20), it is possible to express $Y(d_i)$ as

$$Y(d_i) \leq \frac{\sigma^3\pi}{16} + \left(\frac{d_i}{c}\right)^2 \left(1 + \frac{\left(\frac{d_i}{c}\right)^2}{\sigma^2}\right)^{-3}. \tag{3.39}$$

Since the second term in (3.39) is small, it is clear that $Y(d_i)$ can be approximated by using the first term, which is independent of $d_i$. Therefore, (3.37) can be simplified as

$$F_z \cong \frac{M}{4c^2\sigma^2}. \tag{3.40}$$

The CRLB in 1-D when no CSI is available is

$$\text{CRLB}_{\text{1-D}} \cong \frac{4c^2\sigma^2}{M}. \tag{3.41}$$

Recalling (3.25), we see that when no CSI is available at any anchor, the loss in SNR is a factor of $k = 4$, which is about 6dB. To calculate the CRLB in 2-D we can use (3.17) to calculate the elements of the FIM. Similar to the 1-D case, the loss in SNR compared to the AWGN case is also 6dB.

When the non-coherent estimator in Figure 3.4 is applied, conditioned on the amplitudes and phase of the fading coefficients, the distribution of $\hat{\tau}_{i1}$ and $\hat{\tau}_{i2}$ can be obtained using [75, p.233], (3.6) and (3.7) as

$$\hat{\tau}_{i1} \sim \mathcal{N}\left(\frac{d_i}{c}, \frac{\sigma^2}{|h_i|^2\cos^2(\theta_i)}\right), \tag{3.42}$$

and

$$\hat{\tau}_{i2} \sim \mathcal{N}\left(\frac{d_i}{c}, \frac{\sigma^2}{|h_i|^2 \sin^2(\theta_i)}\right). \tag{3.43}$$

Since $\theta_i$ is uniformly distributed, $\cos^2(\theta_i)$ and $\sin^2(\theta_i)$ have the same distribution. Therefore we will focus on $\hat{\tau}_{i1}$. Using the formula $\cos^2 x = \frac{1}{2}(1-\cos 2x)$, and the fact that $\frac{1}{2}(1-\cos 2x)$ has the same distribution as $\frac{1}{2}(1-\sin 2x)$, comparing (3.42) with (3.32) one can see that the variance of (3.42) is twice of (3.32). Therefore, the CRLB when the quadrature component is extracted is 2 times higher than the CRLB when the previous non-coherent estimation scheme is applied. Also, since the unconditional distribution of $\hat{\tau}_{i1}$ is the same as $\hat{\tau}_{i2}$, the CRLB when the in-phase component is extracted is the same as the CRLB when the quadrature component is extracted. If the average is taken between $\hat{\tau}_{i1}$ and $\hat{\tau}_{i2}$, the final CRLB is the same as the previous non-coherent estimation scheme, which is given in (3.41).

Even though the noncoherent architectures in Figure 3.3 and Figure 3.4 have the same performance, the two schemes have advantages and disadvantages. On the one hand, when there is some prior information on the TOA measurement, the scheme shown in Figure 3.4 is more flexible when combing the two estimates, and therefore can give a better performance. For example, if a range for the TOA measurement is known, between $\hat{\tau}_{i1}$ and $\hat{\tau}_{i2}$, the one within the range can be chosen as the final $\hat{\tau}_i$. On the other hand, the scheme shown in Figure 3.3 is less complex than the scheme shown in Figure 3.4, since the latter scheme requires two correlators.

ML Estimator When No CSI is Available At Anchors

When no CSI is available at any anchor, assuming $m = 1$ and using (3.29) and (3.36), the ML estimator for the location estimate is given by

$$\hat{\mathbf{z}} = \underset{\mathbf{z}}{\operatorname{argmin}} \sum_{i=1}^{M} \ln\left[\frac{1}{\sigma^2}\left(\hat{\tau}_i - \frac{d_i}{c}\right)^2 + 1\right]. \tag{3.44}$$

Consider a comparison of (3.44) with (3.30), which is the ML estimator for the case with known phase and Nakagami envelope. Setting $m = 1$ in (3.30) we see that the only difference between these two ML estimators is a factor of 2 multiplying $\sigma^2$. If we write (3.44) as a function of $\mathbf{T} = [\hat{\tau}_1, \hat{\tau}_2, \ldots, \hat{\tau}_M]$ and $\sigma^2$ as $\hat{\mathbf{z}} = g\left(\mathbf{T}, \sigma^2\right)$, then $\hat{\mathbf{z}}$ in (3.30) can be expressed as $\hat{\mathbf{z}} = g\left(\mathbf{T}, 2\sigma^2\right)$. This indicates that the ML estimator with no CSI needs 3dB higher SNR to use the exact same location estimator as the ML estimator which knows the phases. Note that this does not mean that

the performance of (3.30) and (3.44) are 3dB apart, since the distribution of $\mathbf{T}$ in the two cases is different.

Interestingly, comparing the pdf of the TOA measurements with phase information, given in (3.15), with the pdf of TOA measurements with no CSI information, given by (3.36), one can see that setting $m = \frac{1}{2}$ in (3.15) is identical to (3.36) when $m = 1$. Recalling that $m = \frac{1}{2}$ represents the worst Nakagami fading scenario, we conclude that with phase information, the coherent estimation with $m = \frac{1}{2}$ (worse fading) has identical pdf and performance as the non-coherent estimation with $m = 1$, i.e. under a better fading scenario.

## 3.6 Extension to Cooperative Location Estimation in the Presence of Fading

In the previous sections, we only considered a sensor network with 1 node and $M$ anchors. However, the results can be extended to a cooperative location estimation problem. In this section, we consider a sensor network with $N$ nodes and $M$ anchors, and we assume all nodes communicate with each other. When the fading coefficients are random with Nakagami distributed amplitude, in 1-D, $\mathrm{E}_{\hat{\tau}_i}\left[\left(\frac{\partial l(\hat{\tau}_i|\mathbf{z})}{\partial \mathbf{z}_j}\right)^2\right]$ is given in (3.18), however, $[\mathbf{F}_\mathbf{z}]_{jk}$ is given as

$$[\mathbf{F}_\mathbf{z}]_{jk} = \begin{cases} \sum_{i=1}^{M+N-1} \mathrm{E}_{\hat{\tau}_i}\left[\left(\frac{\partial l(\hat{\tau}_i|\mathbf{z})}{\partial \mathbf{z}_j}\right)^2\right] & j = k \\ -\mathrm{E}_{\hat{\tau}_i}\left[\frac{\partial^2 l(\hat{\tau}_i|\mathbf{z})}{\partial \mathbf{z}_j \partial \mathbf{z}_k}\right] & j \neq k \end{cases} \tag{3.45}$$

Comparing (3.45) with (3.17), due to the cooperation between nodes, when $j = k$, each node receives information from other nodes as well. Therefore, when $j = k$, (3.45) contains $M + N - 1$ terms. Using the first term of $X(d_i)$ in (3.20), and after simplification, we have

$$\mathrm{E}_{\hat{\tau}_i}\left[\left(\frac{\partial l(\hat{\tau}_i|\mathbf{z})}{\partial \mathbf{z}_j}\right)^2\right] = \frac{\Gamma\left(m+\frac{1}{2}\right)!\left(m+\frac{1}{2}\right)^2}{2\Gamma\left(m+\frac{5}{2}\right)c^2\sigma^2}. \tag{3.46}$$

The CRLB for the $i^{th}$ node is the $(i,i)$ element of $\mathbf{F}_\mathbf{z}^{-1}$, which is given by

$$\mathrm{CRLB}_{\text{1-D}}(\mathbf{z}_i) = \frac{2\Gamma\left(m+\frac{5}{2}\right)c^2\sigma^2}{m\Gamma\left(m+\frac{1}{2}\right)\left(m+\frac{1}{2}\right)^2}\frac{M+1}{M(N+M)}. \tag{3.47}$$

When $m = 1$, the ratio between the cooperative location estimation in (3.47) and the non-cooperative location estimation in (3.25) is $r = (M+1)/(N+M)$. Since $N \geq 1$ in a cooperative network, (3.47) is always equal or smaller than (3.25), which proves that cooperation between nodes gives a lower CRLB. In 2-D, the similar conclusion can be reached.

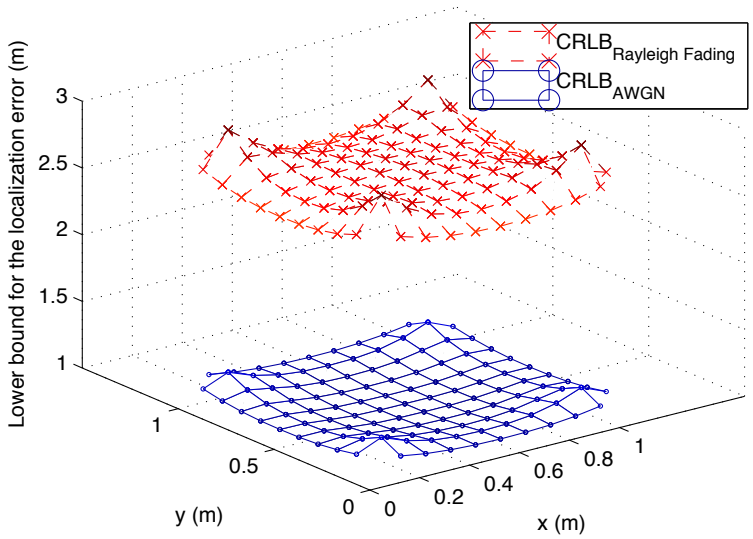


Figure 3.5: CRLBs Comparison Between the non-Fading and the Rayleigh Fading Case. 4 anchors are located in the corners of a 1m $\times$ 1m square. The variance of noise is $\sigma = \frac{1}{c}$.

When no CSI is available at each anchor, with the assumption that the amplitude of fading coefficients is Rayleigh distributed, the pdf of the TOA measurements is given in (3.36). Therefore in 1-D, the CRLB of the $i^{th}$ node in a cooperative WSN with $N$ nodes and $M$ anchors is

$$\text{CRLB}_{\text{1-D}}(\mathbf{z}_i) = \frac{1}{4c^2\sigma^2}\frac{M+1}{M(N+M)}, \tag{3.48}$$

for which the ratio between the cooperative and the non-cooperative is still $r$. Therefore, we can conclude that cooperation between nodes results in a lower CRLB.

## 3.7 Simulation Results

Consider a sensor network with four anchors in the corner of a square, and one node within the square. The fading is Rayleigh distributed. In Figure 3.5 the area of the square is 1m $\times$ 1m. We observe that the loss due to fading is about 2.5 everywhere within the square.

Figure 3.6 shows the loss due to fading as a function of the Nakagami $m$ parameter. As expected, the loss decreases with increasing $m$ and converges to 1.

In Figure 3.7 we consider a 1m $\times$ 1m square, 4 anchors are in the corners, and 1 node is in the middle of the square. We compare estimators (3.30) and (3.31) both in the presence of fading by plotting the normalized SNR (with respect to $c^2$) vs. the variance of localization error in Figure

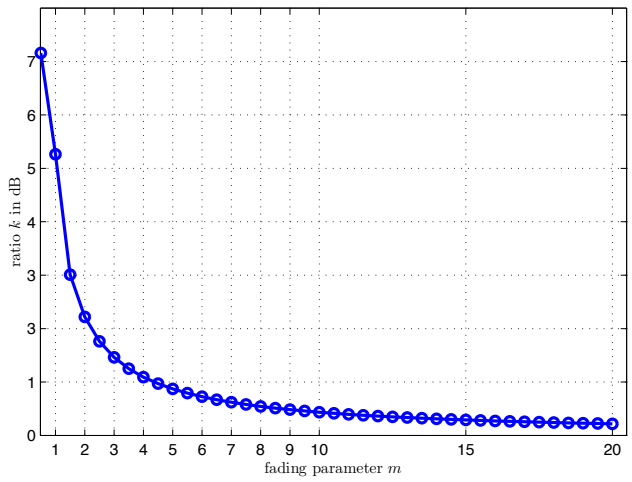


Figure 3.6: The Ratio $k$ in (3.23) versus the Nakagami $m$ Parameter.

As $m$ increases, $k$ decreases. When $m \geq 15$, $k = 0$dB, which indicates that the CRLB when the fading exists converges to the AWGN case.

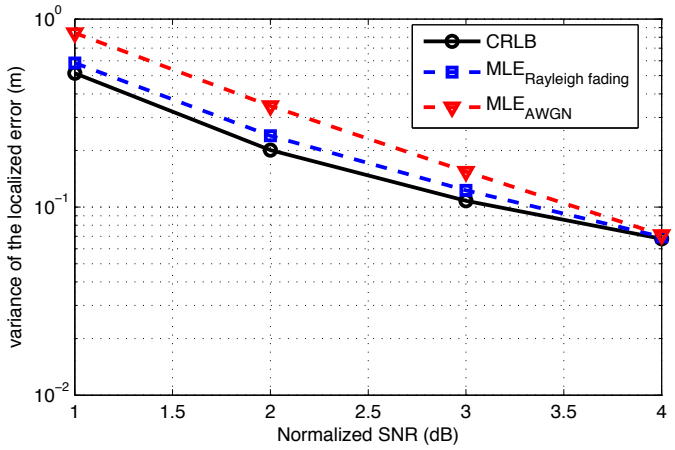


Figure 3.7: ML Estimators Comparison.

3.7. We observe that the fading ML estimator (3.30) performs better than the AWGN ML estimator (3.31) in the presence of fading.

Figure 3.8 shows the CRLB comparison in 1-D between the AWGN case and the presence of Rayleigh fading. From the fading one can see that in the high SNR regime, to maintain the same variance of localization error, CRLB in the presence of Rayleigh fading needs about 5dB more power than the AWGN case.

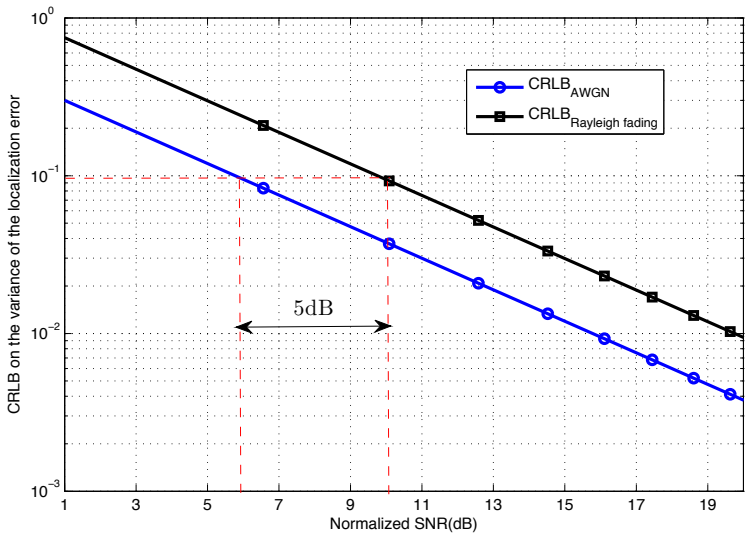


Figure 3.8: CRLB Comparison When SNR is Large.

## 3.8 Conclusions

In this chapter, we derived CRLBs in the presence of fading under TOA measurements. Fading coefficients are first considered as random parameters with a prior Nakagami distribution, the CRLB is derived by averaging out the effect of fading. Also, by comparing the CRLB in the presence of Rayleigh fading and the AWGN case, it is shown in both 1-D and 2-D, the loss in performance due to Rayleigh fading with known phase is about 5dB compared to the case with no fading. Unknown phase causes an additional 1dB loss. Also, the CRLB in the presence of fading converges to the AWGN case as the fading parameter increases. Meanwhile, the ML estimator in the presence of fading is derived, and is different than the ML estimator for the AWGN case. Secondly, the MCRLB is derived when the prior fading distribution is not known at the estimator. In this case, the MCRLB is the same as the CRLB in the absence of fading, proving that fading always leads to loss in performance.

# Chapter 4

# SEQUENTIAL LOCATION ESTIMATION

In large WSNs, centralized localization algorithms, which require anchors transmit measurements to a fusion center, are hard to implement. On the other hand, distributed algorithms, such as the sequential localization algorithm, are more power efficient. However, the localization errors will propagate through the network during the iterative localization process. This is because it is assumed that the estimated locations of nodes are the actual locations. In this chapter, the TOA, TDOA, RSS, DOA and LAA localization algorithms will be expressed as the solution to a set of linear equations. Following this, the performance of a sequential network discovery process when using these different localization algorithms will be compared under different SNR regimes. Also, since the errors will propagate through the network, it is important to study the error characteristics of the sequential localization. Specifically, the CRLB, which provides a performance benchmark for the sequential localization scheme by using the TOA measurement is studied in this chapter. In addition, we consider the sequential localization scheme using the TOA measurement in the absence and in the presence of fading respectively. The sequential localization scheme is compared with the non-sequential localization scheme in [31], and the SNR loss due to the sequential localization scheme is derived. Meanwhile, for the sequential localization scheme, the CRLB when the fading is absent case is compared with the fading is present case, and the SNR loss due to fading is derived.

## 4.1 Performance Comparison of Localization Techniques for Sequential Location Estimation

Consider a homogeneous wireless sensor network with a large number of nodes at random unknown locations in $\mathbb{R}^2$ space. Assume that a small number of anchors at known locations are included in this network. Specifically, we assume the initial number of anchors is $M$, and the initial number of nodes is $N$, where $N \gg M$. Each node or anchor has a circular coverage area with radius $r$, and operates at the frequency $F_c$. The cartesian coordinate of the $i^{th}$ node is denoted by $\mathbf{z}_i$. The locations of all nodes at unknown locations using different localization algorithms. Each algorithm requires a different minimum number of anchors or previously localized nodes for localization to

take place. In $\mathbb{R}^2$ space, for DOA, $M_{\min} = 2$, for TOA, TDOA and RSS, $M_{\min} = 3$ and for LAA, $M_{\min} = 4$.

The sequential location estimation process used in this chapter is described in [38] and may be summarized as follows: Initially, one node transmits at an unknown location in the coverage area of the anchor nodes. If $M_{\min}$ nodes (anchors or the previously localized nodes) are within the coverage area of the node then the node location is estimated. If more than $M_{\min}$ nodes are available, all the available nodes will be used for localization. Otherwise this node is skipped. Following this, another node transmits and the process continues with more nodes at estimated locations being available to perform localization of other nodes. Once localization has been attempted at all nodes, the process is repeated from the beginning, a total of $K$ times. This gives an opportunity for skipped nodes to be revisited in the hope that more nodes in the vicinity of the troublesome nodes will now be at estimated locations to meet the $M_{\min}$ node requirement. In addition, nodes whose locations were successfully estimated may be gradually refined using data fusion techniques (including simple schemes such as averaging).

As errors in the sequential localization algorithm propagate during the estimation process, the choice of the first nodes becomes significantly important. As the anchors will be more likely within the limited coverage area of the closest transmitting nodes, these closest nodes will be localized first. Multiple location estimates are needed to diminish the effect of localization order and noise.

We define $\mathbf{z}$ as the location of a node that needs to be localized, the location of the node may be estimated from measurements from a set of anchors, which are located at $\mathbf{p}_1, \mathbf{p}_2, \cdots, \mathbf{p}_M$, by solving the following set of linear equations:

$$\mathbb{H}\mathbf{z} = \mathbf{b}, \tag{4.1}$$

where the matrix $\mathbb{H}$ and the vector $\mathbf{b}$ are dependent upon the geometry of the receiving anchors with respect to the transmitting node as well as metrics constructed from the data that nodes receive. Hence, (4.1) provides a unified notation allowing solutions to different localization approaches

in the literature to be found. Table 4.1 shows the structure of $\mathbb{H}$ and $\mathbf{b}$ for a selection of common localization algorithms in $\mathbb{R}^2$ space. For the TOA approach, $\hat{\tau}_i$ represents the estimated propagation time of the line-of-sight (LOS) signal between the node (at $\mathbf{z}$) and the $i^{th}$ anchor. For the TDOA approach, $\hat{\tau}_{i1}$ is the time difference from when the LOS signal arrives at the $1^{st}$ anchor to when it arrives at the $i^{th}$ anchor. For the RSS approach, $\hat{d}_i^2$ is the estimated distance between the $i^{th}$ anchor and the node. For the DOA approach, $\theta_i$ and $\rho_i$ represent the angle and range associated with the $i^{th}$ array which has an array reference point at $\mathbf{p}_i$. The angles are estimated using a DOA algorithm (eg. MUSIC [79]), and the ranges to the source may be easily inferred via the sine rule using these estimated directions of arrival and the locations of the array reference points. For example, the triangle $\mathbf{p}_1$, $\mathbf{p}_2$ and $\mathbf{p}_3$,

$$\rho_1 = \frac{\|\mathbf{p}_2 - \mathbf{p}_1\| \sin(\pi - \theta_2 + \psi_{12})}{\sin(\theta_2 - \theta_1)}, \tag{4.2}$$

$$\rho_2 = \frac{\|\mathbf{p}_2 - \mathbf{p}_1\| \sin(\theta_1 - \psi_{12})}{\sin(\theta_2 - \theta_1)}, \tag{4.3}$$

where $\psi_{12}$ is the known angle between the first and second array reference points. Finally, for the LAA approach, $\mathbf{z}$ from (4.1) is a 4 element evector with the final element equal to $\|\mathbf{z}\|^2$ and $\underline{\mathscr{K}} \in \mathbb{R}^{(M-1)\times 1}$ is constructed by rotating the array reference point [34, 38, 61] with reference to a global reference point set at the origin. Note that this is the only approach which uses sensors collectively as a single array system [38].

### 4.1.1 Simulation Results

Consider a two-dimensional 600m$\times$600m sensor field as shown in Figure 4.5. Assume $M = 4$ anchors denoted by blue triangles are placed at known locations in the centre of the field. These anchors are surrounded by 200 sensor nodes denoted by green circles placed randomly at unknown locations following a two dimensional uniform distribution. All nodes transmit at a frequency of $F_c = 2.45$GHz. Each node has a transmission range of $r = 100$m and transmits $L = 100$ snapshots of sinusoid signals. A propagation constant of $a = 4$ exists in the simulation environment and it is assumed that their is no flat frequency fading or multipath. Localization of each transmitting node is attempted $K = 200$ times, after which if no location estimate was made it is declared undiscovered.

| | | |
|---|---|---|
| <u>TOA</u> | | |
| $\mathbb{H}$ | $=$ | $[\mathbf{p}_2-\mathbf{p}_1, \mathbf{p}_3-\mathbf{p}_1, \cdots, \mathbf{p}_M-\mathbf{p}_1]^T$ |
| | $\in$ | $\mathbb{R}^{(M-1)\times 2}$ |
| $\mathbf{b}$ | $=$ | $\frac{1}{2}\begin{bmatrix} \|\mathbf{p}_2\|^2-\|\mathbf{p}_1\|^2-c^2\left(\hat{\tau}_2^2-\hat{\tau}_1^2\right) \\ \|\mathbf{p}_3\|^2-\|\mathbf{p}_1\|^2-c^2\left(\hat{\tau}_3^2-\hat{\tau}_{10}^2\right) \\ \vdots \\ \|\mathbf{p}_M\|^2-\|\mathbf{p}_1\|^2-c^2\left(\hat{\tau}_M^2-\hat{\tau}_1^2\right) \end{bmatrix}$ |
| | $\in$ | $\mathbb{R}^{(M-1)\times 1}$ |
| <u>TDOA</u> | | |
| $\mathbb{H}$ | $=$ | $[\mathbf{p}_2-\mathbf{p}_1, \mathbf{p}_3-\mathbf{p}_1, \cdots, \mathbf{p}_M-\mathbf{p}_1]^T$ |
| | $\in$ | $\mathbb{R}^{(M-1)\times 2}$ |
| $\mathbf{b}$ | $=$ | $\frac{1}{2}\begin{bmatrix} \|\mathbf{p}_2\|^2-\|\mathbf{p}_1\|^2-c^2\left(\hat{\tau}_{21}^2+2\hat{\tau}_1\cdot\hat{\tau}_{21}\right) \\ \|\mathbf{p}_3\|^2-\|\mathbf{p}_1\|^2-c^2\left(\hat{\tau}_{31}^2+2\hat{\tau}_1\cdot\hat{\tau}_{31}\right) \\ \vdots \\ \|\mathbf{p}_M\|^2-\|\mathbf{p}_1\|^2-c^2\left(\hat{\tau}_{M1}^2+2\hat{\tau}_1\cdot\hat{\tau}_{M1}\right) \end{bmatrix}$ |
| | $\in$ | $\mathbb{R}^{(M-1)\times 1}$ |
| <u>RSS</u> | | |
| $\mathbb{H}$ | $=$ | $[\mathbf{p}_2-\mathbf{p}_1, \mathbf{p}_3-\mathbf{p}_1, \cdots, \mathbf{p}_M-\mathbf{p}_1]^T$ |
| | $\in$ | $\mathbb{R}^{(M-1)\times 2}$ |
| $\mathbf{b}$ | $=$ | $\frac{1}{2}\begin{bmatrix} \|\mathbf{p}_2\|^2-\|\mathbf{p}_1\|^2-\left(\hat{d}_2^2-\hat{d}_1^2\right) \\ \|\mathbf{p}_3\|^2-\|\mathbf{p}_1\|^2-\left(\hat{d}_3^2-\hat{d}_1^2\right) \\ \vdots \\ \|\mathbf{p}_M\|^2-\|\mathbf{p}_1\|^2-\left(\hat{d}_M^2-\hat{d}_1^2\right) \end{bmatrix}$ |
| | $\in$ | $\mathbb{R}^{(M-1)\times 1}$ |
| <u>DOA</u> | | |
| $\mathbb{H}$ | $=$ | $\mathbf{p}_1\otimes\mathbb{I}_2$ |
| | $\in$ | $\mathbb{R}^{2M\times 2}$ |
| $\mathbf{b}$ | $=$ | $\begin{bmatrix} \mathbf{p}_1+\rho_1\cdot[\cos\theta_1, \sin\theta_1]^T \\ \mathbf{p}_2+\rho_2\cdot[\cos\theta_2, \sin\theta_2]^T \\ \vdots \\ \mathbf{p}_M+\rho_M\cdot[\cos\theta_M, \sin\theta_M]^T \end{bmatrix}$ |
| | $\in$ | $\mathbb{R}^{2M\times 1}$ |
| <u>LAA</u> | | |
| $\mathbb{H}$ | $=$ | $\begin{bmatrix} 2\left(\underline{1}_{M-1}\mathbf{p}_1^T-[\mathbf{p}_2, \mathbf{p}_3, \cdots, \mathbf{p}_M]^T\right) \\ \left(\underline{1}_{M-1}-\underline{\mathscr{K}}^2\right) \end{bmatrix}$ |
| | $\in$ | $\mathbb{R}^{(M-1)\times 2}$ |
| $\mathbf{b}$ | $=$ | $\left[\|\mathbf{p}_1\|^2\underline{1}_{M-1}-\left[\|\mathbf{p}_2\|^2, \|\mathbf{p}_3\|^2, \cdots, \|\mathbf{p}_M\|^2\right]^T\right]$ |
| | $\in$ | $\mathbb{R}^{(M-1)\times 1}$ |

Table 4.1: Linear Equations for Node Localization Using TOA, TDOA, RSS, DOA and LAA techniques in $\mathbb{R}^2$ Space.

(see Equation 4.1 and Figures 4.1 - 4.4).

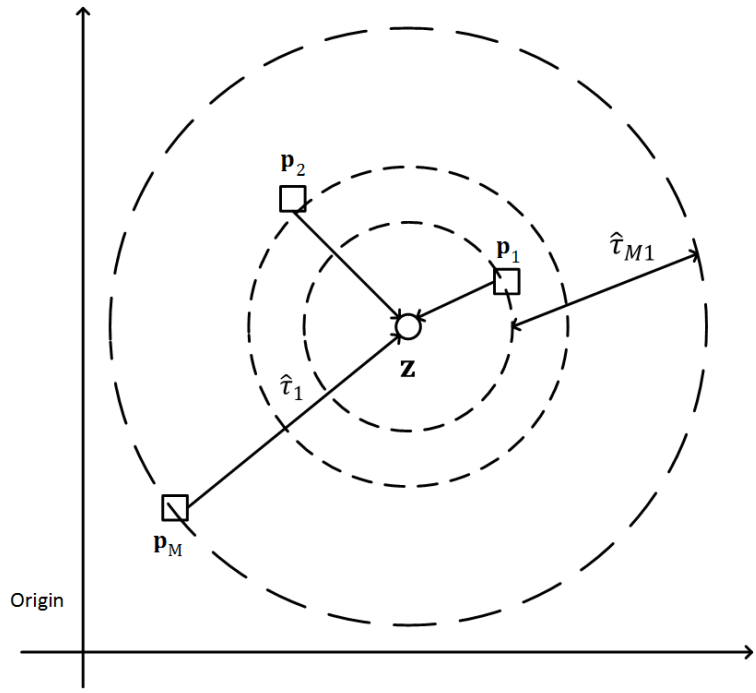


Figure 4.1: TOA/TDOA Based Localization of A Node Located at $\mathbf{z}$ Using $M$ Anchors at Locations $\mathbf{p}_1, \mathbf{p}_2, \ldots, \mathbf{p}_M$.

In Figure 4.5, the results of the sequential discovery process using LAA localization is shown. Estimated locations are represented using red crosses. Two of the nodes remain undiscovered because there are not enough nodes in their coverage range for localization.

Figure 4.6 shows the performance of TOA, TDOA, RSS, DOA and LAA techniques. RMSE values are plotted for different values of SNR $\times L$. From the figure one can see that for all techniques, average RMSE decreases as SNR $\times L$ increases. This is expected as noise reduces and more data is available to produce more statistically efficient metrics. When SNR $\times L$ is below 70dB, DOA has the best performance. However, when the SNR $\times L$ is greater than 70dB, LAA exceeds its performance. Note that the TOA and TDOA schemes are markedly poor due to bandwidth limitations. While the performance of the RSS regime is good in this simulation environment, under scenarios with more complex channel effects, performance will be rapidly degraded.

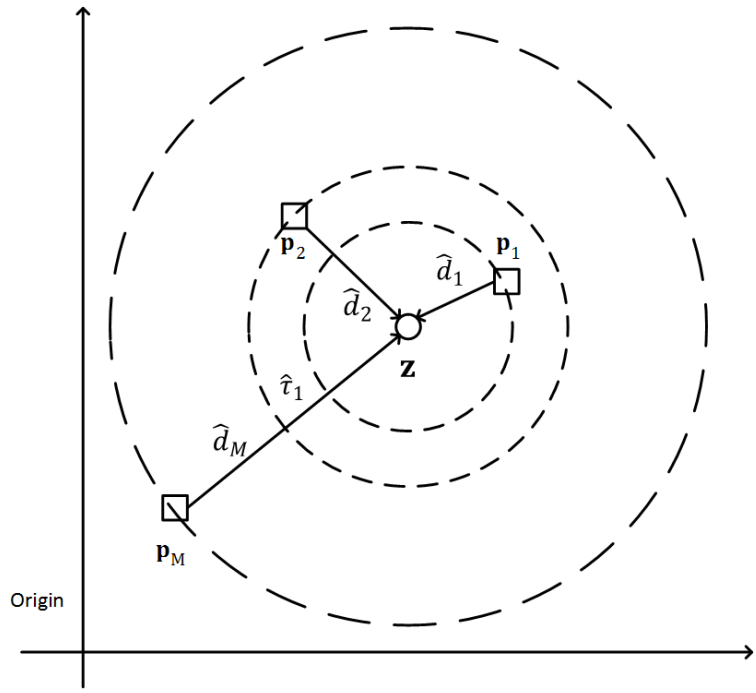


Figure 4.2: RSS Based Localization of A Node Located at $\mathbf{z}$ Using $M$ Anchors at Locations $\mathbf{p}_1, \mathbf{p}_2, \ldots, \mathbf{p}_M$.

## 4.2 CRLB for Sequential Localization in the Absence of Fading

In the previous section, different measurements are compared under different SNR regimes. Since the errors will propagate through the network, it is important to study the error characteristics of the sequential localization theoretically. Therefore, the CRLB is adopted in this section to evaluate the performance of sequential localization. Specifically, the TOA measurement is applied to the sequential localization algorithm.

We assume a sequential localization scheme, in which only one node is localized at a time. After a node is localized, it becomes an anchor and is used to localize other nodes. Therefore, the number of the anchors increases by 1 at each step. At the last step, the last node communicates with all anchors and the previously localized nodes. Figure 4.7 shows the system model of the sequential localization scheme. In this WSN, there is a total of $M$ anchors and $N$ nodes. At the first step, to localize node 1, all anchors make measurements between anchors and node 1. Once node 1 is localized, it becomes an anchor. At the second step, to localize node 2, all anchors and node

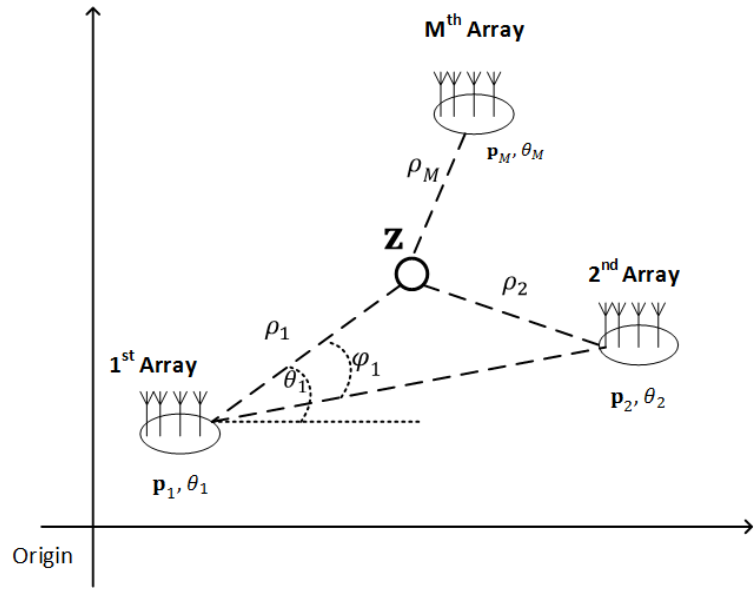


Figure 4.3: DOA Based Localization of A Node Located at $\mathbf{z}$ Using $M$ Arrays with Local Geometries $\mathbf{p}_1, \mathbf{p}_2, \ldots, \mathbf{p}_M$ and DOAs $\theta_1, \theta_2, \ldots, \theta_M$.

1 make measurements. Therefore, an additional measurement is used to estimate the location of node 2. We assume the TOA measurement is used to estimate node locations.

Assume each node communicates with all anchors and previously localized nodes. Define the TOA measurement between the $i^{th}$ node and the $j^{th}$ node or anchor as $\hat{\tau}_{ij}$, where $i = \{1, 2, \ldots, N\}$, $j = \{1, 2, \ldots, N, N+1, \ldots, N+M\}$, and $i \neq j$. Also, $\hat{\tau}_{ij}$ is Gaussian distributed with [31], and is given by

$$\hat{\tau}_{ij} \sim \mathcal{N}\left(\frac{d_{ij}}{c}, \sigma^2\right), \tag{4.4}$$

where $c$ is the speed of propagation of signals in the free space, $\frac{d_i}{c}$ is the true distance between the $i^{th}$ node and the $j^{th}$ node or anchor, and $\sigma^2$ is the variance of the TOA measurements. Therefore, the log likelihood function between the $i^{th}$ node and the $j^{th}$ node or anchor can be written as

$$l(\hat{\tau}_{ij}|\mathbf{z}) = \log \frac{1}{\sqrt{2\pi\sigma^2}} - \frac{\left(\hat{\tau}_{ij} - \frac{||\mathbf{z}_i - \mathbf{z}_j||^2}{c}\right)^2}{2\sigma^2}, \tag{4.5}$$

here $\mathbf{z}_i$ is the location of the $i^{th}$ node, $\mathbf{z}_j$ is the location of the $j^{th}$ node or anchor, and $i \neq j$. Define

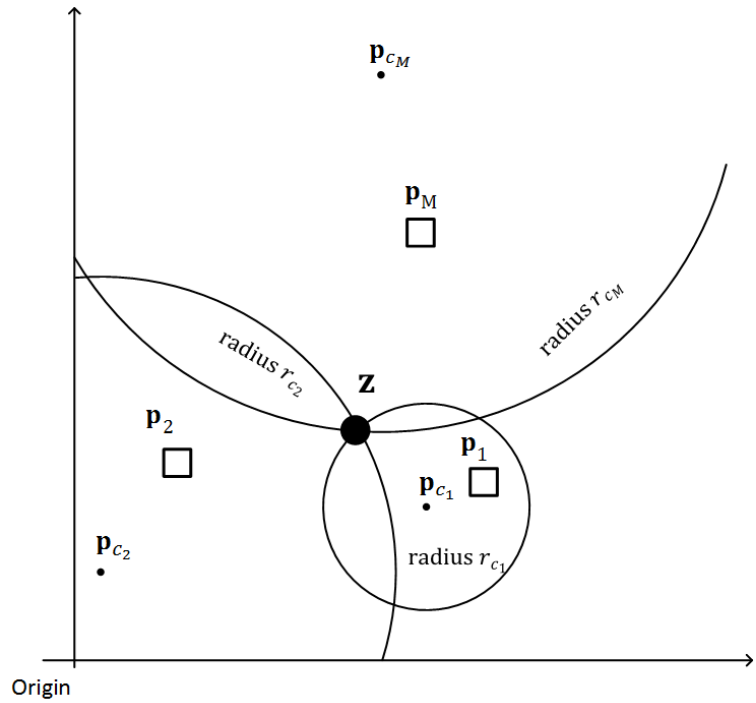


Figure 4.4: LAA Based Localization of A Node Located at $\mathbf{z}$ Using $M$ Anchors at Known Locations $\mathbf{p}_1, \mathbf{p}_2, \ldots, \mathbf{p}_M$ and AOAs $\theta_1, \theta_2, \ldots, \theta_M$.

Here $r_{c_i}$ and $\mathbf{p}_{c_j}$ denote the radius and center of the $j^{th}$ circular locus which may be used to estimate the node location.

$\mathbf{F_z}$ as the $N \times N$ FIM, and each element is given as

$$[\mathbf{F_z}]_{ij} = \begin{cases} \sum_{k=1}^{M} \mathrm{E}_{\hat{\tau}_{ik}} \left[ \left( \frac{\partial l(\hat{\tau}_{ik}|\mathbf{z}_k)}{\partial \mathbf{z}_i} \right)^2 \right] + \sum_{k=1}^{i-1} \mathrm{E}_{\hat{\tau}_{ik}} \left[ \left( \frac{\partial l(\hat{\tau}_{ik}|\mathbf{z}_k)}{\partial \mathbf{z}_k} \right)^2 \right] & j = i \\ -\mathrm{E}_{\hat{\tau}_{ij}} \left[ \frac{\partial^2 l(\hat{\tau}_{ij}|\mathbf{z}_i)}{\partial \mathbf{z}_i \partial \mathbf{z}_j} \right] & j \neq i \end{cases} \tag{4.6}$$

In (4.6), when $j = i$, the first term is the Fisher information from all anchors, and the second term is the Fisher information from all $i-1$ localized nodes. Recall that for the non-sequential localization scheme, when nodes communicate with all other nodes, the summation limit in the second term is from $k = 1$ to $N-1$.

In 1-D, the location of a node or anchor $\mathbf{z} = x$, which is a scalar. The expectation of the second derivative of (4.5) gives $\mathrm{E}_{\hat{\tau}_{ij}} \left[ \left( \frac{\partial l(\hat{\tau}_{ij}|\mathbf{z}_i)}{\partial \mathbf{z}_i} \right)^2 \right] = \frac{1}{c^2 \sigma^2}$. Therefore, the Fisher information matrix

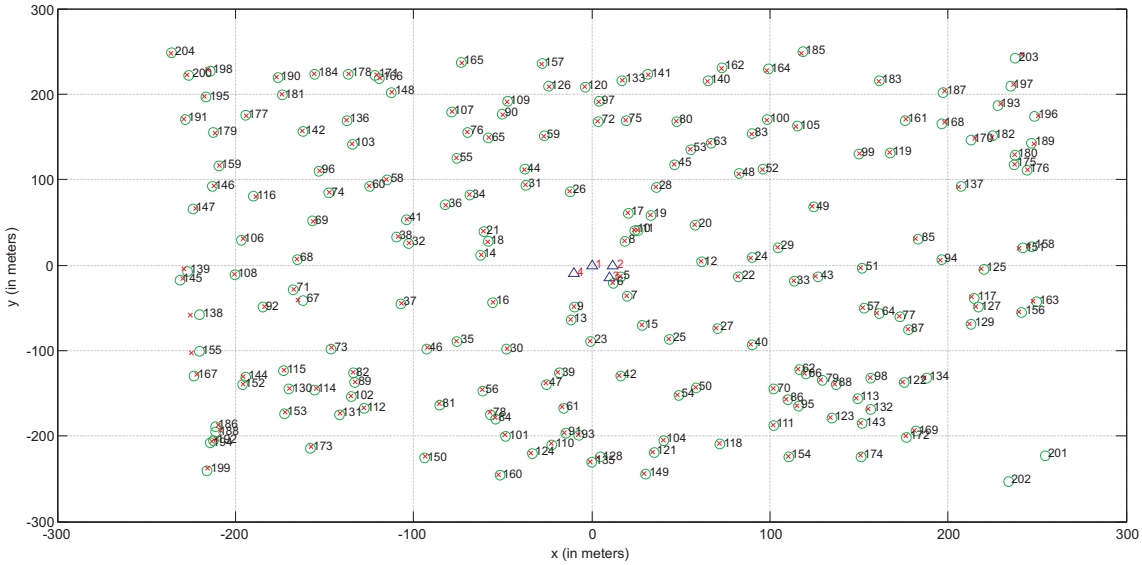


Figure 4.5: Sequential Discovery Using LAA Technique.

Each node having a coverage of $r = 100$m and SNR $= 30$dB; $K = 200$. Green circles represent actual node locations, blue triangles represent anchor nodes at known locations, and red crosses represent location estimates. All but nodes 201 and 202 are localized. Location uncertainties can be seen more predominantly at the edges of the network.

is

$$\mathbf{F_z} = \frac{1}{c^2\sigma^2}\begin{bmatrix} M & -1 & \dots & \dots & -1 \\ -1 & M+1 & -1 & \dots & -1 \\ \vdots & \dots & \ddots & \vdots & \vdots \\ -1 & -1 & \dots & \dots & M+N-1 \end{bmatrix}. \tag{4.7}$$

Define $\sigma_{x_i}^2$ as the variance of the $i^{th}$ node location, using Sherman-Morrison formula, $\sigma_{x_i}^2$ satisfies the following inequality, which is given by

$$\sigma_{x_i}^2 \geq c^2\sigma^2\left(\frac{1}{M+i} + \frac{1}{1-\sum_{i=0}^{N}\frac{1}{M+i}}\frac{1}{(M+i)^2}\right). \tag{4.8}$$

Note that the right hand side of the inequality is the CRLB on the variance of the $i^{th}$ estimated node location. Since the last node communicates with all previously localized node and anchors, we are more interested in the last node. Define CRLB$(x_N)$ as the CRLB on the variance of the last node location, we can derive the CRLB as

$$\text{CRLB}(x_N) = c^2\sigma^2\frac{1}{(M+N)^2}\left(M+N+\frac{1}{1+\frac{\Gamma'(1+M)}{\Gamma(1+M)}-\frac{\Gamma'(1+M+N)}{\Gamma(1+M+N)}}\right). \tag{4.9}$$

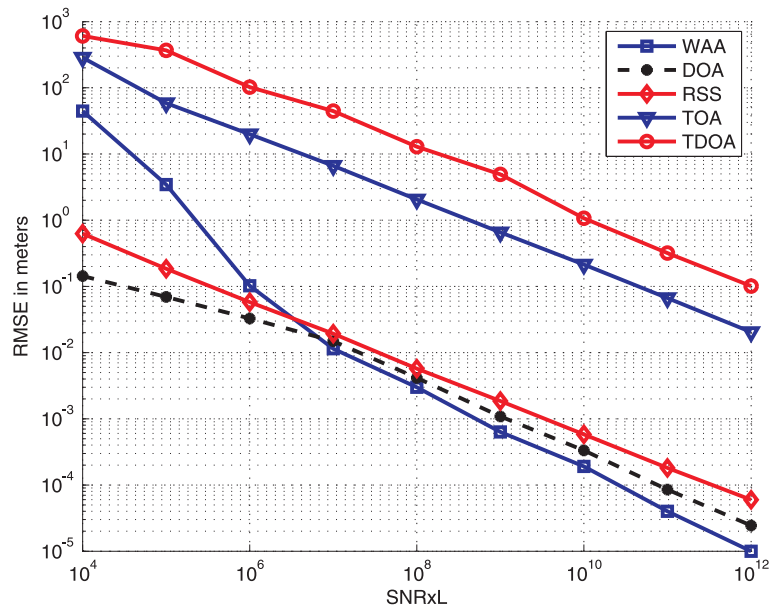


Figure 4.6: Performance Comparison of Different Localization Techniques for Network Discovery. System parameters are $r = 100$m; $L = 100$; $K = 200$. Average RMSE is plotted vs. SNR$\times L$.

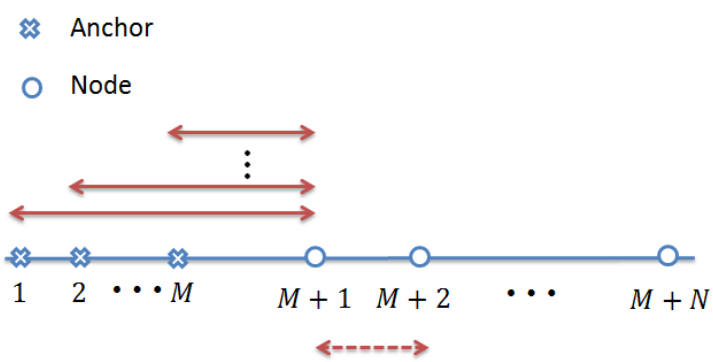


Figure 4.7: System Model of the 1-D Sequential Localization Scheme.

here $\Gamma'(\cdot)$ is the derivative with respect to $\Gamma$, and $\frac{\Gamma'(x)}{\Gamma(x)} = \phi(x)$, which is defined as polygamma function. When $N >> M$, (4.9) can be simplified as

$$\text{CRLB}(x_N) \approx \frac{1}{N^2}\left(N + \frac{1}{\frac{M+1}{M} - \phi(N)}\right) = \frac{1}{N}. \tag{4.10}$$

Therefore, the sequential localization CRLB goes to 0 as $\frac{1}{N}$. Recall that when non-sequential localization scheme is applied, when $N >> M$,

$$\text{CRLB}(x_N) \approx \frac{1}{MN}, \tag{4.11}$$

therefore, the ratio between the sequential localization CRLB and the non-sequential localization CRLB is

$$k = \frac{\text{CRLB}_{\text{1-D}}^{\text{Sequential}}}{\text{CRLB}_{\text{1-D}}^{\text{AWGN}}} = \frac{1}{M}, \tag{4.12}$$

which indicates that the non-sequential localization CRLB goes to 0 is $M$ times faster than the sequential localization CRLB.

In 2-D, $\mathbf{F_z}$ is given as

$$\mathbf{F_z} = \begin{bmatrix} \mathbf{F}_{xx} & \mathbf{F}_{xy} \\ \mathbf{F}_{xy}^T & \mathbf{F}_{yy} \end{bmatrix}, \tag{4.13}$$

where $\mathbf{F}_{xx}$, $\mathbf{F}_{xy}$ and $\mathbf{F}_{yy}$ are $N \times N$ matrix. Each element of $\mathbf{F_z}$ is given as

$$[\mathbf{F}_{xx}]_{ij} = \begin{cases} \frac{1}{c^2\sigma^2}\left(\sum_{k=1}^{M}\frac{(x_k-x_i)^2}{d_{ik}^2} + \sum_{k=1}^{i-1}\frac{(x_k-x_i)^2}{d_{ik}^2}\right) & j = i \\ -\frac{1}{c^2\sigma^2}\frac{(x_i-x_j)^2}{d_{ij}^2} & j \neq i \end{cases} \tag{4.14}$$

$$[\mathbf{F}_{xy}]_{ij} = \begin{cases} \frac{1}{c^2\sigma^2}\left(\sum_{k=1}^{M}\frac{(x_k-x_i)(y_k-y_i)}{d_{ik}^2} + \sum_{k=1}^{i-1}\frac{(x_k-x_i)(y_k-y_i)}{d_{ik}^2}\right) & j = i \\ -\frac{1}{c^2\sigma^2}\frac{(x_i-x_j)(y_k-y_i)}{d_{ij}^2} & j \neq i \end{cases} \tag{4.15}$$

$$[\mathbf{F}_{yy}]_{ij} = \begin{cases} \frac{1}{c^2\sigma^2}\left(\sum_{k=1}^{M}\frac{(y_k-y_i)^2}{d_{ik}^2} + \sum_{k=1}^{i-1}\frac{(y_k-y_i)^2}{d_{ik}^2}\right) & j = i \\ -\frac{1}{c^2\sigma^2}\frac{(y_i-y_j)^2}{d_{ij}^2} & j \neq i \end{cases} \tag{4.16}$$

The CRLB can be computed using

$$\text{CRLB}(\mathbf{z}) = (F_z)^{-1}. \tag{4.17}$$

## 4.3 CRLB for Sequential Localization in the Presence of Nakagami Fading

Similar to section 4.2, we assume there are $M$ anchors and $N$ nodes. When Nakagami fading exists, the pdf of TOA measurements is given as [80]

$$f_{\hat{\tau}_{ii}}(\hat{\tau}_{ij}|\mathbf{z}) = \frac{m^m(m-\frac{1}{2})!}{\sqrt{2\pi\sigma^2}\Gamma(m)\left(\frac{1}{2\sigma^2}(\hat{\tau}_{ij}-\frac{d_i}{c})^2+m\right)^{(m+\frac{1}{2})}}, \tag{4.18}$$

here $m$ is the Nakagami fading parameter. The CRLB in 1-D and 2-D can be derived using the similar approach. The ratio between sequential location estimation in the presence of Nakagami

fading and sequential location estimation in the absence of fading is given as

$$\frac{\text{CRLB}_{\text{1-D}}^{\text{Sequential Fading}}}{\text{CRLB}_{\text{1-D}}^{\text{Sequential}}} \approx k = \frac{\sqrt{\pi}\Gamma(m+\frac{5}{2})}{\Gamma(\frac{3}{2})(m+\frac{1}{2})^2\left(m-\frac{1}{2}\right)!}. \tag{4.19}$$

When $m = 1$, the fading is Rayleigh distributed, and the ratio is

$$k = \frac{10}{3}. \tag{4.20}$$

Similarly, we can derive the ratio in 2-D, which is the same as in (4.20).

Recall from Chapter 3 that in the non-sequential approach, the ratio between the CRLB in the presence of Nakagami fading and the absence of fading equals to $k$, which indicates that in both non-sequential and sequential localization approaches, the SNR loss due to fading is always about 5dB.

### 4.3.1 Simulation Results

In the simulation, we compare the sequential CRLB with the non-sequential CRLB in [31]. First, we assume inside a 10 by 10 square, there are four anchors located at each corner of the square. The node that has the minimum summed distance to 4 anchors is localized first, followed by the node has further summed distance, and the node has the furthest summed distance to anchors is localized at the last step. Figure 4.8 shows the CRLBs comparison between the sequential and non-sequential localization scheme using the TOA method. From the figure one can see that the non-sequential scheme always outperforms the sequential localization scheme for all nodes. Also, as the number of localized nodes increases, the normalized CRLB decreases. In Figure 4.9, we compare the CRLB when the total number of nodes $N = 10$ and $N = 100$ cases, and the CRLB for the first 10 localized nodes are plotted. From the figure one can see that when the number of nodes increases, the CRLB decreases.

## 4.4 Conclusions

In this chapter, we proposed a sequential localization scheme, and studied the CRLB for the sequential localization scheme in the absence and in the presence of fading. We derived the ratio between the sequential localization scheme and the non-sequential localization scheme. Also, we

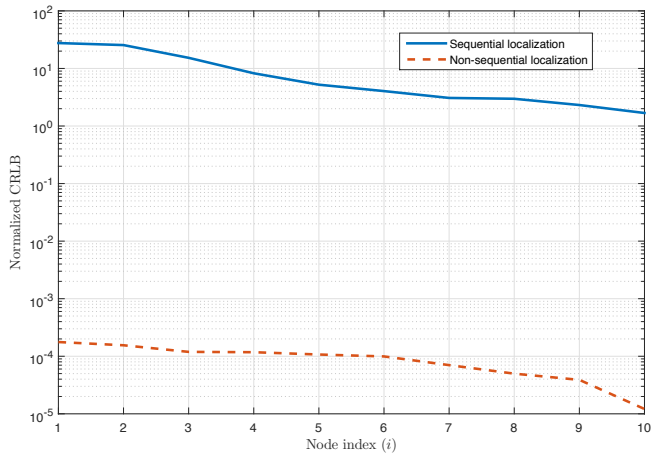


Figure 4.8: Comparisons Between the Sequential CRLB with the Non-sequential CRLB when $N = 10$ Nodes Located Inside a $10 \times 10$ Square.

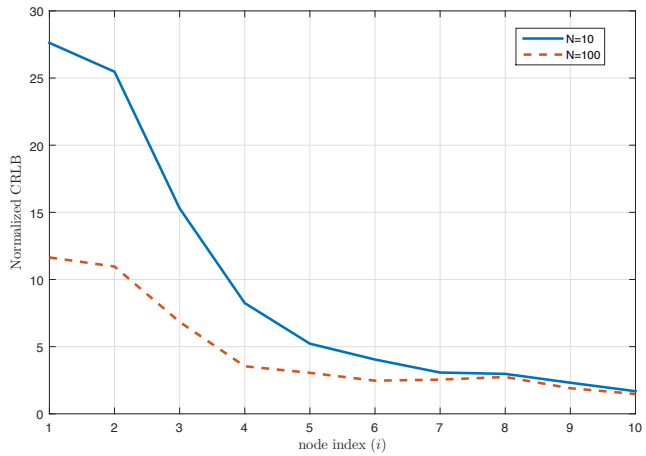


Figure 4.9: Comparisons Between the Sequential CRLB with the Sequential CRLB When $N = 10$ Nodes and $N = 100$ Nodes Located Inside a $10 \times 10$ Square.

compared the CRLBs of the sequential localization in the absence and in the presence of fading, and the result shows that the SNR loss due to fading is also 5dB, which is the same as the non-sequential localization scheme.

# Chapter 5

# DISTRIBUTED LOCATION DETECTION

Localization problems can be classified as location estimation and location detection problems. In the estimation formulation, one or more nodes at unknown locations transmit signals to anchors, and anchors make distance related measurements, such as TOA and RSS, or angle related measurements, such as AOA to locate the node [31, 81]. In Chapter 3 we have considered the case that the location of the node is unknown. However, in some applications, the node location is known to all anchors, but whether the node is active or not is unknown. In many applications such as detecting fire in buildings, each node is placed inside a room, and the location is known to all anchors. Anchors detect an event based on whether the node is transmitting. In location detection, the goal is to determine the presence or absence of a node in a known location, or more generally an unknown location in a known region. More so than location estimation, the detection problem lends itself to distributed implementation based on exchange of bits between the anchors and a fusion center. Moreover, in some cases, location detection needs fewer anchors to detect the node location than estimation. If a node is present at a known location, anchors or a fusion center declare that the node exists based on certain decision rules. On the other hand, if a node is at an unknown location, detection of the node location can be formulated as a composite hypothesis testing problem, in which case estimation theory can be applied to find the maximum likelihood estimates (MLE) of unknown parameters [53].

In this chapter, we propose a distributed location detection scheme and two scenarios are considered. Firstly, a distributed location detection scheme is proposed where one node, when present, is at a known location. In this scheme, each anchor makes its own decision on whether the node is present at a given location, and transmits the decision by sending a binary bit to a fusion center. The fusion center decides if the node is present based on certain decision rules. Secondly, a distributed location detection scheme is proposed where one node, when present, is at a known region. In this scheme, the node can be located anywhere inside a region. Specifically, we consider a circle with known radius. In both scenarios, a fusion center is used to gather all binary bits from anchors, which is different from the centralized methods in the way that the fusion center only

collects binary data sent by each anchor rather than the actual measurements made by anchors. This scheme also has benefits in terms of power and time efficiency.

## 5.1 Distributed Location Detection at A Point

Consider a sensor network with $M$ anchors and one node. The location of the node is known. Therefore, the true time delay between the node and the $i^{th}$ anchor, which is denoted as $n_i$ is known. Anchors make distance related measurements between the node and anchors. Each anchor makes $N$ i.i.d measurements, and correlates the received signal with the transmitted signal, then the measured time delay can be found by the first peak of the correlation. To detect the node, a binary hypothesis testing problem at each anchor can be formulated with the hypothesis $H_0$ and $H_1$, where

$$x_i[n] = \begin{cases} \omega_i[n] & \text{under } H_0 \\ s_i[n-n_i] + \omega_i[n] & \text{under } H_1 \end{cases}. \tag{5.1}$$

Here $s_i[n]$ is the deterministic transmitted signal and its total energy is $\varepsilon = \sum_{n=0}^{N-1} s_i^2[n]$ is normalized; $n = 0, 1, \ldots, N-1$, a total of $N$ i.i.d measurements are made, and $\omega_i[n]$ is additive Gaussian noise with zero mean and variance $\sigma^2$. If the $i^{th}$ anchor detects the node, it will transmit a bit "1" to the fusion center. Otherwise a bit "0" will be transmitted. After the fusion center receives $M$ bits, it counts the number of "1"s and "0"s. The fusion center needs at least $K$ anchors to send bit "1" to declare the node present.

From (5.1), we can calculate the probability of false alarm $P_{\text{FA}}^i$ and the probability of detection $P_{\text{D}}^i$ at the $i^{th}$ anchor. Define $f(\mathbf{x};H_0)$ is the probability density function (pdf) of $\mathbf{x}$ at the $i^{th}$ anchor under $H_0$, where $\mathbf{x} = [x_i[1], x_i[2], \ldots, x_i[N]]$. Also, define $f(\mathbf{x};H_1)$ as the pdf of $\mathbf{x}_i$ at the $i^{th}$ anchor under $H_1$. Let $L_i(\mathbf{x})$ be the likelihood ratio between the two probabilities $f(\mathbf{x};H_1)$ and $f(\mathbf{x};H_0)$ at the $i^{th}$ anchor. Since the $N$ measurements are i.i.d:

$$L_i(\mathbf{x}) = \frac{f(\mathbf{x};H_1)}{f(\mathbf{x};H_0)} = \frac{\left(2\pi\sigma^2\right)^{-N} \exp\left[-\frac{1}{2\sigma^2}\sum_{n=0}^{N-1}\left(x_i[n]-s_i[n-n_i]\right)^2\right]}{\left(2\pi\sigma^2\right)^{-N} \exp\left[-\frac{1}{2\sigma^2}\sum_{n=0}^{N-1}\left(x_i[n]\right)^2\right]} \lessgtr \gamma_i. \tag{5.2}$$

Define $\mathbf{T}_i(\mathbf{x}) = \ln L_i(\mathbf{x})$, based on the Neyman-Pearson theorem [53], the $i^{th}$ anchor decides $H_1$

if $L_i(\mathbf{x}) > \gamma_i$ and otherwise decides $H_0$, where $\gamma_i$ is a threshold. Taking log of $L_i(\mathbf{x})$, and after simplification, $P_{\mathrm{FA}}^i$ and $P_{\mathrm{D}}^i$ can be calculated as

$$P_{\mathrm{FA}}^i = P\{\mathbf{T}_i(\mathbf{x}) > \gamma_i';\, H_0\} = Q\left(\frac{\gamma_i'}{\sqrt{\frac{\sigma^2}{N}}}\right),$$

and

$$P_{\mathrm{D}}^i = P\{\mathbf{T}_i(\mathbf{x}) > \gamma_i';\, H_1\} = Q\left(\frac{\gamma_i' - \varepsilon}{\sqrt{\frac{\sigma^2}{N}}}\right),$$

where $\mathbf{T}_i(\mathbf{x}) = \frac{1}{N}\sum_{n=0}^{N-1} x_i[n]$ and $\gamma_i' = \frac{\sigma^2}{N\varepsilon}\ln\gamma_i + \frac{\varepsilon}{2}$.

After a decision is made at each anchor, it transmits a "1" or "0" to a fusion center. The fusion center needs at least $K$ "1"s to decide the node is active, where $K$ is a predetermined design parameter. Therefore, the total probability of false alarm $\bar{P}_{\mathrm{FA}}^{\mathrm{T}}$ and the total probability of detection $\bar{P}_{\mathrm{D}}^{\mathrm{T}}$ are given by

$$\bar{P}_{\mathrm{FA}}^{\mathrm{T}} = \sum_{m=K}^{M} \binom{M}{m} \left(P_{\mathrm{FA}}^i\right)^m \left(1 - P_{\mathrm{FA}}^i\right)^{M-m}, \tag{5.3}$$

and

$$\bar{P}_{\mathrm{D}}^{\mathrm{T}} = \sum_{m=K}^{M} \binom{M}{m} \left(P_{\mathrm{D}}^i\right)^m \left(1 - P_{\mathrm{D}}^i\right)^{M-m}. \tag{5.4}$$

### 5.1.1 Simulation Results

We consider a sensor network with 4 anchors in each corner of a 1m by 1m square, and one node is in the center of the square, when present. The Neyman-Pearson detector is used to detect the presence of the node. Each anchor makes its own decision and a bit "1" or "0" will be transmitted to a fusion center. The fusion center counts the number of "1"s. If the total number of "1"s is greater than or equal to $K$, then the fusion center will declare the node exists. For the simulation, we set $N = 5$ and $\sigma = 1$ for all simulations, and Monte Carlo simulations were performed.

Figure 5.1.1 and Figure 5.1.1 show the ROC curves for different $K$ values, and all figures are shown on a log-log scale. Figure 5.1.1 shows the entire plot with $\bar{P}_{\mathrm{FA}}^{\mathrm{T}}$ and $\bar{P}_{\mathrm{D}}^{\mathrm{T}}$ ranging from 0 to 1. In order to see the results clearly, we have zoomed into the figure for low $\bar{P}_{\mathrm{FA}}^{\mathrm{T}}$ values as seen in Figure 5.1.1. We observe that $K = 4$ performs the best and $K = 1$ has the worst performance for

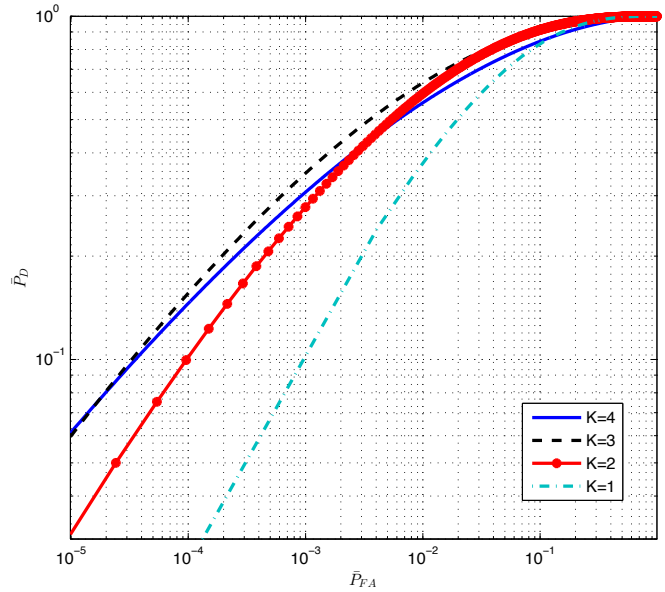


Figure 5.1: The Complete ROC Curve.

a low fixed $\bar{P}_{\text{FA}}^{\text{T}}$. However, in Figure 5.1.1, as $\bar{P}_{\text{FA}}^{\text{T}}$ increases, the system is more tolerant to type I errors. We can see that $K = 4$ is no longer the best choice for a fixed $\bar{P}_{\text{FA}}^{\text{T}}$. From Figure 5.1.1 we can conclude that the choice of $K$ depends on $\bar{P}_{\text{FA}}^{\text{T}}$ and $\bar{P}_{\text{D}}^{\text{T}}$. If the $\bar{P}_{\text{FA}}^{\text{T}}$ is small enough then $K = 4$ can be selected. However, for a higher $\bar{P}_{\text{FA}}^{\text{T}}$, $K = 4$ is not a good choice.

## 5.2 Distributed Location Detection in A Region

In the previous section, we have considered detecting a node at a known location. In this section, instead of a known location, we consider the case that detecting a node in a known region. To formulate the problem, we consider a WSN with $M$ anchors and 1 node. The anchors are outside of a known region, and the node, if actively transmitting, is inside of the region. In the absence of the transmission, each anchor receives pure noise. In the presence of the transmission, each anchor receives signal plus noise. Two distance related measurements are considered. Firstly, the TOA method is used to detect a node in a region. When the TOA method is applied, a correlator is used to extract the time delay, therefore, in the presence of transmission, the estimated distance is extracted. Secondly, the RSS method is applied to detect the node. For the RSS method, the power of the received signal is measured. For both cases, we assume the region is a circle, which is shown

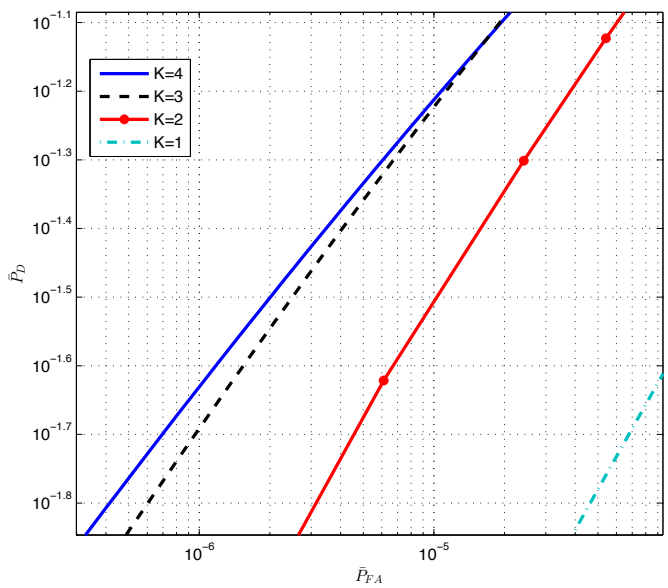


Figure 5.2: ROC Curve When $\bar{P}_{FA}$ is Low.

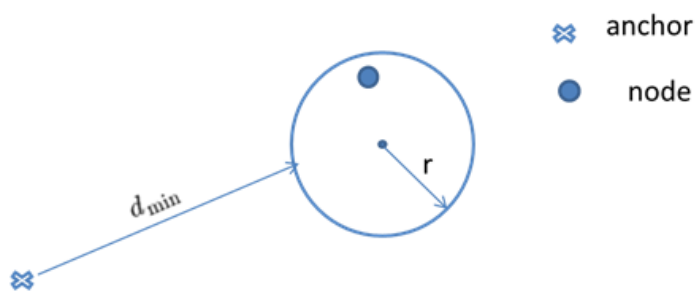


Figure 5.3: System Model for Location Detection in A Circle.

One anchor is located outside a circle with radius $r$, and one node is located inside of the circle with uniform distribution.

in Figure 5.3. The circle has the radius $r$, and one node is uniformly distributed inside the circle. Meanwhile, the minimum distance from an anchor to the region, which is denoted as $d_{\min}$ is also known at each anchor. Each anchor makes its own detection on if the node is transmitting or not. If the $i^{th}$ anchor detects the node, it will transmit a bit "1" to the fusion center. Otherwise a bit "0" will be transmitted. After the fusion center receives $M$ bits, it counts the number of "1"s and "0"s. The fusion center needs at least $K$ anchors to send bit "1" to declare the node present.

### 5.2.1 Detecting A Node in A Region Using the TOA Method

We assume each anchor has the prior information on the distance measurements. Therefore, the detection problem at the $i^{th}$ anchor can be formulated as

$$z_i = \begin{cases} \omega_i & \text{under } H_0 \\ d_i + \omega_i & \text{under } H_1 \end{cases}, \tag{5.5}$$

where $d_i$ is the true distance between the $i^{th}$ anchor and the node, $\omega_i$ is the Gaussian noise with 0 mean and variance $\sigma^2$.

Since the location of the node is uniformly distributed inside a circle, we can write the pdf of $d_i$ as [82]

$$f_{d_i}(x) = \frac{2x}{\pi r^2} \arccos\left[\frac{\left(x^2 + R^2 - r^2\right)}{2xR}\right], \tag{5.6}$$

where $R = r + d_{\min}$, and $d_{\min} \leq x \leq d_{\min} + 2r$. Also, in [82], the $j^{th}$ moment of $d_i$ is given by

$$E\left[d_i^j\right] = R^j \times {}_2F_1\left(-\frac{j}{2}, -\frac{j}{2}, 2; \left(\frac{r}{R}\right)^2\right), \tag{5.7}$$

where ${}_2F_1$ is the Gauss Hypergeometric function. From (5.7) one can calculate the mean and the second moment of $d_i$, which are

$$E\left[d_i\right] = R \times {}_2F_1\left(-\frac{1}{2}, -\frac{1}{2}, 2; \left(\frac{r}{R}\right)^2\right), \tag{5.8}$$

and

$$E\left[d_i^2\right] = \frac{r^2 + 2R^2}{2R^2}. \tag{5.9}$$

From (5.8) and (5.9) we can calculate the variance of $d_i$ as

$$\sigma_{d_i}^2 = E\left[d_i^2\right] - \left(E\left[d_i\right]\right)^2 = \frac{r^2 + 2R^2}{2R^2} - \left(R \times {}_2F_1\left(-\frac{1}{2}, -\frac{1}{2}, 2, \left(\frac{r}{R}\right)^2\right)\right)^2. \tag{5.10}$$

Therefore, conditional on $d_i$, the Neyman-Pearson detector at the $i^{th}$ anchor can be formulated as

$$L(z_i) = \frac{f(z_i; H_1)}{f(z_i; H_0)} = \frac{f_{d_i}(x) * f_{\omega_i}(x)}{f_{\omega_i}(z_i)} \lessgtr \gamma_i. \tag{5.11}$$

Here, $f_{d_i}(x) * f_{\omega_i}(x)$ is the convolution between two pdfs, which is $\int_{R+r}^{R-r} f_{d_i}(x) f_{\omega_i}(z-x)\,dx$. Also, $f_{\omega_i}(x)$ is the pdf of the noise, which is denoted as $f_{\omega_i}(x) = \frac{1}{\sqrt{2\pi\sigma^2}} \exp\left[\frac{-x^2}{2\sigma^2}\right]$.

According to (5.11), $P_{\text{FA}}^i$ can be calculated as

$$P_{\text{FA}}^i = \int_{\gamma_i}^{\infty} f_{\omega_i}(z_i) = Q\left(\frac{\gamma_i}{\sigma}\right). \tag{5.12}$$

For a given $P_{\text{FA}}^i$, the threshold can be calculated as

$$\gamma_i = \sigma Q^{-1}\left(P_{\text{FA}}^i\right). \tag{5.13}$$

The probability of detection can be calculated as

$$P_{\text{D}}^i = \int_{\gamma_i}^{\infty} \int_{R-r}^{R+r} \frac{2x}{\pi r^2} \arccos\left[\frac{x^2+R^2+r^2}{2xR}\right] \frac{1}{\sqrt{2\pi\sigma^2}} \exp\left[\frac{-(z_i-x)^2}{2\sigma^2}\right] dx dz_i \tag{5.14}$$

However, (5.14) is not trackable. To make it more trackable, we assume $d_i$ is Gaussian distributed with the mean given in (5.8) and variance in (5.10). Therefore, under both $H_0$ and $H_1$, $z$ is Gaussian distributed, which is given as

$$z_i \sim \begin{cases} \mathcal{N}\left(0, \sigma^2\right) & \text{under } H_0 \\ \mathcal{N}\left(\mu_i, \sigma_i^2\right) & \text{under } H_1 \end{cases}, \tag{5.15}$$

where $\mu_i = E[d_i]$, and $\sigma_i^2 = \sigma_{d_i}^2 + \sigma^2$. The Neyman Pearson detector can be found as

$$L(z_i) = \frac{f(z_i;H_1)}{f(z_i;H_0)} = \frac{\frac{1}{\sqrt{2\pi\sigma_1^2}} \exp\left[\frac{-(z_i-\mu_1)^2}{2\sigma_1^2}\right]}{\frac{1}{\sqrt{2\pi\sigma^2}} \exp\left[\frac{-z_i^2}{2\sigma^2}\right]} \lessgtr \gamma_i. \tag{5.16}$$

Define $T(z_i) = \ln L(z_i)$, after simplification, we have

$$L(z_i) = \left(z_i + \frac{\sigma^2 \mu_i}{\sigma_{d_i}^2}\right)^2 \lessgtr \gamma_i', \tag{5.17}$$

The detector in (5.17) is Chi square distributed under both hypothesis. Since under $H_0$, $z$ is Gaussian distributed, we can calculate $P_{\text{FA}}^i$ as

$$P_{\text{FA}}^i = \int_{\gamma_i}^{\infty} f(z_i;H_0) = Q\left(\frac{\gamma_i}{\sigma}\right). \tag{5.18}$$

The threshold can be calculated by inverting (5.12), which is

$$\gamma_i = \sigma Q^{-1}\left(P_{\text{FA}}^i\right). \tag{5.19}$$

Also, since under $H_1$, $z$ is Gaussian distributed, we can calculate $P_{\mathrm{D}}^i$ as

$$P_{\mathrm{D}}^i = Q\left(\frac{\gamma_i - \mu_i}{\sigma_d}\right) = Q\left(\frac{\sigma Q^{-1}\left(P_{\mathrm{FA}}^i\right) - \mu_i}{\sigma_i}\right). \tag{5.20}$$

After each anchor makes a decision, it transmits a "1" or "0" to a fusion center. Therefore, similar to the previous sections, the total probability of the false alarm and the total probability of detection can be calculated using (5.3) and (5.4) respectively.

#### 5.2.1.1 Simulation Results

Figure 5.4 shows the ROC curves at the $i^{th}$ anchor under different $r$ but with the same $d_{\min}$. In one case, we fix the radius of the circle to 1m. In another case, we fix the radius of the circle to 10m. One can see that with larger radius, $P_{\mathrm{D}}^i$ converges faster.

Figure 5.5 shows the ROC curves at the $i^{th}$ anchor under different $d_{\min}$ but with the same $r$, and $r = 1$. One can see that with smaller $d_{\min}$, $P_{\mathrm{D}}^i$ converges faster.

Figure 5.6 we compare the original detector in (5.11) with the Gaussian approximation in (5.17). We set the variance of the noise to 5 and 0.5 respectively. Under both high and low SNR scenarios, the performance of the Gaussian approximated detector is very close to the original detector, which indicates that the Gaussian approximation is a good substitution for the original detector since it is more trackable.

Figure 5.7 shows the effect of the choice of the design parameter $K$ when the original detector is used. Figure 5.8 shows the effect of the choice of the design parameter $K$ when the Gaussian approximation is applied. Similar to the node detection at a known location case, there is no optimal choice of $K$ for all $\bar{P}_{\mathrm{FA}}^{\mathrm{T}}$.

### 5.2.2 Detecting A Node in A Region Using the RSS Method

In this section, we consider location detection using RSS method. Similar to the TOA approach, we consider a WSN with $M$ anchors and 1 node. The anchors are outside of a known region, and the node, if actively transmitting, is inside of the region. In the absence of the transmission, each anchor measures the power of pure noise. In the presence of the transmission, each anchor receives the power of signal plus noise. Each anchor makes its own detection on if the node is transmitting

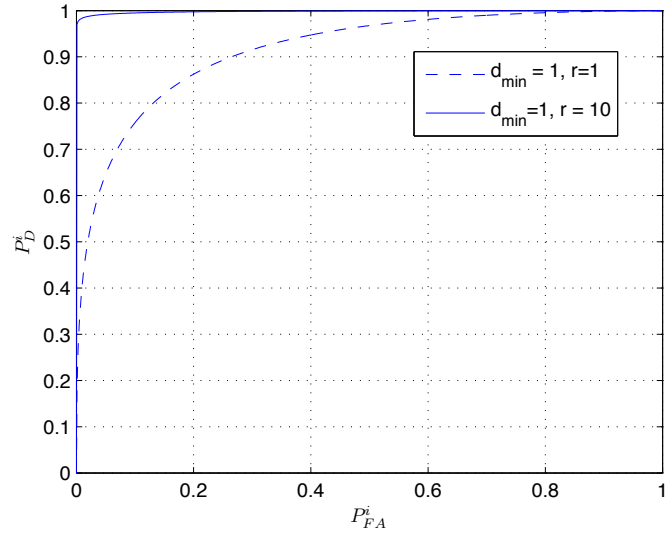


Figure 5.4: ROC Curves at the $i^{th}$ Anchor Under Different Circle Radius.

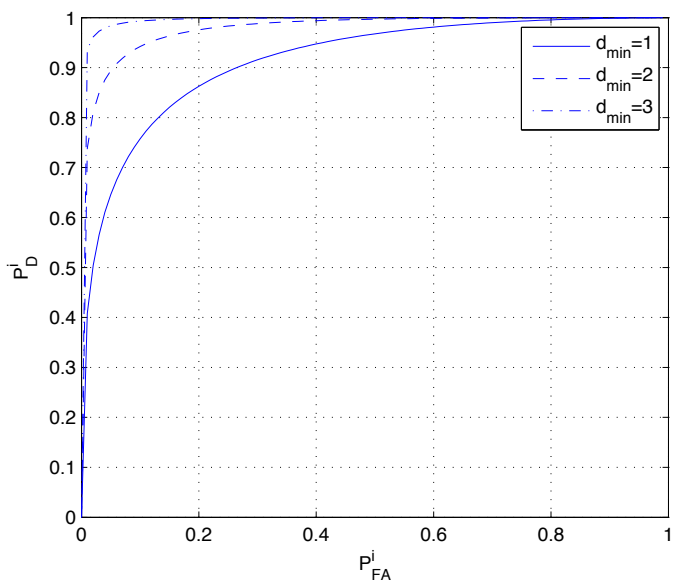


Figure 5.5: ROC Curves at the $i^{th}$ Anchor Under Different $d_{\min}$.

or not. we assume one node is located inside a region, and $M$ anchors are located outside of the region. The detection problem at the $i^{th}$ anchor can be formulated as

$$z_i = \begin{cases} \sum_{n=0}^{N-1} \omega_i^2[n] & \text{under } H_0 \\ \sum_{n=0}^{N-1} \left(g(d_i)s_i[n-n_i] + \omega_i[n]\right)^2 & \text{under } H_1 \end{cases}, \tag{5.21}$$

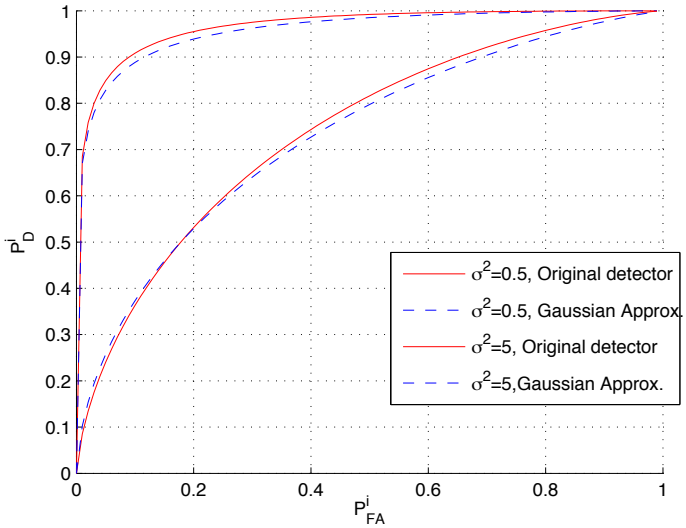


Figure 5.6: ROC Curves Comparison Between the Gaussian Approximation and the Original Detector.

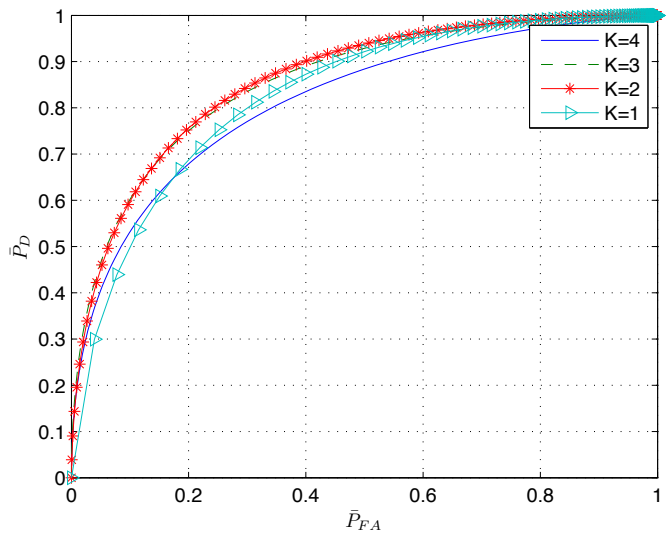


Figure 5.7: ROC Curves Under Different Choices of $K$ When Using (5.11).

where $\omega_i$ is the Gaussian noise with 0 mean and variance $\sigma^2$, $n_i$ is the time delay, $n$ is the sample index, and $N$ is the total samples is sent by the node. $g(d_i)$ is a function of the true distance $d_i$, and we assume $g(d_i) = \frac{1}{d_i^2}$.

The pdf of $d_i$ is given in (5.6), conditional on $d_i$, the Neyman-Pearson detector at the $i^{th}$

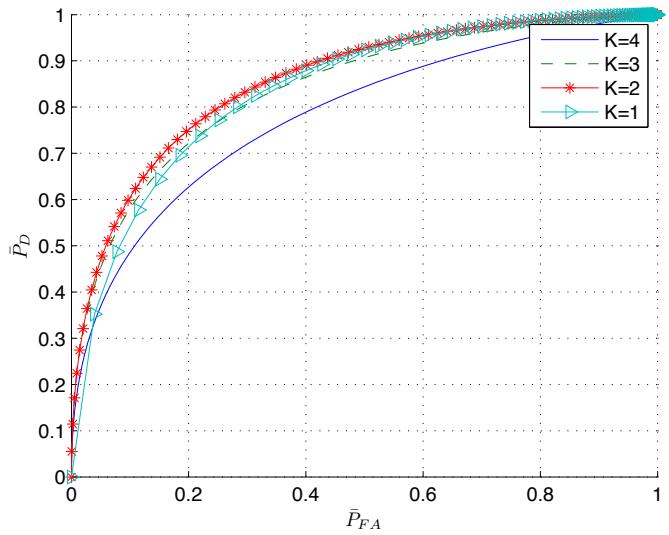


Figure 5.8: ROC Curves Under Different Choices of $K$ When Using (5.17).

anchor can be formulated as

$$L_i(z) = \frac{f(z_i;H_1)}{f(z_i;H_0)} = \frac{\int_{d_{\min}}^{d_{\max}} f(z_i|x) f_{d_i}(x)dx}{\frac{1}{2\sigma^2\Gamma(m)}\left(\frac{z_i}{2\sigma^2}\right)^{N-1}\exp\left(-\frac{z_i}{2\sigma^2}\right)} \lessgtr \gamma_i. \tag{5.22}$$

Here,

$$f(z_i|x) = \frac{1}{2\sigma^2}\left(\frac{z_i}{a^2}\right)^{\frac{N-1}{2}} \exp\left(-\frac{z_i+a^2}{2\sigma^2}\right) \mathrm{I}_{N-1}\left(\sqrt{\frac{a^2 z_i}{\sigma^4}}\right), \tag{5.23}$$

where $a$ is the non-central parameter, which is defined as $a = g(d_i)\sqrt{N\varepsilon}$; $\varepsilon$ is the energy of the signal, which is defined as $\varepsilon = \sum_{n=0}^{N-1} s_i^2[n]$. $\mathrm{I}_b(\cdot)$ is the modified Bessel function of the first kind.

The probability of false alarm and probability of detection at the $i^{th}$ anchor can be calculated as

$$P_{\mathrm{FA}}^i = \int_{\gamma}^{\infty} f(z_i;H_0)d\mathbf{z}_i = \exp\left(-\frac{\gamma}{2\sigma^2}\right)\sum_{k=0}^{N-1}\frac{\left(\frac{\gamma}{2\sigma^2}\right)^k}{\Gamma(k+1)}, \tag{5.24}$$

and

$$P_{\mathrm{D}}^i = \int_{\gamma}^{\infty} f(z_i;H_1)d\mathbf{z}_i = \int_{\gamma}^{\infty}\int_{d_{\min}}^{d_{\max}} f(z_i|x)f_{d_i}(x)dxdz_i. \tag{5.25}$$

Since (5.25)is not trackable, similar to the TOA case, we can approximate $g(d_i)$ as Gaussian distribution. Recall the $j^{th}$ moment of $d_i$ is given in (5.7), therefore the mean of $g(d_i)$ is given as

$$E\left[g(d_i)\right] = E\left[d_i^{-2}\right] = R^{-2}{}_2F_1\left(1,1,2;\left(\frac{r}{R}\right)^2\right). \tag{5.26}$$

The variance of $g(d_i)$ is

$$\mathrm{var}(d_i^{-2}) = R^{-4}\left({}_2F_1\left(2,2,2;\left(\frac{r}{R}\right)^2\right) - \left({}_2F_1\left(1,1,2;\left(\frac{r}{R}\right)^2\right)\right)^2\right). \tag{5.27}$$

By applying the Gaussian approximation, $z_i$ under $H_1$ is non-central Chi square distributed with $N$ i.i.d Gaussian random variables. The mean of each random variable is given in (5.26) and the variance is

$$\sigma_i^2 = \mathrm{var}(d_i^{-2}) + \sigma^2, \tag{5.28}$$

where $\mathrm{var}(d_i^{-2})$ is given in (5.27).

Applying the Neyman-Pearson theorem, The detector at the $i^{th}$ anchor is

$$L_i(z_i) = \frac{\frac{1}{2\sigma_i^2}\left(\frac{z_i}{a^2}\right)^{\frac{N-1}{2}} \exp\left(-\frac{z_i+a^2}{2\sigma_i^2}\right) \mathrm{I}_{N-1}\left(\sqrt{\frac{a^2 z_i}{\sigma_i^4}}\right)}{\frac{1}{2\sigma^2\Gamma(m)}\left(\frac{z_i}{2\sigma^2}\right)^{N-1} \exp\left(-\frac{z_i}{2\sigma^2}\right)} \lessgtr \gamma_i. \tag{5.29}$$

After simplification, we have

$$L_i(z_i) = z_i^{\frac{1-N}{2}} \exp\left(z_i\left(\frac{1}{2\sigma^2} - \frac{1}{2\sigma_i^2}\right)\right) \mathrm{I}_{N-1}\left(\sqrt{\frac{a^2 z_i}{\sigma_i^4}}\right) \lessgtr \gamma_i. \tag{5.30}$$

We found that $L_i(z_i)$ is a monotonically decreasing function of $z_i$. Therefore, we can use $z_i$ as the detector. A new detector by using the Gaussian approximation can be found as

$$z_i \lessgtr \gamma_i', \tag{5.31}$$

where $\gamma_i'$ is not a function of the measured data.

#### 5.2.2.1 Simulation Results

For the simulation, we set the number of samples $N = 20$, and the Monte Carlo simulations are performed. In Figure 5.9, Figure 5.10 and Figure 5.11, we compare we compare the original detector derived in (5.22) and the Gaussian approximation in (5.31) under different $d_{\min}$, $r$, and SNR values respectively. From Figure 5.9 one can see that as $d_{\min}$ decreases, the performance of Gaussian approximation is much closer to the original detector. However, the original detector outperforms the Gaussian approximation under both $d_{\min}$ values. From Figure 5.10, one can see that when $r$ decreases, the performance of Gaussian approximation is much closer to the original detector. However, the original detector outperforms the Gaussian approximation under both $r$ values. From

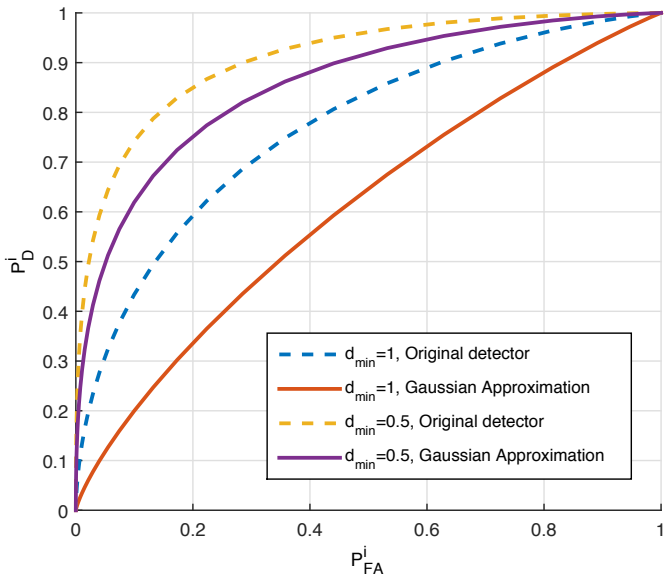


Figure 5.9: ROC Curves at the $i^{th}$ Anchor Under Different $d_{\min}$.

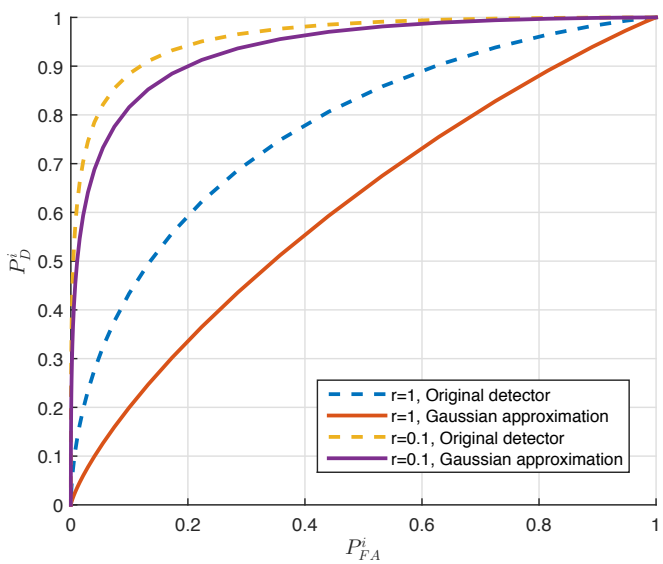


Figure 5.10: ROC Curves at the $i^{th}$ Anchor Under Different $r$.

Figure 5.11, one can see that as SNR increases, the performance of Gaussian approximation is much closer to the original detector. However, the original detector outperforms the Gaussian approximation under both SNR values. Therefore, we can conclude that the Gaussian approximation is not a good approximation for the RSS method. Figure 5.12 shows the total probability of detec-

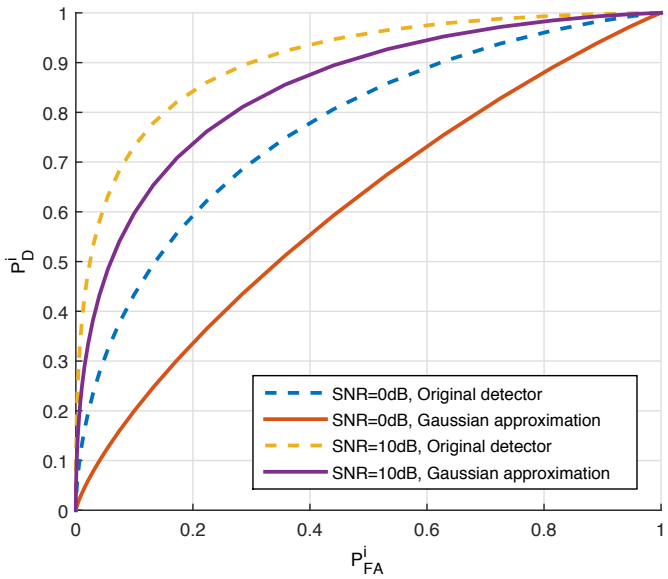


Figure 5.11: ROC Curves at the $i^{th}$ Anchor Under Different SNR.

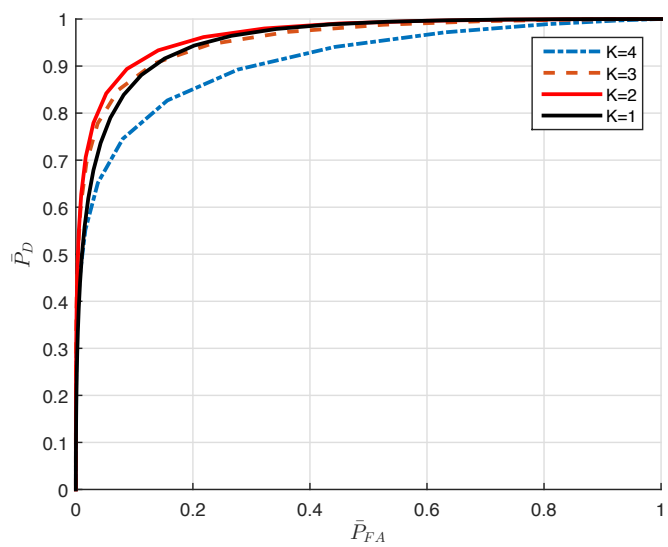


Figure 5.12: ROC Curves at the $i^{th}$ Anchor Under Different Choice of $K$ Using the RSS Method.

tion versus the total probability of false alarm under different choice of $K$. From the figure one can see that similar to the TOA method, none of the choice of $K$ always performs best among all the range of the false alarm probability.

## 5.3 Conclusions

In this chapter, we proposed a distributed location detection scheme in WSNs. The proposed scheme is different from the the centralized location detection schemes because each anchor makes its own decision of whether the node is present and transmits a binary bit to a fusion center. We considered two schemes, one is detecting a node at a known location. Another one is locating a node in a known region. In both schemes, each anchor makes its own decision and a fusion center is used to collect binary bits from anchors. The fusion center needs at least $K$ anchors to agree that the node exists to detect the presence of the node. The proposed scheme is more power and time efficient than centralized methods. Simulation results show that in both schemes the optimum choice of $K$ depends on the requirements of $\bar{P}_{FA}$ and $\bar{P}_D$, and none of the $K$ values outperform others for all $\bar{P}_{FA}$.

Chapter 6

# DISTRIBUTED LOCATION DETECTION IN THE PRESENCE OF FADING

In the previous chapter, we have studied location detection in the absence of fading. In this chapter, we consider a location detection problem in the presence of fading. Consider a sensor network with $M$ anchors and one node. In the absence of the node, each anchor receives only noise. In the presence of the node, each anchor receives faded signal with noise. If the phases of the fading coefficients are known at each anchor, a coherent detection scheme, needs only one phase-synchronized matched filter, can be applied. In this case, the received signal is sampled and a total number of $N$ samples are extracted. Next, the $N$ samples are correlated with the sampled transmitted signal and compared with a threshold. If the phase is unknown at any anchor, a non-coherent detection scheme is applied. In this case, two demodulators with 90 degree phase shift of each other are needed. After two analog to digital converters, both real (in-phase) and imaginary (quadrature) components of the signal are extracted, then both components are correlated with the generated real and quadrature elements separately. By combining the power of the output of correlators (or a synchronized single branch) and comparing with a threshold, a final decision is made at each anchor. If an anchor detects the node, it transmits a bit "1" to the FC, otherwise it transmits a bit "0". The FC needs at least $K$ anchors to declare the node exists at the given location, where $K$ is a design parameter.

To detect the node, a binary hypothesis testing problem at the $i^{th}$ anchor can be formulated as

$$x_i[n] = \begin{cases} \omega_i[n] & \text{under } H_0 \\ h_i s_i[n-n_i] + \omega_i[n] & \text{under } H_1 \end{cases}. \tag{6.1}$$

As before the fading coefficients, $h_i$, are complex Gaussian random variables. Both real and imaginary parts of $h_i$ have 0 mean and variance $\frac{1}{2}$, to satisfy $\mathrm{E}\left[|h_i|^2\right] = 1$; $\omega_i[n]$ is additive Gaussian noise with 0 mean and variance $\sigma^2$; $s_i[n]$ is the modulated deterministic transmitted signal and its total energy $\mathscr{E} = \sum_{n=0}^{N-1} s_i^2[n]$ is normalized; $n_i$ is the true time delay between the node and the $i^{th}$ anchor, where $i = 1, 2, \ldots, M$. The following three cases are considered in this work. (a) The fading coefficients are assumed to be known at each anchor. In this case, conditioned on the fading coefficients,

$x_i[n]$ is Gaussian distributed under both $H_0$ and $H_1$; (b) Amplitudes of the fading coefficients are unknown at any anchor but with a known prior distribution. In this case, the Neyman-Pearson detector can be found by integrating the fading effect [53]; (c) No CSI is available at any anchor. In this case, a non-coherent detection scheme which extracts both in-phase and quardrature components is used.

## 6.1 Fading Coefficients Known at Anchors

When the fading coefficients are known at each anchor, the phases can be synchronized, and the coherent detection scheme can be used. The hypothesis testing problem at each anchor can be formulated as

$$x_i[n] = \begin{cases} \omega_i[n] & \text{under } H_0 \\ |h_i| s_i[n-n_i] + \omega_i[n] & \text{under } H_1 \end{cases}. \tag{6.2}$$

Since $h_i$ is a zero-mean complex Gaussian random variable, $|h_i|$ is Rayleigh distributed. Conditioned on $|h_i|$ and based on Neyman-Pearson theorem, the $i^{th}$ anchor detects the node if the likelihood ratio $L_i(\mathbf{x})$ satisfies

$$L_i(\mathbf{x}) = \frac{f\left(\mathbf{x}\middle||h_i|;H_1\right)}{f(\mathbf{x};H_0)} \lessgtr \gamma_i, \tag{6.3}$$

for some threshold $\gamma_i$, which balances the false alarm and detection probabilities at each anchor. Here, $f\left(\mathbf{x}\middle||h_i|;H_1\right)$ is the probability density function (pdf) of the received signal conditioned on $|h_i|$ under $H_1$, and $\mathbf{x} = [x_i[0], x_i[1], \ldots, x_i[N-1]]^T$. Similarly, $f(\mathbf{x};H_0)$ is the pdf of the received signal under $H_0$. Under both $H_0$ and $H_1$, $\mathbf{x}$ is Gaussian distributed, given by

$$f(\mathbf{x};H_0) = \frac{1}{(2\pi\sigma^2)^{\frac{N}{2}}} \exp\left(-\frac{1}{2\sigma^2}\sum_{n=0}^{N-1} x_i^2[n]\right), \tag{6.4}$$

and

$$f\left(\mathbf{x}\middle||h_i|;H_1\right) = \frac{1}{(2\pi\sigma^2)^{\frac{N}{2}}} \exp\left(-\frac{1}{2\sigma^2}\sum_{n=0}^{N-1} \left(x_i[n] - |h_i| s_i[n-n_i]\right)^2\right). \tag{6.5}$$

Taking the log of (6.3), and substituting (6.4) and (6.5) into (6.3), and simplifying, we have

$$\ln L_i(\mathbf{x}) = \sum_{n=0}^{N-1} x_i[n] s_i[n-n_i] \lessgtr \frac{\sigma^2 \ln \gamma_i}{|h_i|} + \frac{|h_i|}{2}. \tag{6.6}$$

Define $T_i(\mathbf{x}) = \frac{1}{\sigma} \ln L_i(\mathbf{x})$, so that (6.6) can be expressed as

$$T_i(\mathbf{x}) \lessgtr \gamma_i'(|h_i|), \tag{6.7}$$

where

$$\gamma_i'(|h_i|) = \sqrt{\frac{\sigma^2}{|h_i|^2}} \ln \gamma_i + \frac{1}{2}\sqrt{\frac{|h_i|^2}{\sigma^2}} \tag{6.8}$$

is the threshold for the statistic $T_i(\mathbf{x})$ and depends on both $\gamma_i$ and $|h_i|$. Note that conditioned on $|h_i|$, $T_i(\mathbf{x})$ is Gaussian:

$$T_i(\mathbf{x}) \sim \begin{cases} \mathcal{N}(0,1) & \text{under } H_0 \\ \mathcal{N}\left(\sqrt{\frac{|h_i|^2}{\sigma^2}}, 1\right) & \text{under } H_1 \end{cases}. \tag{6.9}$$

The instantaneous probability of false alarm at the $i^{th}$ anchor $P_{\text{FA}}^i$ is

$$P_{\text{FA}}^i = Q\left(\gamma_i'(|h_i|)\right), \tag{6.10}$$

and the probability of detection at the $i^{th}$ anchor $P_{\text{D}}^i$ is

$$P_{\text{D}}^i = Q\left(\gamma_i'(|h_i|) - \sqrt{\frac{|h_i|^2}{\sigma^2}}\right), \tag{6.11}$$

both of which are functions of $|h_i|$. The average false alarm probability $\bar{P}_{\text{FA}}$ can be calculated by averaging out the fading effect, which is given by

$$\bar{P}_{\text{FA}} = \text{E}\left[P_{\text{FA}}^i\right] = \int_0^\infty Q\left(\gamma_i'(|h_i|)\right) f_{|h_i|^2}(x)\, dx, \tag{6.12}$$

where the pdf of $|h_i|^2$ is given in (3.13). Similarly, the averaged $\bar{P}_{\text{D}}$ can be calculated by

$$\bar{P}_{\text{D}} = \int_0^\infty Q\left(\gamma_i'(|h_i|) - \sqrt{\frac{|h_i|^2}{\sigma^2}}\right) f_{|h_i|^2}(x)\, dx. \tag{6.13}$$

After a decision is made at each anchor, it transmits a "1" or "0" to a fusion center. The fusion center needs to receive at least $K$ "1"s to decide the node is active, where $K$ is a predetermined design parameter. Therefore, the total probability of false alarm and the total probability of detection are given by

$$\bar{P}_{\mathrm{FA}}^{\mathrm{T}} = \sum_{m=K}^{M} \binom{M}{m} \left(\bar{P}_{\mathrm{FA}}\right)^{m} \left(1-\bar{P}_{\mathrm{FA}}\right)^{M-m}, \tag{6.14}$$

and

$$\bar{P}_{\mathrm{D}}^{\mathrm{T}} = \sum_{m=K}^{M} \binom{M}{m} \left(\bar{P}_{\mathrm{D}}\right)^{m} \left(1-\bar{P}_{\mathrm{D}}\right)^{M-m}. \tag{6.15}$$

Recall that the threshold $\gamma_i'(|h_i|)$ given in (6.7) depends on the random channel amplitude $|h_i|$. The question arises as to whether this choice is optimal in the sense of maximizing $\bar{P}_{\mathrm{D}}$ when $\bar{P}_{\mathrm{FA}} \leq \alpha$, where $\alpha$ is a constant. Now we want to prove that the threshold $\gamma_i'(|h_i|)$ in (6.8) has the optimal dependence on $|h_i|$. We do this by casting the threshold optimization problem as a variational problem where the variable $\gamma_i'(|h_i|)$ is a function of the channel:

**Theorem 1.** Consider the following optimization problem

$$\begin{array}{ll} \text{maximize} & \bar{P}_{\mathrm{D}} = \int_0^\infty Q\left(\gamma_i'(|h_i|) - \sqrt{\frac{|h_i|^2}{\sigma^2}}\right) f_{|h_i|^2}(x)\,dx \\ \text{subject to} & \bar{P}_{\mathrm{FA}} = \int_0^\infty Q\left(\gamma_i'(|h_i|)\right) f_{|h_i|^2}(x)\,dx \leq \alpha \end{array},$$

where the variable function is $\gamma_i'(|h_i|)$. The optimal threshold function is given in (6.8).

Proof: To prove the Theorem, we express the Lagrangian as

$$\int_0^\infty Q\left(\gamma_i'(|h_i|) - \sqrt{\frac{|h_i|^2}{\sigma^2}}\right) f_{|h_i|^2}(x)\,dx + \lambda\left(\int_0^\infty Q\left(\gamma_i'(|h_i|)\right) f_{|h_i|^2}(x)\,dx - \alpha\right). \tag{6.16}$$

Taking the derivative of (6.16) with respect to $\gamma_i'$, we have

$$\int_0^\infty \frac{\partial Q\left(\gamma_i'(|h_i|) - \sqrt{\frac{|h_i|^2}{\sigma^2}}\right)}{\partial \gamma_i'(|h_i|)} f_{|h_i|^2}(x)\,dx + \lambda \int_0^\infty \frac{\partial Q\left(\gamma_i'(|h_i|)\right)}{\partial \gamma_i'(|h_i|)} f_{|h_i|^2}(x)\,dx. \tag{6.17}$$

Setting (6.17) to 0, applying the formula $\frac{dQ(x)}{dx} = -\frac{1}{\sqrt{2\pi}}\exp\left(-\frac{x^2}{2}\right)$, and solving for $\gamma_i'$, we have

$$\gamma_i'(|h_i|) = \ln\lambda\sqrt{\frac{\sigma^2}{|h_i|^2}} + \frac{1}{2}\sqrt{\frac{|h_i|^2}{\sigma^2}}. \tag{6.18}$$

Setting $\lambda = \gamma$, (6.18) is equivalent to (6.8), which proves Theorem I.

## 6.2 Fading Coefficients with Known Phase but Unknown Amplitude

Now assume that the amplitude of the fading are unknown at every anchor with a known distribution. In this case, $|h_i|$ in (6.2) is unknown but with a known distribution. The Neyman-Pearson detector at the $i^{th}$ anchor can be formulated as

$$L_i(\mathbf{x}) = \frac{f(\mathbf{x};H_1)}{f(\mathbf{x};H_0)} = \frac{\int_0^\infty f\left(\mathbf{x}\middle||h_i|;H_1\right) f_{|h_i|}(x)\,dx}{f(\mathbf{x};H_0)} \lessgtr \gamma_i \tag{6.19}$$

Defining $T_i(\mathbf{x}) = \frac{1}{\sigma^2}\sum_{n=0}^{N-1} x_i[n]s_i[n-n_i]$ and assume $|h_i|$ is Rayleigh distributed, we can express (6.19) as

$$L_i = T_i \exp\left(\frac{T_i^2}{2\left(1+\frac{1}{\sigma^2}\right)}\right)\left(1-Q\left(\frac{T_i}{\sqrt{1+\frac{1}{\sigma^2}}}\right)\right) \lessgtr \gamma_i', \tag{6.20}$$

where

$$\gamma_i' = \frac{\left(\gamma_i - \frac{1}{\left(1+\frac{1}{\sigma^2}\right)}\right)\left(1+\frac{1}{\sigma^2}\right)^{\frac{3}{2}}}{\sqrt{2\pi}}, \tag{6.21}$$

and we drop the dependence of $L_i$ and $T_i$ on $\mathbf{x}$ to emphasize their functional relationship.

We found that for all SNR values, $L_i$ is a monotonically increasing function of $T_i$. Therefore, we can rewrite (6.20) as

$$T_i(\mathbf{x}) = \sum_{n=0}^{N-1} x_i[n]s_i[n-n_i] \lessgtr \gamma_i'', \tag{6.22}$$

here $\gamma_i''$ is a constant, which is not a function of the measured data, and can be calculated numerically as we now explain. Since the distribution of $T_i(\mathbf{x}) \sim \mathcal{N}(0,1)$, $\bar{P}_{\mathrm{FA}}$ can be calculated as

$$\bar{P}_{\mathrm{FA}} = Q\left(\gamma_i''\right), \tag{6.23}$$

where $\gamma_i''$ can be found by taking the inverse of (6.23).

Since under $H_1$ shown in (6.9), conditioned on $|h_i|$, the distribution of $T_i(\mathbf{x}) \sim \mathcal{N}\left(\sqrt{\frac{|h_i|^2}{\sigma^2}}, 1\right)$, the detection probability $P_{\mathrm{D}}^i$ can be calculated as

$$P_{\mathrm{D}}^i = Q\left(Q^{-1}(\bar{P}_{\mathrm{FA}}) - \sqrt{\frac{|h_i|^2}{\sigma^2}}\right). \tag{6.24}$$

The averaged $\bar{P}_{\mathrm{D}}$ can be calculated using

$$\bar{P}_{\mathrm{D}} = \int_0^{\infty} Q\left(Q^{-1}\left(\bar{P}_{\mathrm{FA}}\right) - \sqrt{\frac{|h_i|}{\sigma^2}}\right) f_{|h_i|^2}(x)\, dx, \tag{6.25}$$

which is different from (6.13), since $\gamma_i''$ does not depend on $|h_i|$ anymore. Finally, the total probability of false alarm and detection can be calculated using (6.14).

Recalling that (6.6), is the detector for the case when $h_i$ is known to anchors. Comparing it with (6.22), which is the detector for the case when $|h_i|$ is a random variable with Rayleigh distribution, one can see that the detector for both cases rely on the same statistic $T_i(\mathbf{x})$. However, in (6.6) the threshold is a function of the fading coefficients, whereas in (6.22) the threshold is a constant that only depends on the prescribed $\bar{P}_{\mathrm{FA}}$. In Section 5.2.1.1 we will show (6.6) outperforms (6.22) as expected. The closed form expression for $\bar{P}_{\mathrm{D}}$ in (6.25) is not tractable. However, when no CSI is available at each anchor, we will have a closed form expression for $\bar{P}_{\mathrm{D}}$ as seen next.

## 6.3 No CSI is Available at Any Anchor

When the knowledge of CSI is not available at any anchor, a non-coherent detection scheme is applied. The received bandpass signal is sampled and both in-phase and quadrature components of the signal are extracted [83]. The problem statement can be formulated as

$$x_i[n] = \begin{cases} \omega_i[n] & \text{under } H_0 \\ h_{\mathrm{R}i} s_{1i}[n-n_i] + h_{\mathrm{I}i} s_{2i}[n-n_i] + \omega_i[n] & \text{under } H_1 \end{cases}, \tag{6.26}$$

where $s_{1i}[n]$ and $s_{2i}[n]$ are the sampled signal $s_i[n]$ multiplied by $\cos(2\pi f_c n)$ and $\sin(2\pi f_c n)$ respectively, and $f_c$ is the carrier frequency. $\omega_i[n] = \omega_{\mathrm{R}i}[n] + \omega_{\mathrm{I}i}[n]$, which contains both in phase and quadrature components. Similarly, $h_{\mathrm{R}i}$ and $h_{\mathrm{I}i}$ are the real and imaginary parts of the fading coefficients respectively. We can rewrite the hypothesis testing problem in vector format as

$$\mathbf{x}_i = \begin{cases} \boldsymbol{\omega}_i & \text{under } H_0 \\ \mathbf{S}_i \mathbf{h}_i + \boldsymbol{\omega}_i & \text{under } H_1 \end{cases}, \tag{6.27}$$

where $\mathbf{x}_i = [x_i[0], x_i[1], \ldots, x_i[N-1]]^T$, and $\mathbf{S}_i$, $\mathbf{h}_i$, and $\boldsymbol{\omega}_i$ are defined as

$$\mathbf{S}_i = \begin{bmatrix} s_{1i}[-n_i] & s_{2i}[-n_i] \\ s_{1i}[1-n_i] & s_{2i}[1-n_i] \\ \vdots & \vdots \\ s_{1i}[N-1-n_i] & s_{2i}[N-1-n_i] \end{bmatrix}, \tag{6.28}$$

$$\mathbf{h}_i = [h_{\mathrm{R}i} \quad h_{\mathrm{I}i}]^T \tag{6.29}$$

and

$$\boldsymbol{\omega}_i = \begin{bmatrix} \omega_{\mathrm{R}i}[0] + \omega_{\mathrm{I}i}[0] \\ \omega_{\mathrm{R}i}[1] + \omega_{\mathrm{I}i}[1] \\ \vdots \\ \omega_{\mathrm{R}i}[N-1] + \omega_{\mathrm{I}i}[N-1] \end{bmatrix}. \tag{6.30}$$

The detector at the $i^{th}$ anchor can be computed by calculating the log likelihood ratio which is a quadratic function of $\mathbf{x}_i$

$$L_i(\mathbf{x}) = \mathbf{x}_i^T \mathbf{S}_i \mathbf{S}_i^T \left(\mathbf{S}_i \mathbf{S}_i^T + \sigma^2 \mathbf{I}\right)^{-1} \mathbf{x}_i \lessgtr \gamma_i, \tag{6.31}$$

After simplifications, $L_i(\mathbf{x})$ can be expressed as

$$L_i(\mathbf{x}) = \frac{1}{N} \mathbf{x}_i^T \mathbf{S}_i \mathbf{S}_i^T \mathbf{x}_i \lessgtr \gamma_i. \tag{6.32}$$

The probability of false alarm and the probability of detection at the $i^{th}$ anchor can be calculated as

$$\begin{aligned} \bar{P}_{\mathrm{FA}} &= \Pr\{L_i(\mathbf{x}) > \gamma_i; H_0\} \\ &= \exp\left(-\frac{\gamma_i}{12\sigma^2}\right). \end{aligned} \tag{6.33}$$

In addition, the averaged probability of detection $\bar{P}_{\mathrm{D}}$ can be expressed as a function of the $\bar{P}_{\mathrm{FA}}$ in closed form:

$$\begin{aligned} \bar{P}_{\mathrm{D}} &= \Pr\{L_i(\mathbf{x}) > \gamma_i; H_1\} \\ &= (\bar{P}_{\mathrm{FA}})^{\frac{1}{1+\frac{N}{4\sigma^2}}}. \end{aligned} \tag{6.34}$$

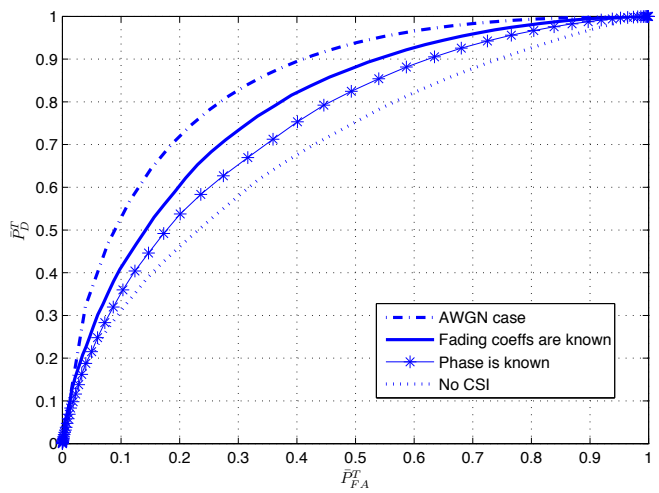


Figure 6.1: ROC Curves for Different Scenarios.

The overall $\bar{P}_{\text{FA}}^{\text{T}}$ and $\bar{P}_{\text{D}}^{\text{T}}$ can be calculated by substituting (6.33) and (6.34) into (6.14) and (6.15).

### 6.3.1 The Choice of the Design Parameter $K$

As mentioned before, $K$ is a predetermined design parameter which is used to fuse the binary decisions from each anchor in the following manner. If $K$ or more anchors detect a node, a final *detect* decision is made. When $K$ is large, which means the fusion center requires most of the anchors to claim the node exists, both $\bar{P}_{\text{FA}}^{\text{T}}$ and $\bar{P}_{\text{D}}^{\text{T}}$ decrease. On the other hand, When $K$ is small, both $\bar{P}_{\text{FA}}^{\text{T}}$ and $\bar{P}_{\text{D}}^{\text{T}}$ increase. However, for a given total false alarm threshold $\bar{P}_{\text{FA}}^{\text{T}} \leq \alpha$, it appears that there is an optimal value of $K$ which maximizes $\bar{P}_{\text{D}}^{\text{T}}$. In Section 5.2.1.1 we will see the choice of $K$ under different values of $\bar{P}_{\text{FA}}^{\text{T}}$.

## 6.4 Simulation Results

In the location detection formulation, we consider a 1m $\times$ 1m square, 4 anchors are at the corners, and 1 node is in the middle of the square. The location of the node (when active) is known to all anchors. Figure 6.1 shows the comparison between the AWGN case, fading coefficients are known to the anchors, the amplitude of fading coefficients are unknown but with a prior distribution, and the no CSI case. Here we fix the design parameter $K = 1$ for all cases so that a single anchor's detection is sufficient for the FC to detect the node. One can see from the figure that the AWGN

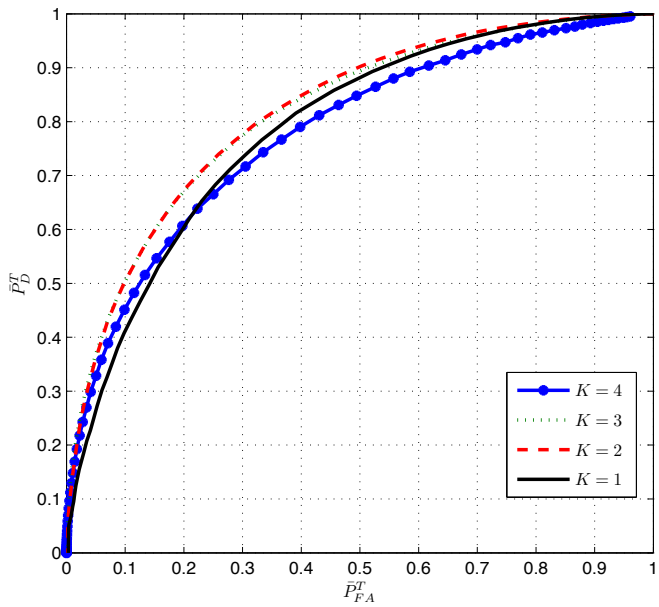


Figure 6.2: ROC Curves When the Fading Coefficients are Known to All Anchors When SNR = 15dB.

case outperforms all other cases as we expected, followed by the fading coefficients are known to anchors, the amplitude of fading coefficients are unknown but with a prior distribution, and no CSI case gives the worst performance. Intuitively speaking, we expect higher probability of detection when more information is available.

Figure 6.2 through Figure 6.4 show the ROC curves for different cases as $K$ changes. From the figures one can see that for small $\bar{P}_{\mathrm{FA}}^{\mathrm{T}}$, $K = 4$ performs best, however as $\bar{P}_{\mathrm{FA}}^{\mathrm{T}}$ increases, $K = 4$ is not a good choice. Therefore, none of the $K$ values outperform others for all $\bar{P}_{\mathrm{FA}}^{\mathrm{T}}$.

Figure 6.5 shows $\bar{P}_{\mathrm{D}}^{\mathrm{T}}$ vs. SNR when $\bar{P}_{\mathrm{FA}}^{\mathrm{T}} = 10^{-1}$, $K = 1$ and the amplitude of fading is Rayleigh distributed. From the figure one can see that to maintain the same $\bar{P}_{\mathrm{D}}^{\mathrm{T}} = 0.85$, the no CSI case needs 21.5dB SNR, followed by the case when $|h_i|$ is unknown, which is about 19.6dB, and $|h_i|$ is known needs the least amount of SNR, which is about 18.5dB. Therefore, the SNR loss due to Rayleigh fading is about 2dB, and unknown phase causes an additional 1dB. However, one can also see that as $\bar{P}_{\mathrm{D}}^{\mathrm{T}}$ increases, the SNR losses decrease.

Figure 6.6 shows the ROC curve comparisons between (6.22) and (6.6) at the first anchor.

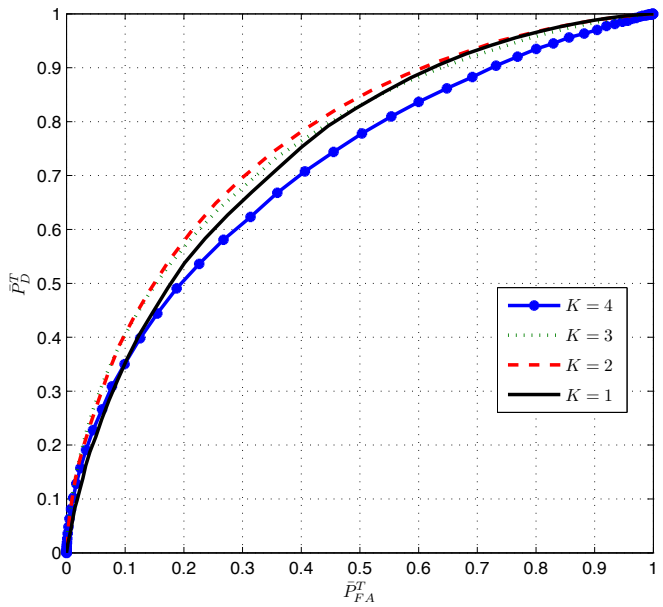


Figure 6.3: ROC Curves When the Amplitude of the Fading Coefficients are Unknown to the Anchors but with A Prior Distribution When SNR = 15dB.

From the figure we can see that by using the knowledge of the magnitude of the fading coefficients to set the threshold in (6.6), the performance is better than the no CSI case (6.22).

## 6.5 Conclusions

In this chapter, we consider distributed location detection in the presence of fading. Each anchor makes its own decision, and transmits the decision to a fusion center. The fusion center needs $K$ anchors to agree that the node exists to detect the presence of the node. Three scenarios are considered, which includes the fading coefficients are known at anchors, the fading coefficients with known phase but unknown amplitude, and no CSI is available at any anchor. The ROC curves are plotted under different channel assumptions. From the plots we can see that the optimal $K$ depends on the requirements of $\bar{P}_{\mathrm{FA}}^{\mathrm{T}}$ and $\bar{P}_{\mathrm{D}}^{\mathrm{T}}$, and none of the $K$ values outperform others for all $\bar{P}_{\mathrm{FA}}^{\mathrm{T}}$. Finally, the simulation results show that using the knowledge of the fading coefficients to choose the threshold gives better performance.

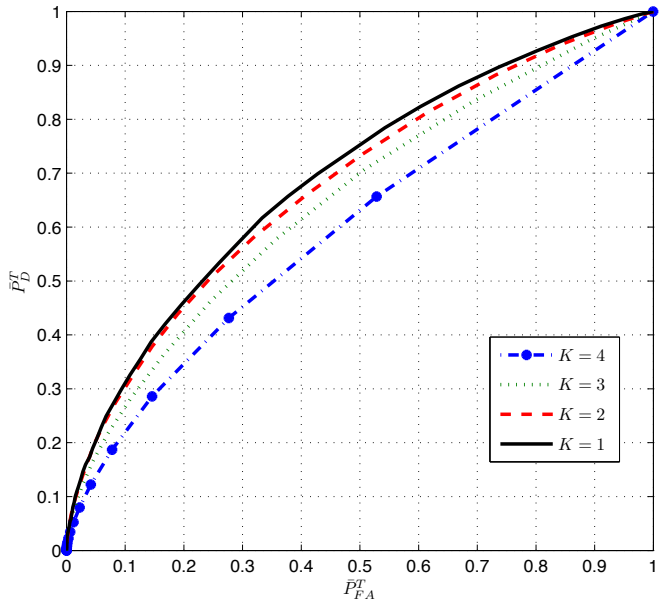


Figure 6.4: ROC Curves When No CSI is Available at Any Anchor When SNR = 15dB.

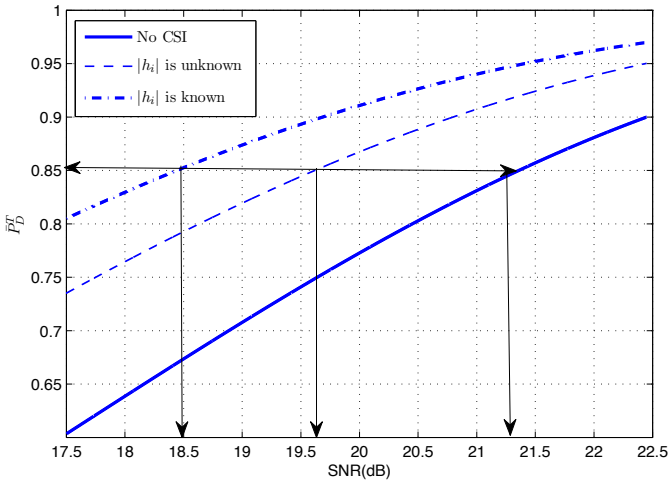


Figure 6.5: $\bar{P}_{\mathrm{D}}^{\mathrm{T}}$ vs. SNR Under Different Fading Scenarios.

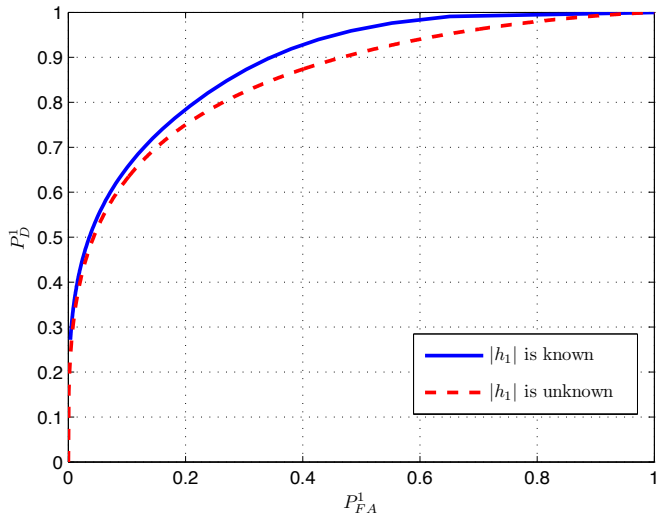


Figure 6.6: Comparisons Between the Threshold is A Function of Fading Coefficients and the Threshold is not A Function of Fading Coefficients When SNR = 15dB.

Using the Channel Knowledge Gives a Better Performance.

# Chapter 7

# CONCLUSIONS

In the preceding chapters, location estimation and detection problems were presented. In Chapter 2, different localization methods were revisited. In general, distance and angle related measurements are used to estimate the node location. Distance related measurements include TOA, RSS, and TDOA. Angle related measurements include AOA. The LAA method, which uses both distance and angle measurements, is one of hybrid localization methods. After measurements are made, many algorithms can be applied to estimate the location. In Chapter 2, NLS, LLS, POCS, and POR were reviewed.

In Chapter 3, a non-sequential localization scheme, which uses the TOA measurements was considered when the Nakagami fading is present. The CRLBs for localization errors were derived under different fading assumptions. Firstly, we considered the case where the phase is known at each anchor. In this case, the CRLB depends on the amplitude of the fading coefficient. Secondly, the amplitude of fading coefficients is assumed to be Nakagami distributed. In this case, the unconditional distribution of the TOA measurement can be calculated by using the total probability theorem. Thirdly, we assume no CSI is available at any anchor. In addition, the amplitude and the phase of fading coefficients are Nakagami distributed and uniformly distributed respectively. In this case, we calculated the unconditional distribution of the TOA measurement by integrating the effect of both amplitude and phase. The analytical results showed that the loss in performance due to Rayleigh fading with known phase is about 5dB compared to the case with no fading. Unknown phase caused an additional 1dB loss. Following this, the MLEs were also derived for different fading scenarios.

In Chapter 4, a sequential localization scheme, in which the locations of nodes are sequentially estimated, was applied to estimate node locations. The TOA, TDOA, RSS, DOA, and LAA localization algorithms were expressed as the solution to a set of linear equations. Following this, the performance of a sequential network localization process when using these different localization algorithms were compared. The simulation results showed that the DOA method outperformed

in low SNR and the LAA method outperformed in high SNR. Next, the CRLB on the localization error using the TOA method for the sequential localization scheme was studied. In the absent of fading, the CRLB for the sequential localization scheme was compared with the CRLB for the non-sequential localization scheme. The analytical results show that the non-sequential CRLB converges to zero $N$ times faster than the sequential scheme, where $N$ is the total number of nodes in the network. For the sequential localization scheme, the CRLB when the fading is present was also compared to the CRLB when the fading is absent case. Interestingly, the loss due to Rayleigh fading in both non-sequential and sequential schemes is the same, which is about 5dB.

In Chapter 5, a distributed location detection scheme was proposed. In the distributed detection formulation, each anchor receives a noisy signal from a node at a known location or within a known region. Each anchor makes a decision as to whether the node is active or not and transmits a bit to a fusion center once a decision is made. The fusion center combines all the decisions and uses a design parameter $K$ to make the final detection. Two cases were considered in this chapter. Firstly, locating a node at a known location was considered. Secondly, locating a node in a known region was considered. In both cases, the simulation results showed that the choice of the design parameter $K$ depends on the total probability of false alarm, and none of the $K$ values outperformed others for all $\bar{P}_{\mathrm{FA}}^{\mathrm{T}}$. To locate a node in a known region, the simulation results showed that the Gaussian approximation performs better when the TOA method was applied than the RSS case.

In Chapter 6, distributed location detection at a known location when fading exists was discussed. When the node is actively transmitting, each anchor receives a faded signal from the node. Three scenarios were considered, which include the fading coefficients are known at anchors, the fading coefficients with known phase but unknown amplitude, and no CSI is available at any anchor. When the fading coefficients are known at anchors, the optimal threshold depends on the fading coefficients. When the amplitude of the fading coefficients are random with Rayleigh distribution, the optimal threshold can be found by integrating the fading effect. When no CSI is available at any anchor, two non-coherent detection schemes can be applied and both in phase and quadrature components of the fading coefficients are extracted. The simulation results showed that

similar to the distributed location detection in the absence of fading case, none of the $K$ values outperformed others for all $\bar{P}_{\mathrm{FA}}^{\mathrm{T}}$.

REFERENCES


[1] D. Culler, D. Estrin, and M. Sivastava, "Overview of sensor networks," *IEEE Computer Society*, pp. 41–49, August 2004.

[2] I. Akyildiz, W. Su, Y. Sankarasubramaniam, and E. Cayirci, "A survey on sensor networks," *IEEE Communications Magazine*, vol. 40, no. 8, pp. 102–114, August 2002.

[3] J. Yick, B. Mukherjee, and D. Ghosal, "Wireless sensor network survey," *Computer Networks*, vol. 52, no. 12, pp. 2292–2330, August 2008.

[4] V. Chandramohan and K. Christensen, "A first look at wired sensor networks for video surveilance systems," *IEEE 27th Annual Conference on Local Computer Networks*, pp. 728–729, November 2002.

[5] V. Mhatre, "Homogeneous vs heterogeneous clustered sensor networks: a comparative study," in *IEEE International Conference on Communications*, June 2004, pp. 3646–3651.

[6] [Online]. Available: http://www.defence-industries.com/company/army/base-camp-protection-security-systems/genetlab-bilgi

[7] R. Frank. Sensor advance medical and healthcare applications. [Online]. Available: http://www.designworldonline.com/sensors-advance-medical-and-healthcare-applications/

[8] Logical neighborhoods: programming wireless sensor networks. [Online]. Available: http://logicalneighbor.sourceforge.net/

[9] Introduction to wireless sensor networks and its applications. [Online]. Available: https://wirelessmeshsensornetworks.wordpress.com/tag/wireless-sensor-network-technology-and-its-application-using-vlsi/

[10] U. Bilstrup, K. Sjoberg, B. Svensson, and P. Wiberg, "Capacity limitations in wireless sensor networks," *IEEE Emerging Technologies and Factory Automation*, pp. 529–536, September 2003.

[11] G. Pottie and W. Kaiser, "Wireless integrated network sensors," *Communications of the ACM*, vol. 43, no. 5, pp. 51–58, May 2000.

[12] ——, *Principles of Embedded Networked Systems Design*. Cambridge University Press, 2005.

[13] A. Chehri, P. Fortier, and P. Tardif, "Security monitoring using wireless sensor networks," *IEEE Annual Conference on Communication Networks and Services Research*, pp. 13–17, May 2007.

[14] J. Ko, C. Lu, M. Srivastava, J. Stankovic, A. Terzis, and M. Welsh, "Wireless sensor networks for healthcare," *IEEE Proceedings*, pp. 1947–1960, September 2010.

[15] D. Basu, G. Moretti, G. Gupta, and S. Marsland, "Wireless sensor network based smart home: sensor selection, deployment and monitoring," *IEEE Sensors Applications Symposium*, pp. 49–54, February 2013.

[16] J. Zhang, W. Li, Z. Yin, S. Liu, and X. Guo, "Forest fire detection system based on wireless sensor network," *IEEE Conference on Industrial Electronics and Applications*, pp. 520–523, May 2009.

[17] T. Alhmiedat, A. Taleb, and M. Bsoul, "A study on threats detection and tracking systems for military applications using WSNs," *International Journal of Computer Applications*, no. 15, pp. 12–18, February 2012.

[18] T. Arampatzis, J. Lygeros, and S. Manesis, "A survey of applications of wireless sensors and wireless sensor networks," *13th Mediterranean Conference on Control and Automation*, pp. 719–724, June 2005.

[19] J. Tavares, F. Velez, and J. Ferro, "Application of wireless sensor networks to automobiles," *Measurement Science Review*, vol. 8, no. 3, pp. 65–71, 2008.

[20] G. Sun, J. Chen, W. Guo, and K. Liu, "Signal processing techniques in network-aided positioning: A survey of state-of-the-art positioning designs," *IEEE Signal Processing Magazine*, vol. 22, no. 4, pp. 12–23, June 2005.

[21] C. Yawut and S. Kilaso, "A wireless sensor network for weather and disaster alarm systems," *2011 International Conference on Information and Electronics Engineering*, vol. 6, pp. 155–159, 2011.

[22] K. Khedo, R. Perseedoss, and A. Mungur, "A wireless sensor network air pollution monitoring system," *International Journal of Wireless and Mobile Networks*, vol. 2, no. 2, pp. 31–45, 2010.

[23] P. Curtis, M. Banavar, S. Zhang, A. Spanias, and V. Weber, "Android acoustic ranging," in *IEEE International Conference on Information, Intelligence, Systems, and Applications*, July 2014, pp. 118–123.

[24] E. Kaplan, *Understanding GPS: Principles and Applications*. Artech House Telecommunication Library, 1996.

[25] S. Miller, X. Zhang, and A. Spanias, "A new asymmetric correlation kernel for gnss multipath mitigation," *IEEE Sensor Signal Processing for Defence*, pp. 1–5, September 2015.

[26] A. Pal, "Localization algorithms in wireless sensor networks: Current approaches and future challenges," *Network Protocols and Algorithm*, vol. 2, no. 1, pp. 45–74, January 2010.

[27] Y. Shen and M. Win, "Fundamental limits of wideband localization- Part I: A general framework," *IEEE Transactions on Information Theory*, pp. 4956–4980, September 2010.

[28] Y. Shen, H. Wymeersch, and M. Win, "Fundamental limits of wideband localization- Part II: Coopeartive networks," *IEEE Transactions on Information Theory*, pp. 4981–5000, June 2010.

[29] F. Commission, "Revision of the commissions rules to insure compatibility with enhanced 911 emergency calling systems," *FCC Docket*, no. 94-102, December 1996.

[30] S. Gezici, I. Guvenc, and Z. Sahinoglu, "On the performance of linear least-squares estimation in wireless positiong systems," *IEEE Communication Society*, pp. 4203–4208, May 2008.

[31] N. Patwari, A. Hero, M. Perkins, N. Correal, and R. O'Dea, "Relative location estimation in wireless sensor networks," *IEEE Transactions on Signal Processing*, vol. 51, no. 8, pp. 2137–2148, July 2003.

[32] S. Muruganathan, D. Ma, R. Bhasin, and A. Fapojuwo, "A centralized energy-efficient routing protocol for wireless sensor networks," *IEEE Communications Society*, pp. 8–13, March 2005.

[33] L. Lu and C. Lim, "Position-based, energy-efficient, centralized clustering protocol for wireless sensor networks," *4th IEEE Conference on Industrial Electronics and Applications*, pp. 139–144, May 2009.

[34] N. Patwari, J. Ash, S. Kyperountas, A. Hero, R. Moses, and N. Correal, "Locating the nodes: cooperative localization in wireless sensor networks," *IEEE Signal Processing Magazine*, vol. 22, no. 4, pp. 54–59, June 2005.

[35] Y. Shen, "Fundamental limits of wideband localization," Master's thesis, Massachusetts Institute of Technology, Feburary 2008.

[36] A. Catovic and Z. Sahinoglu, "The Cramér-Rao bounds of hybrid TOA/RSS and TDOA/RSS location estimation schemes," *IEEE Communications Letters*, vol. 8, no. 10, pp. 626–628, October 2004.

[37] J. Xu, M. Ma, and C. Law, "AOA cooperative position localization," in *Global Telecommunications Conference, IEEE*, December 2008, pp. 1–5.

[38] M. Willerton, M. Banavar, X. Zhang, A. Manikas, C. Tepedelenlioglu, A. Spanias, T. Thomoton, E. Yeatman, and A. Constantinides, "Sequential wireless sensor network discovery using wide aperture array signal processing," *European Signal Processing Conference*, pp. 2278–2282, August 2012.

[39] M. Laaraiedh, L. Yu, S. Avrillon, and B. Uguen, "Comparison of hybrid localization schemes using RSSI, TOA, and TDOA," in $11^{th}$ *European Wireless Conference*, April 2011, pp. 1–5.

[40] S. Gezici, "A survey on wireless position estimation," *Wireless Personal Communications*, vol. 44, no. 3, pp. 263–282, February 2008.

[41] E. Huang and R. W. Herring, "Comparisons of error characteristics between TOA and TDOA positioning," *IEEE Transactions on Acoustics, Speech, Signal Processing*, no. 1, pp. 307–311, October 1981.

[42] H. Wymeersch, J. Lien, and M. Z.Win, "Cooperative localization in wireless networks," *Proceeding of the IEEE*, vol. 97, no. 2, pp. 427–450, February 2009.

[43] D. Niculescu and B. Nath, "Ad-hoc positioning system," in *USENIX Technical Annual Conference*, June 2002, pp. 317–327.

[44] S. Shioda and K. Shimamura, "Anchor-free localization: estimation of relative locations of sensors," *IEEE International Symposium on Personal, Indoor and Mobile Raido Communications: Mobile and Wireless Networks*, pp. 2087–2092, September 2013.

[45] X. Zhang, M. Banavar, M. Willerton, A. Manikas, C. Tepedelenlioğlu, A. Spanias, T. Thornton, E. Yeatman, and A. Constantinides, "Performance comparison of localization thechniques for sequential WSN discovery," in *IEEE Sensor Signal Processing for Defence*, London, September 2012, pp. 1–5.

[46] L. Doherty, K. Pister, and L. Ghaoui, "Convex position estimation in wireless sensor networks," *IEEE Infocom*, pp. 1655–1663, April 2001.

[47] E. Larsson, "Cramer-Rao bound analysis of distributed positioning in sensor networks," *IEEE Signal Processing Letters*, no. 3, pp. 334–337, March 2004.

[48] P. Biswas and Y. Ye, "Semidefinite programming for ad hoc wireless sensor network localization," *IEEE Information Processing in Sensor Networks*, pp. 45–54, April 2004.

[49] ——, "A distributed method for solving semidefinite programming for ad hoc wireless sensor network localization," Stanford University, Tech. Rep., October 2003.

[50] W. Pries, T. de Paula Figueiredo, H. Wong, and A. Loureiro, "Malicious node detection in wireless sensor networks," *IEEE Parallel and Distributed Processing Symposium*, April 2004.

[51] J. Ho, M. Wright, and S. Das, "Distributed detection of mobile malicious node attacks in wireless sensor networks," *Ad Hoc Networks*, pp. 512–523, May 2012.

[52] H. Van Trees, *Detection, estimation and modulation Theory*. John Wiley and Sons, Inc., 1968.

[53] S. Kay, *Fundamentals of Statistical Signal Processing: Detection Theory*. Prentice Hall, 1993.

[54] M. Z. Win, Y. Shen, and H. Wymeersch, "On the position error bound in cooperative networks: a geometric approach," *Spread Spectrum Techniques and Applications. IEEE*, pp. 637–643, September 2008.

[55] P. Bergamo and G. Mazzini, "Localization in sensor networks with fading and mobility," *IEEE international symposium on personal, indoor and mobile radio communications*, pp. 750–754, 2002.

[56] S. Sattarzadeh and B. Abolhassani, "TOA extraction in multipath fading channels for location estimation," *IEEE 17th International Symposium on Personal, Indoor and Mobile Radio Communications*, pp. 1–4, September 2006.

[57] S. Ray, W. Lai, and I. Paschalidis, "Statistical location detection with sensor networks," *IEEE Transactions on Information Theory*, vol. 52, no. 6, pp. 2670–2683, 2006.

[58] N. Vankayalapati and S. Kay, "Asymptotically optimal detection of low probability of intercept signals using distributed sensors," *IEEE Transactions on Aerospace and Electronic Systems*, vol. 48, no. 1, pp. 737–748, January 2012.

[59] A. Weiss, "Direct position determination of narrowband radio frequency transmitters," *IEEE Signal Processing Letter*, vol. 11, no. 5, pp. 513–516, May 2004.

[60] F. Zhao and L. Guibas, *Wireless Sensor Networks: An Information Processing Approach*. Morgan Kaufmann Publishers, 2004.

[61] G. Mao, *Localization Algorithms and Strategies for Wireless Sensor Networks*. Information Science Reference, 2009.

[62] M. Willerton, M. Banavar, X. Zhang, A. Manikas, C. Tepedelenlioglu, A. Spanias, T. Thomoton, E. Yeatman, and A. Constantinides, "Sequential wireless sensor network discovery using wide aperture array signal processing," *European Signal Processing Conference*, pp. 2278–2282, August 2012.

[63] S. Khan, A. Pathan, and N. Alrajeh, *Wireless Sensor Networks: Current Status and Future Trends*. CRC Press, 2012.

[64] R. Peng, "Angle of arrival localization for wireless sensor networks," in *IEEE Communications Society on Sensor and Ad Hoc Communications and Networks*, September 2006, pp. 374–382.

[65] R. Moses, O. Moses, D. Kishnamurthy, and R. Patterson, "A self-localization method for wireless sensor networks," *EURASIP Journal on Applied Signal Processing*, no. 4, pp. 348–358, 2003.

[66] D. Torrieri, "Statistical theory of passive location systems," *IEEE Transactions on Aerospace and Electronic Systems*, vol. 20, no. 2, March 1984.

[67] J. Costa, N. Patwari, and A. Hero, "Distributed multidimensional scaling with adaptive weighting for node localization in sensor networks," *ACM Journal*, vol. 5, no. N, pp. 1–23, June 2004.

[68] K. Langendoen and N. Reijers, "Distributed localization in wireless sensor networks: a quantitative comparison," *avaliable online at: www.ElsevierComputerScience.com*, 2003.

[69] S. Kay, *Fundamentals of Statistical Signal Processing: Estimation Theory*. Prentice Hall, 1993.

[70] J. Yi and L. Zhou, "Enhanced location algorithm with received-signal-strength using fading kalman filter in wireless sensor networks," *IEEE Conference Publishing*, pp. 458–461, 2011.

[71] M. Gholami, H. Wymeersch, E. Strom, and M. Rydstrom, "Wireless network positioning as a convex feasibility problem," *EURSIP Journal on Wireless Communications and Networking*, January 2011.

[72] A. Hero and D. Blatt, "Sensor network source localization via projection onto convex sets," *IEEE International Conference on Acoustics, Speech and Signal Processing*, vol. 3, March 2005.

[73] M. Alsheikh, S. Lin, D. Nyato, and H. Tan, "Machine learning in wireless sensor networks: algorithms, strategies, and applications," *IEEE Communications Surveys and Tutorials*, pp. 1553–877x, April 2014.

[74] P. Jarabo-Amo, R. Rosa-Zurera, R. Gil-Pita, and F. Lopez-Ferreras, "Sufficient condition for an adaptive system to approximate neyman-pearson detector," *IEEE 13th Workshop on Statistical Signal Processing*, pp. 295–300, July 2005.

[75] C. Helstrom, *Elements of Signal Detection and Estimation*. Prentice Hall, 1994.

[76] A. Andrea, U. Mengali, and R. Reggiannini, "The modified Cramer-Rao bound and its application to synchronization problems," *IEEE Transactions on Communications*, vol. 42, no. 234, pp. 1391–1399, April 1994.

[77] A. Goldsmith, *Wireless communications*. Combridge University Press, 2005.

[78] I. Gradshteyn and I. Ryzhik, *Tables of Integrals, Series, and Products*. Elsevier Inc., 2007.

[79] J. Foutz, A. Spanias, and M. K. Banavar, *Narrowband Direction of Arrival Estimation for Antenna Arrays*. Morgan and Claypool Publishers, 2008.

[80] X. Zhang, C. Tepedelenlioğlu, M. Banavar, and A. Spanias, "CRLB for the localization error in the presence of fading," in *IEEE International Conference on Acoustics, Speech, and Signal Processing*, Vancouver, BC, May 2013, pp. 5150–5154.

[81] G. Mao and B. Fidan, *Localization Algorithms and Strategies for Wireless Sensor Networks*. Information Science Reference, 2009.

[82] A. Mathai, *An Introduction to Geometrical Probability*. CRC Press, December 1999.

[83] A. Ong, "Bandpass analog-to-digital conversion for wireless applications," Stanford University, Tech. Rep., 1998.